

PATHFINDING INTERPLANETARY BUS CAPABILITY FOR THE CAL POLY  
CUBESAT LABORATORY THROUGH THE DEVELOPMENT OF A  
PHOBOS-DEIMOS MISSION CONCEPT

A Thesis  
presented to  
the Faculty of California Polytechnic State University,  
San Luis Obispo

In Partial Fulfillment  
of the Requirements for the Degree  
Master of Science in Aerospace Engineering

by  
Alyssa Ralph  
August 2020

© 2020

Alyssa M. Ralph

ALL RIGHTS RESERVED

## COMMITTEE MEMBERSHIP

TITLE: Pathfinding Interplanetary Bus Capability for the  
Cal Poly CubeSat Laboratory Through the  
Development of a Phobos-Deimos Mission  
Concept

AUTHOR: Alyssa M. Ralph

DATE SUBMITTED: August 2020

COMMITTEE CHAIR: Pauline Faure, Ph.D.  
Assistant Professor of Aerospace Engineering

COMMITTEE MEMBER: Kira Abercromby, Ph.D.  
Professor of Aerospace Engineering

COMMITTEE MEMBER: Amelia Greig, Ph.D.  
Assistant Professor of Mechanical Engineering  
University of Texas, El Paso

COMMITTEE MEMBER: Andrea Hsu, Ph.D.  
Senior Scientist  
The Aerospace Corporation

## ABSTRACT

### Pathfinding Interplanetary Bus Capability for the Cal Poly CubeSat Laboratory Through the Development of a Phobos-Deimos Mission Concept

Alyssa M. Ralph

With the rise of CubeSats and the demonstration of their many space applications, there is interest in interplanetary CubeSats to act for example as scientific investigations or communications relays. In line with the increasing demand for this class of small satellites, the Cal Poly CubeSat Lab (CPCL) seeks to develop a bus that could support an interplanetary science payload. To facilitate this, a mission concept to conduct science of the moons of Mars, Phobos and Deimos, is investigated by determining the mission needs for a CubeSat in a Phobos-Deimos cyler orbit through the development of a baseline design to meet mission objectives. This baseline design is then compared by subsystem to CPCL's current capabilities to identify technology, facility, and knowledge gaps and recommend a path forward to close them. The resulting baseline design is a 16U bus capable of transferring from an initial low Mars orbit to a Phobos-Deimos cyler orbit using a combined chemical and electric propulsion system. The bus is designed for a 3.5 year mission lifetime collecting radiation data and images, utilizing a relay architecture to downlink payload data. Estimates for mass, volume, and power available for an additional payload are up to 2.3 kg in ~4U with power consumption up to 13 to 38 W. This baseline requires further iteration due to non-closure of the thermal protection subsystem and improvement of other subsystems but serves as a starting point for exploration into CPCL's next steps in becoming an interplanetary bus provider. Major subsystem areas identified for hardware performance improvement within CPCL are propulsion, communications, power, and mechanisms.

Keywords: Small Satellites, Planetary, Systems Engineering, Mission Architecture

## ACKNOWLEDGMENTS

Thank you to my professors and mentors who have acted as role models throughout my undergraduate career and encouraged me to pursue a graduate education. In particular, thank you to Dr. Andrea Hsu, Dr. Kira Abercromby, and Dr. Amelia Greig for providing me opportunities to expand my engineering experience beyond the classroom, leading me to take on this endeavor and generously donating their time to help me see it through. Extra thanks to Dr. Pauline Faure for being a patient and supportive advisor through multiple setbacks and being a wealth of knowledge on the topic of systems engineering practice. Thank you to Kendra Bubert for her help and positivity over the years and to Brandon Goddard for providing me with the computational resources needed for this work. I am also grateful to my peers for the comradery and many motivational pep talks as we tackled this program together. Finally, thank you to my friends and family for checking in on me and cheering me on-- your care means the world to me.

## TABLE OF CONTENTS

	Page
LIST OF TABLES .....	viii
LIST OF FIGURES .....	x
CHAPTER	
1. INTRODUCTION .....	1
1.1 Problem Statement .....	4
1.2 Thesis Objectives and Scope .....	6
2. BACKGROUND .....	8
2.1 The Cal Poly CubeSat Laboratory .....	8
2.2 CubeSats and CubeSat Specifications .....	8
2.3 Environment Beyond Earth Orbit and Other Challenges .....	10
2.3.1 Power .....	11
2.3.2 Communications .....	11
2.3.3 Propulsion .....	12
2.3.4 Thermal .....	15
2.3.5 Radiation .....	16
2.4 Phobos-Deimos Cypher Orbit .....	17
3. MISSION OBJECTIVES .....	20
3.1 Defining the Mission Objectives .....	20
3.2 Stand-in Payloads .....	22
3.3 Developing the Mission Concept .....	22
4. SYSTEM OVERVIEW AND CONCEPT OF OPERATIONS .....	26
4.1 Spacecraft Overview .....	28
4.2 Concept of Operations .....	26
5. PROPULSION SUBSYSTEM .....	32
5.1 Orbit Analysis .....	32
5.2 Propulsion System Survey and Requirements .....	34
5.3 Electric Propulsion .....	37
5.4 Chemical Propulsion .....	39
5.5 Propulsion Subsystem Summary .....	40
5.6 Propulsion Subsystem Results in Relation to CPCL .....	41
6. COMMUNICATIONS SUBSYSTEM .....	43
6.1 Direct-to-Earth Architecture .....	43
6.2 Relay Architecture .....	49
6.3 Communications Subsystem Results in Relation to CPCL .....	56
7. POWER SUBSYSTEM .....	58
7.1 Power Consumption Requirements .....	58
7.2 Sizing the Solar Panels .....	62
7.3 Sizing the Batteries .....	66
7.4 Power Management and Distribution System Selection .....	68
7.5 Power Subsystem Summary .....	69
7.6 Power Subsystem Results in Relation to CPCL .....	69
8. ATTITUDE DETERMINATION AND CONTROL SYSTEM .....	71
8.1 Attitude Control Requirements .....	71
8.2 Attitude Sensors .....	73
8.3 Reaction Control Actuation .....	74
8.4 ADCS Subsystem Results in Relation to CPCL .....	80

9. COMMAND AND DATA HANDLING SUBSYSTEM.....	82
9.1 Memory Storage.....	82
9.2 Command and Data Handling Subsystem Results in Relation to CPCL .....	84
10. SPACECRAFT CONFIGURATION .....	86
10.1 EXOpod 16U Specification.....	86
10.2 Mass Budget.....	88
10.3 Configuration Process .....	91
10.4 Configuration Results.....	93
10.4.1 Stowed .....	94
10.4.2 Deployed.....	97
10.5 Bus as a Payload Host .....	100
10.6 Configuration Results in Relation to CPCL .....	101
11. RADIATION CONSIDERATIONS.....	104
12. THERMAL PROTECTION SYSTEM.....	108
12.1 Thermal Requirements .....	108
12.2 Determining the Thermal Load .....	110
12.3 Initial Analysis .....	112
12.4 Thermal Desktop Model.....	114
12.5 Thermal Subsystem Summary and Needed Work.....	118
12.6 Thermal Subsystem Results in Relation to CPCL.....	119
13. SUMMARY OF RECOMMENDATIONS TO CPCL.....	121
14. CONCLUSIONS AND FUTURE WORK .....	125
14.1 Future Work .....	126
BIBLIOGRAPHY.....	128
APPENDICES .....	134
A. Propulsion Trade and Calculations .....	134
B. Detailed Link Budgets .....	135
C. EXOlaunch Specifications.....	137
D. N2 Diagram for Configuration Trade .....	140
E. CubeSats Manifested for Artemis-1.....	141
F. STK Inputs.....	143
G. Thermal Desktop Inputs.....	150

## LIST OF TABLES

Table	Page
1-1: Phobos Deimos Strategic Knowledge Gaps outlined by NASA [20, 22].....	4
2-1: Orbital parameters of Phobos/Deimos cycler orbits [44]. .....	19
3-1: Summary of mission objectives.....	22
3-2: Payload mass, volume, power, and data allocations.....	23
3-3: Mission elements and their assumed tradability.....	25
5-1: Definition of transfer orbits considered.....	34
5-2: Transfer trajectory options and delta-Vs. ....	34
5-3: Surveyed propulsion systems with TRL 6 or greater. ....	36
5-4: Electric propulsion system trade. ....	38
5-5: Busek BIT-3 RF Ion Thruster Parameters [58]. ....	39
5-6: Performance parameters of surveyed chemical propulsion systems. ....	40
5-7: Aerojet Rocketdyne MPS-135-6U Thruster Module Parameters [59, 60]. ....	40
5-8: Delta-V budget and resulting propellant masses. ....	41
6-1: Link parameters used for analysis. ....	46
6-2: Antennas considered for high gain DTE, adapted from [33, 66].....	48
6-3: Summary of Ka-Band DTE architecture parameters.....	49
6-4: Surveyed UHF radios considered for relay architecture.....	51
6-5: Relay link parameters. ....	53
6-6: Summary of UHF relay architecture option parameters.....	55
6-7: Comparison of UHF Relay and DTE Ka-band architectures. ....	56
7-1: Power consumption of selected components.....	59
7-2: Power consumption modes throughout mission. ....	61
7-3: Solar panel sizing parameters and results.....	65
7-4: Battery sizing parameters and results. ....	67
7-5: Surveyed battery technology [56].....	68
7-6: Power subsystem summary. ....	69
8-1: Required pointing accuracy for components. ....	72
8-2: Physical and performance parameters of selected ADCS components. ....	74
8-3: Mass and area properties of deployed configurations. ....	77
8-4: Worst case disturbance torques. ....	78
8-5: Derived reaction wheel performance requirements.....	79
8-6: Baselined reaction wheel performance and physical parameters. ....	80
9-1: Surveyed C&DH systems [56].....	84
9-2: Baselined C&DH system summary.....	84
10-1: EXOpod Allowed Maximum Dimensions with Axes Referring to Figure 10-1 [26]. ..	88
10-2: Mass and volume budget ( $U = 1000 \text{ cm}^3$ ). ....	90
10-3: Mass properties of the stowed configuration.....	96
10-4: Post-deployment mass properties.....	99
10-5: Post-low thrust phase and pre-impulsive transfer mass properties.....	99
10-6: Cycler orbit mass properties.....	100



10-7: Baseline SWaP summary. .... 101  
11-1: Radiation tolerances of selected components where provided by manufacturer..... 106  
12-1: Component physical and material specifications/assumptions..... 109  
12-2: Component operating temperature ranges and internal heat generation..... 110  
12-3: Thermal finishes utilized [23, 97]..... 114  
12-4: Mitigations applied to the presented model..... 119  
13-1: Summary of CPCL capability, baseline results for mission concept, and  
recommendations. .... 122

## LIST OF FIGURES

Figure	Page
2-1: Illustration of 12U CubeSat adapted from CDS with optional “tuna can” volume. Note: axes do not correspond to CDS [7].	9
2-2: Encounter geometry of Phobos, Deimos, and resonance orbits.	19
3-1: Stand-in payload with dosimeter (left) and camera (right); not to scale [47, 48].	24
4-1: Stowed configuration overview.	27
4-2: +Y view of spacecraft depicting deployables.	27
4-3: Internal configuration.	28
4-4: Mission concept of operations.	29
4-5: Entire mission trajectory.	31
5-1: Time required for electric propulsion options to achieve 1250 m/s.	37
6-1: Earth-Mars distances over time.	44
6-2: Antenna gain versus antenna diameter for various frequency bands.	46
6-3: Encounter geometry of cycler orbit and MRO for link analysis.	50
6-4: Data rate change through the 3.5 hr pass near cycler periapsis.	54
6-5: Number of MRO passes needed to downlink various data packets with varying compression levels.	54
7-1: Eclipse duration during low-thrust transfer.	63
7-2: Eclipse duration during cycler orbit.	63
7-3: Deployed configuration (top) and proposed folding strategy for MMA arrays (bottom) [77].	66
10-1: Maximum allowable outer dimensions for CubeSats launched in an EXOpod with additional dimensions listed in Table 10-1 [26].	87
10-2: Internal configuration.	93
10-3: Stowed configuration.	95
10-4: Stowed configuration showing compliance with EXOpod deployer specification. Dimensions are in mm.	96
10-5: Deployed configuration showing relative interior configuration.	97
10-6: Deployed configuration showing side panels with apertures.	98
10-7: Center of mass aligning with BIT-3 thruster.	100
11-1: Total ionizing dose in silicon for 1.64 years exposure in a 4624 km altitude, 0° inclination circular orbit.	105
11-2: Total ionizing dose in silicon for 1.88 years exposure in the cycler orbit.	105
12-1: Resulting component temperatures for initial thermal analysis.	113
12-2: Hot case component temperature Thermal Desktop results over two orbits.	115
12-3: Hot case component temperature post-processing Thermal Desktop results at hottest point in orbit.	116
12-4: Cold case component temperature Thermal Desktop results over an orbit.	117
12-5: Cold case component temperature post-processing Thermal Desktop results at coldest point in orbit.	118

## Chapter 1

### INTRODUCTION

Earth orbiting missions have historically been conducted by large and costly satellite missions, with 73% of those launched between 1990 and 2008 being greater than 500 kg at launch [1]. Missions of masses greater than 500 kg, such as Jason 1 at 500 kg and TOPEX/POSEIDON at 2400 kg, both Earth science missions, carried price tags of \$255 million and \$882 million, respectively, in Fiscal Year 2020 dollars [2, 3, 4]. In low Earth orbit (LEO), there has been a change in the large and costly satellite mission paradigm with the rise of Small Satellites (SmallSats), defined as a satellite with a mass less than 180 kg [5]. In particular, the SmallSat sub-class of CubeSats, has become popular with 93% of satellites less than 54 kg developed since 1998 following a CubeSat form factor [6]. CubeSats are defined in units, or “U,” which are 10 x 10 x 10 cm cubes, each of which can be up to 2 kg and combined to form sizes from 1U to 27U [7, 8]. The CubeSat Standard, co-created by California Polytechnic State University and Stanford University in 1999, was started as a means to increase access to space for university programs by decreasing cost of development, launch, and operations through project standardization, increased use of commercial off the shelf parts (COTS), and reduced testing [9]. The applications of CubeSats have expanded to benefit the scientific, academic, and engineering communities with government agencies, private engineering companies, and educational institutions across the globe utilizing the cost-effective CubeSat platform for performing technology demonstrations and science investigations, as well as proving advanced mission concepts with development times of one to two years; depending on their application, the cost can range from tens of thousands to a few million USD [5, 8, 9].

The potential applications for CubeSats beyond LEO were recognized as early as 2012 through NASA’s Innovative Advanced Concepts (NIAC) studies for mineral mapping of asteroids, deep

space astronomy, and Phobos sample return [10]. The NASA 2018 Strategic Plan, which outlines the direction of the space agency, has placed emphasis on missions that perform science and develop technologies that will help enable human exploration of the solar system, starting with the Moon, and then eventually Mars. As part of this effort, NASA is going beyond conceptual NIAC studies to actively expand “*the use of lower-cost CubeSats and SmallSats to accomplish ... science goals*” [11]. As of 2020, of the approximately 1200 CubeSats launched, only four were in non-LEO orbits, with the US Air Force Research Laboratory’s 12U TDO and TDO-2 CubeSats in a geostationary transfer orbit and NASA’s 6U MarCO-A and MarCO-B in an interplanetary Mars flyby orbit [6]. Despite there being only two deep space CubeSats flown, there is increasing demand for them, as shown in a 2014 Small Business Innovation Research (SBIR) call from NASA for deep space CubeSat technology proposals, seeking bus technologies that enable a flight demonstration mission in deep space, such as propulsion systems that can enable orbit insertion, for mission objectives such as remote sensing or in-situ science data collection [12]. More recent indications of this trend are the thirteen 6U CubeSats manifested as secondary payloads on Artemis-1, expected to launch in 2021, which will be the first CubeSats deployed in cislunar space with five going into interplanetary trajectories [13]. Though not a direct comparison of mission types, the relatively low cost of the CubeSat platform can also be illustrated for interplanetary applications with MarCO costing \$19 million compared to the Mars Reconnaissance Orbiter (MRO) mission at ~\$955 million in 2020 USD [14, 15].

This expansion into deep space CubeSat technology and missions puts demand not only on the commercial industry but also the academic field as NASA sponsors development through cash-prize Cube Quest Challenges such as the Deep Space Derby and by providing free launches for student payloads that address aspects of science, exploration, or technology development relevant to NASA’s strategic goals through the CubeSat Launch Initiative (CSLI) [16, 17]. The Cal Poly CubeSat Lab (CPCL), which maintains the CubeSat Standard through the CubeSat Design Specification (CDS), is one organization that takes advantage of these funding and launch

opportunities to provide industry applicable educational experiences to university students. The lab acts as a bus provider, providing the structure, software, and ground support to host payloads in collaboration with other universities and organizations including The Naval Research Laboratory, NASA Jet Propulsion Laboratory, and SRI International [18]. CPCL has launched eleven CubeSats and has two in assembly or awaiting integration; all these missions were or will be in LEO though very recently the lab developed two collaborative lunar CubeSat concepts [19]. With the industry demand trend following NASA's "Moon then Mars" direction and development of lunar CubeSats already in the works, CPCL has an interest in further investigating interplanetary bus capability, taken to mean CubeSats for applications beyond Earth or lunar orbit and in particular, at Mars.

Strategic knowledge gaps (SKGs), or gaps between what an organization needs to know and what it knows now, have been identified by NASA in relation to accomplishing human exploration of Near Earth Objects (NEOs) and other small bodies such as Mars' moons, Phobos and Deimos, as part of the greater effort of lunar and Mars human exploration [20]. These gaps pinpoint measurements that need to be obtained by satellites and robotic missions to characterize the environment such that a safe human mission can be designed [20]. Phobos and Deimos are of interest because their origin is uncertain; they are theorized to be captured asteroids or fragmentations from an impact with Mars. Their composition could provide information on the evolution of the surface of Mars due to Martian sediment accumulation and if formed from a collision, containing parts of a younger Mars surface. If captured asteroids, their composition can provide information on how water was and can be transported to Mars [21]. Multiple SKGs call for science in Phobos and Deimos orbit and on the surface; these are outlined in Table 1-1 [22]. The Martian Moons eXplorer (MMX) is a flagship sample return mission from JAXA, planning to address science goals in line with the SKGs located on the Phobos/Deimos surface by remote sensing both moons and landing on Phobos [21]. Considering surface location goals covered by MMX, the remaining SKGs that need to be addressed are those that encounter Phobos/Deimos in orbit. These Phobos/Deimos rendezvous SKGs can be used to guide a small satellite mission

concept as they provide a recognized need which in turn increases the chances of funding and launch opportunities.

**Table 1-1: Phobos Deimos Strategic Knowledge Gaps outlined by NASA [20, 22].**

<b>SKG</b>	<b>Science Investigation</b>	<b>Potential Instrument</b>	<b>Location</b>	<b>Duration</b>
<b>Surface Science</b>	Surface composition	Spectrometers, imagers	Surface	Sufficient to map potential landing zones and interact with materials at site
<b>Surface Operations</b>	Regolith composition and physical/electrical properties	Spectrometers, imagers, ground penetrating radar, mechanical probes	Surface	Sufficient to map potential landing zones, interact with and characterize site materials
	Thermal environment	Thermal imager/probes	Surface	Sufficient to characterize properties over diurnal timescales
	Gravitational fields of Phobos/Deimos	Radioscience tracking	Phobos/Deimos rendezvous	Sufficient to map gravity field for proximity operations
	Electrical and plasma environments of Phobos/Deimos	Radiation detector suite, Langmuir probe	Phobos/Deimos rendezvous	Periodically throughout 1 Martian year
<b>Technology</b>	Anchoring and surface mobility	Surface anchoring/mobility demonstration	Surface	Surface interaction at site of interest

### 1.1 Problem Statement

The needs for remote science at Phobos/Deimos and development of CubeSats capable of missions beyond LEO and lunar orbit can be addressed simultaneously by a CubeSat capable of conducting science in an orbit encountering Phobos/Deimos. The challenges associated with this solution stem from overcoming the environment near Mars while adhering to a CubeSat design specification. As Mars is farther than the Sun than Earth with a semi-major axis of 1.5 AU compared to 1 AU, solar irradiation is reduced from 1367.5 W/m<sup>2</sup> to 607.8 W/m<sup>2</sup> according to Equation (1.1) where  $R$  is the

distance from the Sun in AU, requiring larger solar cell areas to generate the same amount of electrical power and reducing the absorbed heat not converted to electrical power [23]; to generate 1 W of power in LEO, 7.3 cm<sup>2</sup> of solar cell area is needed compared to 16.5 cm<sup>2</sup> at Mars. Reduced power per area restricts the possible performance of all other subsystems, namely propulsion and communications for missions performing orbital maneuvers and payload data transmission [24]. Other considerations for Mars CubeSats that differ from LEO CubeSats are increased radiation exposure without protection of Earth's Van Allen belts and lack of magnetic field for attitude determination and control [24].

$$\text{Solar flux} = \frac{1367.5 \text{ W/m}^2}{R^2} \quad (1.1)$$

Further, the CDS provides design boundaries in volume and mass, which combined with area's relation to power generation, can be referred to as size, weight, and power (SWaP) constraining. The combination of the difference in environment and SWaP constraints derived from the CDS create an engineering challenge, calling for engineering and technology solutions that miniaturize and simultaneously increase the functionality of critical space systems [24].

CPCL has begun work to increase bus capability both for LEO and beyond with updated specifications for up to a 12U form factor and mass per "U" increasing from 1.33 kg to 2 kg as of 2020 [7]. Concepts for lunar CubeSats to perform science and technology demonstrations of a CPCL deep space radio have been developed [19]. The lab has also invested in developing an interplanetary CubeSat deployer with studies into radiation shielding and relay capability. However, the lab has not yet performed studies of a CubeSat bus designed for the environment at Mars. This work seeks to fill that gap, using the interest in Phobos and Deimos science to develop a mission concept for investigation of the Martian moons. Designing a mission concept located beyond LEO can inform areas of needed improvement within CPCL in terms of hardware

performance, in-house technology development, and student experience to achieve the goals of such a mission, helping determine a path forward to interplanetary bus capability.

## 1.2 Thesis Objective and Scope

The objective of this thesis is to identify the technology gaps between CPCL's current bus capabilities and what is needed for interplanetary missions. To identify these gaps, a mission concept to perform scientific investigations of the Martian moons, Phobos and Deimos, is developed. The top level mission objectives for the concept in this thesis are derived from the Phobos/Deimos SKGs in Table 1-1: perform science of Mars' moons and do so for one Martian year. As will be explained in Chapter 2, a rideshare to Mars is assumed which requires transfer from the primary mission's insertion orbit to the science orbit. The selected science orbit is referred to as a cycler orbit, providing repeated encounters with the Martian moons; the rationale and description of this orbit is explained in Chapter 2. Performance objectives for the communications and data handling subsystems address science data collection, storage, and transmission time. Rationale for these objectives will also be explained in Chapter 2. The top-level mission and performance objectives are listed below:

- Perform science of Mars' moons
- Maneuver from an initial insertion orbit to a Phobos/Deimos cycler orbit
- Perform science for one Martian year
- Establish a communications link with Earth and maintain a data rate of at least 100 bps
- Downlink one week of science data within three downlink opportunities
- Store up to four weeks of science data onboard

The development of a baseline design for this mission concept is the focus of this work, determining solutions for a CubeSat to meet the listed objectives while surviving the environment experienced at Mars. This involves deriving performance requirements and trading design solutions



to meet those requirements for all major subsystems. For propulsion, requirements and subsequent trades will be explained in Chapter 5, the communications subsystem in Chapter 6, the power subsystem in Chapter 7, attitude determination and control subsystem in Chapter 8, and command and data handling subsystem in Chapter 9. Configuration rationale and results are detailed in Chapter 10 while radiation and thermal considerations and analysis are explored in Chapter 11 and Chapter 12, respectively. Throughout this thesis, baseline results are compared to CPCL flight heritage, current technology development, and planned development on a subsystem level to identify gaps and recommend a path forward to close them.

The baseline design is high level, focusing on subsystem performance for a near future (2025-2030) technology demonstration of the bus, and therefore prioritizing components that have been demonstrated in a relevant environment, corresponding to technology readiness levels (TRLs) of 6 or greater [25]. The presented design is a first iteration, acting as a starting point for the development of a bus capable of hosting a scientific payload at Mars and providing an estimate of how much mass, space, and power could be offered to that payload. To begin the design, several assumptions were made, such as ridesharing to Mars, the initial orbit, and the selected cycler orbit. Additionally, mass, volume, and configuration constraints for CubeSats larger than 12U are not defined by the CDS so commercial deployer specifications were used to inform sizing and configuration as explained in Chapter 2. These assumptions may become untrue as the CubeSat industry and technologies evolve, requiring revision of assumptions and consequently, the baseline design. However, this work can still be used to inform revision of the baseline. It should be noted that selection of commercial components in this work is not intended as an endorsement for purchase and integration of those parts, rather they provide a guide for performance of subsystem components using available technologies. Areas outside the scope of this thesis include trajectory optimization, structural analysis, software design, and detailed subsystem interfacing.

## **Chapter 2**

### **BACKGROUND**

This chapter contains provides background information relevant to the design of a mission concept for a CubeSat mission for Martian moon science and how that concept can be used by CPCL. The role of CPCL is explained and CubeSat design specifications detailed before addressing the design challenges faced for CubeSats beyond LEO with mitigation techniques used by the only CubeSat mission to experience the space environment near Mars, MarCO, provided for reference. Finally, the cycler orbit assumed for this research is described.

#### **2.1 The Cal Poly CubeSat Laboratory**

The CubeSat Standard was co-developed and is maintained by CPCL. It is a student-run program, advised by dedicated staff, that also develops, builds, tests, integrates, and operates CubeSats. In addition to providing busses to host payloads, the lab also develops and tests new in-house technologies, such as a CubeSat sized plasma thruster, star tracker software, and a deep space radio to continually expand bus capabilities. The lab also assembles and integrates CubeSats into their deployers in the on-campus cleanroom and has testing facilities for thermal, vacuum, and launch environments, as well as ground stations to perform amateur radio ultra-high frequency (UHF) operations from the university campus. Specific subsystem capabilities and planned development will be detailed at the end of each chapter relevant to that subsystem.

#### **2.2 CubeSats and CubeSat Specifications**

The CubeSat Standard is a design specification providing design boundaries in volume, mass, and content restrictions CubeSat developers shall comply with to ensure safe integration with any

launch vehicle. Units, or “U,” of 10 x 10 x 10 cm cubes of up to 2 kg can be combined in various configurations, with common ones being 3U (10 cm x 10 cm x 30 cm), and in MarCO’s case, 6U (~20 cm x 10 cm x 30 cm). As the need for more capable small satellites grows, configurations to 16U (20 cm x 20 cm x 40 cm) have been proposed; as of 2020, 65 12U CubeSat and 33 16U CubeSats have been developed [6]. The CDS provides specifications for up to 12U CubeSats to ensure compatibility with most deployers though the dimensions, masses, and extra volume allowed outside of the rails and in “tuna cans” of configurations greater than 12U which vary by the company providing the deployer; as an example, EXOLaunch provides payload specifications for CubeSats up to 16U for their 12U/16U EXOpod deployer [26]. An example of a 12U CDS-compliant CubeSat using “tuna can” volume is shown in Figure 2-1; EXOpod allows for similar use of volume for 16U CubeSats but expands the limitations of the CDS, allowing features to extend an additional 4.7 mm beyond the rails [26]. The purpose of these specifications is to create a standard that if adhered to on a wide-level, will allow compatibility with cost-effective mass produced parts, satellite deployers, and launch vehicles in order to “reduce cost and development time, increase accessibility to space, and sustain frequent launches” [27]. While deviations from CDS and deployer specifications are possible, they are not ideal and must be reviewed thoroughly, going through a waiver process [7, 8, 27].

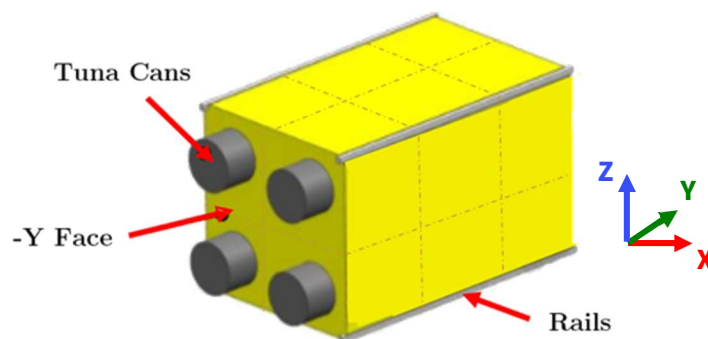


**Figure 2-1: Illustration of 12U CubeSat adapted from CDS with optional “tuna can” volume. Note: axes do not correspond to CDS [7].**

In addition to volume and mass constraints there are other requirements to be taken into account with CubeSat specifications that limit the design space including [27]:

- Recommended limit on battery capacity at 100 Wh per battery
- Pyrotechnics and propulsion systems designed in accordance with the Air Force Space Command Range Safety Manual 90-710, Vol. 3 (AFSPCMAN 91-710, Vol. 3)
- Offset of the center of gravity from the geometric center on each major axis up to  $\pm 4.5$  cm in the X and Z axes and  $\pm 7$  cm in the Y axis for 12U, corresponding to Figure 2-1

### **2.3 Environment Beyond Earth Orbit and Other Challenges**

The space environment and varying distance from the Sun are the drivers for difference in design of an interplanetary CubeSat compared to one near Earth. Factors such as radiation, power generation and storage, thermal effects, communications, and propulsion capabilities must be considered for a successful interplanetary mission. The only interplanetary satellites to date are the MarCO satellites which were launched in May 2018 and arrived at Mars in November 2018. The MarCO mission was developed to have two twin 6U CubeSats accompany the InSight Mars lander and perform a flyby of Mars while relaying real-time communications back to Earth during entry, descent, and landing. It was also used as a technology demonstration to show that a CubeSat could communicate with the Deep Space Network (DSN) using the Iris Radio deep space transponder, navigate independently from Earth to Mars, and flight test multiple COTS parts [28]. Other firsts are being the first CubeSats to take photos of Earth from deep space, photograph Mars up close, and make the first trajectory correction maneuvers performed by CubeSats [14]. Their success demonstrated the survivability of CubeSats in interplanetary space and near Mars, providing a reference for proven design and performance of such CubeSats which can be compared to the

mission concept developed in this thesis. For each of the following challenges detailed, the flight-proven solution from MarCO is provided as reference.

### **2.3.1 Power**

A design driver for CubeSats at Mars is power generation due to the small satellite surface area and volume available and greater distance from the Sun. As mentioned in Chapter 1, at 1.5 AU from the Sun, power generation is  $\sim 608 \text{ W/m}^2$  at Mars. Compounding on this power constraint is the increased need for telecommunications and thermal systems that require more heater power than at Earth due to the increased distance from the Earth and Sun. Identified solutions for equalizing power input and power consumption are deployable solar arrays which are found in every interplanetary CubeSat design, greater energy storage capacity in batteries, and low-power modes and duty cycling [29]. A promising technology in development is thin flexible solar arrays which could offer high stowed power density and mass savings compared to standard arrays [30].

The MarCO CubeSats had rigid deployable solar arrays that each stowed to the size of a 3U side panel and unfurled to be  $1800 \text{ cm}^2$ . At Earth, they provided 35 W of power, resulting in 17 W available at Mars. A 3 series-4 parallel battery configuration of COTS 18650B Lithium-ion batteries for a total energy capacity of 126 Wh was used in conjunction with a 12V battery bus [31, 32].

### **2.3.2 Communications**

The increased distance between a Mars CubeSat and Earth also causes telecommunications design constraints if using a direct-to-Earth architecture. Compared to LEO, the communications subsystem must overcome larger space path losses; for X-band at 500 km, losses are  $\sim 144 \text{ dB}$  compared to  $\sim 247 \text{ dB}$  at 0.5 AU from Earth, the closest Mars approaches. SWaP and thermal constraints limit transmit power for 6U CubeSats to  $\sim 5 \text{ W}$  and gain to  $\sim 30 \text{ dB}$  if utilizing an X-band transponder [33]. On the ground station side, high power ground stations are required to catch

the faint and distant signal; so far only the Deep Space Network has been utilized. Ways to deal with these limitations include onboard data compression, high power S, X, and Ka-band transponders, deployable antennas and reflectarrays, and disruption tolerant networking. Deployable “whip” antennas are common in Earth orbit but reflectarrays are new for the CubeSat community [29]. Alternatively, relay architectures utilizing the Electra UHF relay payload onboard larger Mars orbiting missions such as MRO have been proposed [34].

Trades were performed on the high-gain antenna for MarCO and included patch arrays, mesh reflectors, and reflectarrays. Patch arrays were discarded due to insufficient area for the required gain and mesh reflectors were discarded due to large stowage requirements, deploying complexity, and poor pointing capability, leaving the reflectarray [33]. MarCO successfully employed a custom designed deployable reflectarray with 29 dB of gain for high-speed downlink to Earth at Mars [33]. Near Earth, a low-gain patch antenna was used and for safe-mode communications far from Earth a medium gain patch array was used; to communicate with the InSight lander, a custom deployable UHF antenna with 2.5 dB gain at  $\pm 30^\circ$  and 5 dB peak gain was used [35]. The communications subsystem consists of an Iris V2 radio with an UHF receiver, providing 4 W radio frequency (RF) output in X-Band and is compatible with the Deep Space Network (DSN). At 1.05 AU, the high gain antenna and radio can maintain an 8 kbps link. It should be noted that this design might be excessive for a different mission, as the MarCO satellites were acting as real-time, direct-to-earth communications relays for the InSight lander, requiring high-speed, high-volume data transmissions [31].

### **2.3.3 Propulsion**

Nanosatellites generally do not get to choose their launcher or injection orbit and flown CubeSat propulsion systems do not offer significant maneuvering capability, limited by mass, volume, and power constraints. The CDS, in compliance AFSPCMAN 91-710, Vol. 3, provides several restrictions on propulsion systems, both directly and indirectly. According to AFSPCMAN90-710,

Vol. 3 there are no pyrotechnics permitted without a waiver, discarding solid chemical propulsion, which even if waived provides thrust levels that would quickly tumble a CubeSat and require a robust attitude determination and control subsystem (ADCS) [36]. The AFSPCMAN 91-710, Vol. 3 also defines any systems with operating pressures greater than 100 psig as hazardous hardware. The requirement can be waived, but requires additional testing, inspection, and certification to obtain Range Safety acceptance which is costly. As of 2017, no waivers for range safety had been permitted for secondary payload CubeSats and as a consequence of restrictions on chemical propulsion systems, flight tested and/or proven CubeSat propulsion technologies only included cold gas thrusters, electrospray thrusters, and vacuum arc thrusters [36]. Other methods such as solar sails have been proposed as a propulsion solution for interplanetary CubeSats [37].

Considering these restrictions, a promising propulsion candidate for interplanetary orbits is electric propulsion as it can deliver a high specific impulse with lower thrust than chemical propulsion systems, reducing propellant mass at the cost of time and power. Capable of delta-Vs up to 1-3 km/s, these systems also have the potential to eventually break rideshare dependence on interplanetary primary missions which are rare, instead entering low-thrust Earth-escape trajectories from rideshares on commercial geostationary orbit launches; for Mars missions, there are only six planned major launches from JPL's Perseverance Rover in Summer 2020 to the JAXA's MMX in 2024 [38]. As of 2017, only ten CubeSats have had propulsion systems and six of them were cold gas, limiting the availability of electric propulsion flight data [36]. There have also been discussions of individual dedicated launches and large groups of CubeSats contracting a common vehicle though this capability has not been developed for orbits beyond LEO [36].

Power generation limitations must be considered due to the power intensive nature of electric propulsion, which converts onboard electricity into thrust. Power consumption for electric propulsion systems range from 1 W to 10 W for  $\mu\text{N}$ -level thrust to  $>50$  W for thrust on the order of mN [36]. There are three main types of electric propulsion: electrothermal, electromagnetic, and electrostatic [36]. Electrothermal methods heat gas and accelerate it out of a nozzle such as in

resistojets and RF heating thrusters; this method is promising because it can use inert, storable propellants and provide a higher specific impulse (Isp) than cold gas thrusters. However, as of 2017, only one electrothermal thruster has flown which was the NanoSpace CubeSat MEMS propulsion module on CubeSat TW-1 in 2015. An electrothermal plasma microthruster was developed at Australia National University and has been undergoing research testing at California Polytechnic State University to develop a CubeSat sized propulsion module; this system uses RF to ionize Argon, Helium, or Xenon, which then expands into vacuum [39]. Electromagnetic thrusters use electric and magnetic fields to accelerate a plasma; examples include pulsed plasma thrusters and vacuum arc thrusters. Pulsed plasma thrusters were the go-to propulsion system for early CubeSats due to their use of solid propellant, flexible power constraints, and modularity but only have an efficiency of ~10%. Vacuum arc thrusters (VAT) work by producing vacuum arcs that can be used as high-velocity plasma jets or as a plasma to be electrostatically accelerated; a VAT was tested on the US Naval Academy's BRICSat-P CubeSat, successfully detumbling the spacecraft. Electrostatic methods ionize a propellant then accelerate it electrostatically such as in Hall thrusters, RF ion engines, and electrospray thrusters. Ion engines use an electric field to create plasma and biased grids to accelerate ions to create thrust. RF ion engine systems require conversion of DC solar array power to RF power and a secondary cathode to neutralize the plasma plume but can utilize high density propellants such as iodine; such a system, the Busek BIT-3, is set to fly on two Artemis-1 CubeSats [36]. Electrospray thrusters eject ions by using a strong electric field at the tip of an emitter with an ionic propellant with a surface tension. This type of system has been proven on the European Space Agency's LISA Pathfinder mission and tabletop development has been investigated at California Polytechnic State University [36, 40].

As electric propulsion comes with increased flight time due to low thrust and long-duration high power consumption, some high delta-V mission architectures may favor higher thrust chemical propulsion systems. As mentioned previously, solid propellants are not heavily considered due to the restrictions on pyrotechnics and bipropellants are complex and massive,



requiring two separate propellant storage and feed systems. For monopropellant systems, alternatives to hydrazine, hydroxylammonium nitrate (HAN)-based and ammonium dinitramide (AND)-based propellants, have increased in popularity due to their lower toxicity and higher specific impulse; these are referred to as “green monopropellants.” Out of these, HAN-based AF-M315E has a higher increase in density specific impulse and flight heritage on the 2019 Green Propulsion Infusion Mission (GPIM) [36].

MarCO was directly injected into a Mars-bound orbit, performing correction maneuvers and reaction wheel desaturation using a VACCO cold-gas, R-236FA propellant and eight thrusters to perform its flyby. The propulsion subsystem occupied approximately a 2U volume [31].

#### **2.3.4 Thermal**

Another challenge caused by the increased distance from the Sun is colder thermal environments due to less incident solar irradiance at Mars. The decreased temperature can be illustrated through the concept of a perfect blackbody “reference sphere” with an absorptance and emittance of 1.0; in equilibrium, the reference sphere would be  $-47\text{ }^{\circ}\text{C}$  at Mars compared to  $6\text{ }^{\circ}\text{C}$  at Earth [23]. Decreased absorbed heat can cause greater temperature differences between “hot” in-Sun or high-power modes and “cold” eclipse or low-power modes. The thermal protection system must design for both cases, balancing passive control methods with active control. For CubeSats utilizing the potential propulsion or communications solutions discussed in this chapter, “hot cases” would arise from heat dissipated from high-power electric propulsion systems and radios. Mitigation techniques include modelling and testing to determine the appropriate area allocations for radiators and multi-layer insulation (MLI) as well as using heaters [29].

For reference, the thermal design solution for MarCO included two radiators, multi-layer insulation, and temperature sensors. These worked in conjunction with appropriately timed power usage and heaters. For the most temperature restrictive component, the batteries, a dedicated

radiator was used to isolate them from the temperature swings experienced by the rest of the spacecraft [31].

### **2.3.5 Radiation**

Satellites in LEO benefit from the protection of the Earth's magnetic field that deflects charged particles. In interplanetary space and at Mars, radiation exposure is increased. Radiation can penetrate critical electronics, causing transient or permanent errors depending on the type of radiation to critical devices such as flight computers, field programmable gate arrays (FPGAs), and memory storage devices. There are three primary types of damage to electronics: displacement damage, total ionizing dose, and single-event effects. Displacement damage removes atomic nuclei of materials from the lattice position having effects such as decreased semiconductor performance and lifetime, which can degrade efficiency of solar cells. Total ionizing dose (TID) is cumulative ionizing radiation, which can cause electron-hole pairs in semiconductors and insulators resulting in runaway current, increasing power consumption, reducing gain, and changing device time constants and threshold voltages. Single-event effects are caused by small, isolated energetic particle encounters. They can cause soft errors in code resulting in bit flips that can be corrected with error detection and control algorithms. On the more extreme end, it can cause permanent bit flips and corrupt memory, as well as latchups and burnout that cause excessive power draw resulting in overheating. Damages increase with the larger energetic particle fluxes that accompany increased solar activity, called Solar Particle Events (SPE), and longer exposures to chronic low-dose Galactic Cosmic Rays (GCR) [41]. These effects need to be mitigated for a Martian moon mission.

Mitigation techniques are employed through both hardware and software. Hardware protections are shielding, radiation hardening, and redundancy. Shielding of sensitive components may be accomplished through adding layers of metal such as aluminum or positioning them within the spacecraft to be shielded by other existing components. Radiation hardening is done by

electronics manufacturers and having more than one of the same component can provide physical redundancy in case of failure of one. Error detection and correction (EDAC) algorithms can maintain the accuracy of stored data, watchdog timers can force reboots if they indicate anomalous behavior, and redundant systems are used to check against each other [41].

Mitigating radiation for CubeSats is difficult due to the volume restrictions that limit the amount of shielding as more volume for shielding is less volume available for other components. Additionally, radiation hardened parts are specialized components, not mass produced COTS parts, making them expensive. Literature suggests that 2 to 3 krad is considered tolerable by COTS, while a dose above 20 to 30 krad is dangerous to all but rad-hardened components [37]. In-situ measurements of the radiation environment at Mars has been gathered by the Fine Resolution Epithermal Neutron Detector (FREND) onboard the Trace Gas Orbiter (TGO). FREND characterized the radiation environment around Mars in a highly elliptic 250 x 101,000 km orbit, measuring an average dose rate in silicon of 40.4 mrad/day with no SPE events observed during the ~130 day data collection period [42]. While the relatively constant GCR flux has been quantified, SPE are randomly distributed events, though more prevalent during high solar activity. Therefore, exposure is dependent on a mission's timeline in relation to the solar cycle and must be analyzed on a mission-by-mission basis using radiation modelling. Exposure for specific time periods can be predicted using industry-standard space radiation models such as those implemented in the open-source SPace ENVironment Information System (SPENVIS) program from ESA [43]; this method was used for the analysis in Chapter 11. No literature on MarCO's radiation mitigation method was found.

## **2.4 Phobos-Deimos Cycler Orbit**

The mission objectives introduced in Chapter 1 to address Martian moon SKGs call for maneuvering into a Phobos/Deimos cycler orbit. Cyclor orbits have been investigated as candidate for encountering both of Mars' moons regularly, up to once every 23 hours for Phobos and once

every 30 hours for Deimos, providing many opportunities for science and surface coverage of both moons with minimal resources over a long period of time [44]. This contrasts with studies of Quasi-Satellite Orbits (QSOs), fixed-point station keeping, and Lagrange-point orbits which focused primarily on visiting either Phobos or Deimos. As advanced orbit design and optimization are outside the scope of this thesis and to maximize potential to address SKGs at both moons, a cycler orbit defined in [44] was an assumed top-level mission objective.

In the study, cycler orbits that would be able to be reached by small satellites ridesharing on a primary Mars mission from the insertion orbit of that primary mission were targeted to encounter different sides of Phobos and Deimos at an altitude of 50 to 150 km. The orbits of Phobos and Deimos are nearly circular with inclinations of  $\sim 1^\circ$ , with Phobos having an orbital radius of  $\sim 9376$  km and Deimos having an orbital radius of  $\sim 23463$  km. The parameters of the Phobos cycler orbit used for this mission concept are provided in Table 2-1; a similar Deimos cycler orbit is provided to show that transition between them is feasible if desired. The resonance indicates the number of orbits the moon makes and the number of orbits the spacecraft makes before an encounter; for example, 12:5 Phobos resonance means that Phobos will make 12 orbits around Mars while the spacecraft will make 5 orbit before they meet again. The argument of periapsis is given as  $\omega$  and the right ascension of ascending node as  $\Omega$ , both in degrees; these are the only elements that change substantially over time due to gravitational perturbations. The delta-V required each week to maintain the orbit given the dominant gravitational perturbation from Mars is given as  $\Delta V1$  in m/s and the delta-V to reach the cycler orbit from the initial circular,  $0^\circ$  inclination, 300 km altitude Mars orbit is given as  $\Delta V2$  in km/s. The cycler orbit geometry used for this mission concept, corresponding to the 12:5 Phobos orbit in Table 2-1 can be visualized in relation to Mars and the orbits of Phobos and Deimos in Figure 2-2.

**Table 2-1: Orbital parameters of Phobos/Deimos cycler orbits [44].**

Resonance Body	Phobos	Deimos
Resonance	12:5	3:5
Semi-major axis (km)	16802.9	16691.7
Period (days)	0.7654	0.7576
Eccentricity	0.4497	0.4461
Radius of Apoapsis (km)	24359.7	24137.3
$\omega$ ( $^\circ$ )	163.03	164.52
$\Delta\Omega$ ( $^\circ$ /day)	-0.0887	-0.0902
$\Delta\omega$ ( $^\circ$ /day)	0.1773	0.1804
$\Delta V1$ (m/s)	0.4760	0.4768
$\Delta V2$ (km/s)	1.3890	1.3936

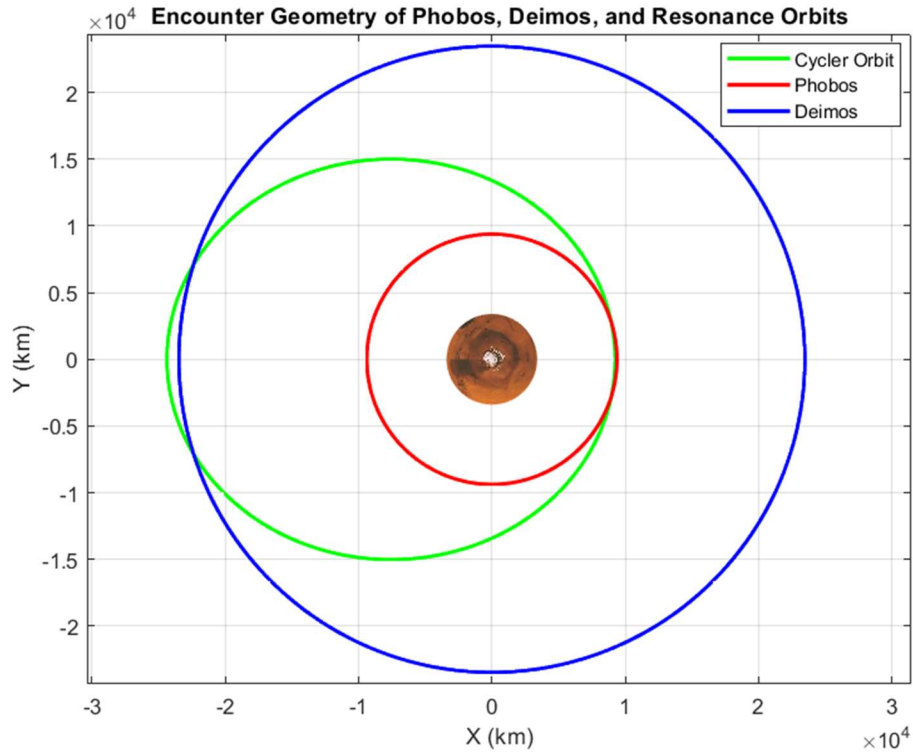


**Figure 2-2: Encounter geometry of Phobos, Deimos, and resonance orbits.**

## **Chapter 3**

### **MISSION OBJECTIVES**

To begin working towards a baseline design, mission objectives and constraints first need to be defined. As this mission concept is theoretical, the mission objectives were inspired by the research into NASA's SKGs, Phobos-Deimos cypher orbits, and the NASA Deep Space Derby for small satellite communications presented in Chapter 1 and Chapter 2. The synthesis of these provide high level objectives concerning mission location, duration, and telecommunications. Additional performance objectives were applied to further narrow the design space. These objectives and their derivation are explained in this chapter.

#### **3.1 Defining the Mission Objectives**

NASA's SKGs were reviewed to determine what mission types are in need leading to the selection of missions that could be done from Mars orbit. Phobos and Deimos remote science objectives were chosen as few missions have explored these moons yet despite asteroids and Mars' moons being identified as the next location of human spaceflight missions on the greater roadmap to human exploration of Mars. This results in the first mission constraint: perform science investigations of Mars' moons. Referring to Table 1-1, the SKG for surface operations involving radiation environment characterization has a time duration of 1 Martian year, equivalent to 1.88 Earth years, in order to obtain a complete set of data. This duration results in the second mission constraint: perform science collection for 1 Martian year.

Though dedicated interplanetary launches for CubeSats may someday be an option and Earth-escape with CubeSat propulsion is theorized, the only current viable route is ridesharing as a secondary payload on a primary mission considering cost and volume required for radiation

shielding of low-thrust Earth-escape travelling through the Van Allen belts [37]. As mentioned in Chapter 2, MarCO was directly injected into a Mars-bound trajectory while the Artemis-1 CubeSats will be deployed in cis-lunar space. As there are multiple primary missions to Mars in the coming years, the assumption was made that the CubeSat would rideshare to Mars and deploy from a primary spacecraft once that mission reached a stable orbit [38]. Combined with the selected Phobos cyclor orbit described in Table 2-1 these assumptions form the third mission constraint: rideshare to Mars and transfer from the insertion orbit to the cyclor orbit.

To constrain the mission further, communications link and command and data handling (C&DH) subsystem performances were chosen. Expected capabilities of deep space small satellite communications subsystems competing in technology development challenges, such as that of CU-E3, have data rates as low as 13 bps at 0.2 AU from Earth [45]. As this is considered competitive for student developed CubeSat technology demonstration and is scaled to the assumed payload data volume, a slightly greater performance of 100 bps was set as the minimum allowable data rate throughout the mission and therefore at Earth-Mars distances up to  $\sim 2.5$  AU. Two more performance objectives were assumed involving science data storage and transmission. First, to ensure science data is not lost, the C&DH subsystem must be able to store four weeks of data onboard in case of limited downlink opportunities or mission anomalies preventing downlink. The second is to downlink a week's worth of data within three downlink opportunities; this is to set a performance parameter such that time utilizing costly deep space link capable ground stations, such as the DSN, is capped. No constraints were provided for cost as the goal was to identify the best enabling technologies regardless of cost as it could likely be reduced with in-house development depending on the component.

Finally, the mission concept design must adhere to a CubeSat specification. Though seemingly obvious, this objective is included because the required specification is not necessarily the CDS as it does not define dimensions and mass properties for CubeSats larger than 12U. For 16U CubeSats,

the allowable dimensions and mass properties for an EXOpod payload were used [26]. A summary of the mission objectives is listed in Table 3-1.

**Table 3-1: Summary of mission objectives.**

<b>Mission Objectives</b>	
1	Perform science investigations of Mars' moons.
2	Perform science collection for 1 Martian year.
3	Rideshare to Mars and transfer from the insertion orbit (circular, 300 km altitude, 0° inclination), to the cycler orbit (defined in [44])
4	Maintain a minimum data rate of 100 bps throughout the mission.
5	Downlink 1 week of data within 3 downlink opportunities.
6	Have the ability to store 4 weeks of data onboard.
7	Adhere to a CubeSat specification.

### **3.2 Stand-in Payloads**

As this mission concept is developed as a technology demonstration of a bus that could address the Phobos/Deimos SKGs, a stand-in payload was selected based on the potential instruments suggested in the SKGs. The payload is referred to as “stand-in” as this mission is not focused on its performance, rather it is used to provide concrete mass, volume, power, and data allocations for an instrument that could address an SKG, however minimally. Corresponding to the Surface Operations SKG regarding radiation environment that provided the mission objective of collecting data for 1 Martian year, a radiation detector, the piDOSE Digital CubeSat Dosimeter from SkyFox Labs, was selected. The dosimeter provides dose-rate per hour for background radiation and local gamma ray environments. Though suggested as a potential instrument in the radiation SKG, a Langmuir probe was not considered due to the involved payload design that would be required for



probe boom deployment needed to avoid contamination from the plasma sheath around the CubeSat and need to hold the electric potential of the CubeSat constant for measurement [46]. It is also of interest to a university mission to include an imager for outreach purposes. Therefore, a COTS imager, the 2 Megapixel CMOS OV2640 Camera Module from OmniVision, selected for its low SWaP, was included as well. With a field of view of 194° x 142° and resolution of 1632 x 1232 pixels, the camera, at the expected cycloidal orbit distances of 50 km to 150 km would be able to achieve Phobos ground resolution of 0.24 m/pixel to 0.71 m/pixel; if used in the initial insertion orbit, Mars could be imaged at up to 1.41 m/pixel [47]. For the selected orbit, the spacecraft will encounter Phobos twice a week. The baselined science return is considered one maximum resolution color photo per encounter, or two photos per week, along with dosimeter data for a total of 13.2 MB of data collected per week. Relevant physical and data parameters of these components are provided in Table 3-2 and are shown in Figure 3-1.

**Table 3-2: Payload mass, volume, power, and data allocations.**

	<b>Skyfox Labs piDOSE Digital CubeSat Dosimeter [48]</b>	<b>2 MP CMOS OV2640 Camera Module [47]</b>
Mass (g)	30	50
Volume (U)	0.02	0.02
Average Power (mW)	70	125
Data per Week (MB)	1.2	12 (2 max. resolution color photos)

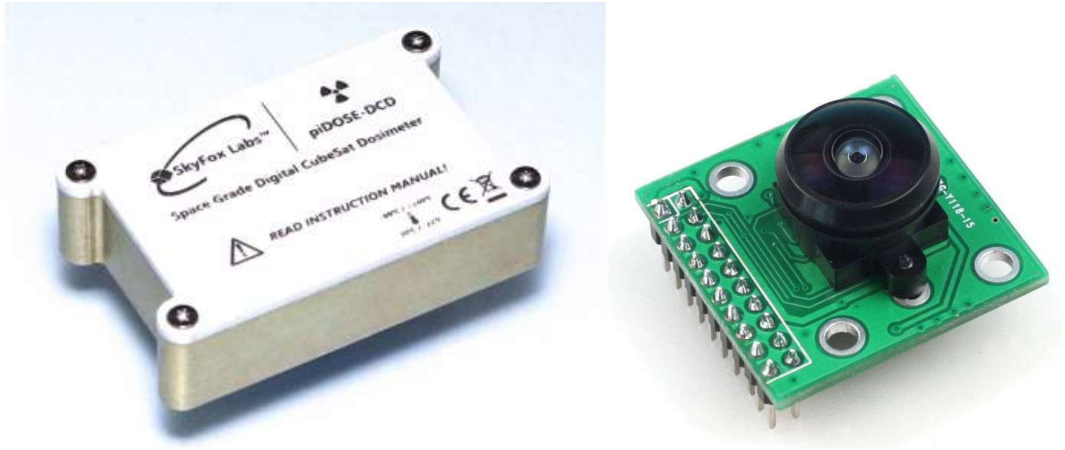


**Figure 3-1: Stand-in payload with dosimeter (left) and camera (right); not to scale [47, 48].**

These payloads are also relevant to CPCL experience and planned development. The CP-8 IPEX mission utilized a similar camera, an OV3642 3MP with on-camera image compression, providing some experience in reducing data size to maximize data return which will be addressed in Chapter 6 [49]. CPCL creates the printed circuit boards (PCBs) to interface the payload with the onboard computer and has planned implementation of an in-house developed radiation event counter and dosimeter for ionizing radiation, which could be used in place of the selected commercial dosimeter.

### **3.3 Developing the Mission Concept**

Common mission elements that can and cannot be traded based on the assumptions provided to this point were identified (Table 3-3) to investigate alternative mission architectures and work towards general concept of operations. Options were characterized through analysis and mass, power, link, and pointing budgets while considering the SWaP system drivers for CubeSats.

**Table 3-3: Mission elements and their assumed tradability.**

<b>Mission Element</b>	<b>Can be Traded?</b>	<b>Reason and/or Options</b>
Payload	No	Assumed
Orbit	No/Yes	Initial and final orbits assumed; transfer can be traded
Communications Architecture	Yes	Direct to Earth vs. Relay
Launch System	No	Assumed rideshare
Spacecraft Bus		
<i>Propulsion</i>	Yes	Low-thrust, high thrust, combined electric and chemical propulsion systems
<i>Power</i>	Yes	Body-mounted vs. solar arrays, array configurations, energy storage, power modes
<i>ADCS</i>	Yes	Passive vs. 3-axis stabilization, sensors, actuators

For the level of detail needed to get to a baseline design, focus was put on *system-level* trades and requirements, these will be the focus of the remainder of this work. From the mission constraints, design drivers were identified to begin the design process. As the delta-V required to reach the cycler orbit, at least 1.4 km/s (see Table 2-1), is high for a CubeSat, this was the first trade to occur. Following propulsion system selection, communications and ADCS subsystem designs were traded. Using the resulting power requirements for these systems, the power subsystem was designed and using that, a preliminary configuration was chosen in order to perform a thermal analysis. Throughout this process, volume, mass, and TRL were considered. It should be noted that there are many potential outcomes, but the focus of this thesis is not to design an optimized spacecraft, but rather a capable one to serve as a comparison for CPCL bus capability.

## Chapter 4

### SYSTEM OVERVIEW AND CONCEPT OF OPERATIONS

The baseline presented in this thesis was the result of multiple iterations of subsystem design which could be further iterated. The presented design is meant to be a baseline that can be improved upon, serving as a starting point for considerations that need to be included when designing an interplanetary bus. For the following mission analyses and resulting design solutions to have more context, the baselined concept of operations and bus design are overviewed in this chapter. Design decisions are discussed in detail in the following chapters corresponding to each subsystem with this chapter serving as a preview.

#### 4.1 Spacecraft Overview

The baseline stowed configuration, shown in Figure 4-1, is designed to fit within the 16U envelope specified by the EXOpod User Guide, the details of which are discussed in Chapter 10. The outer rail dimensions are ~20 cm x 20 cm x 45 cm, with additional volume utilized for solar panel and antenna stowage as allowed by EXOpod's specification.

After release from the EXOpod, the spacecraft will deploy its solar panel array and antenna; details on the communications subsystem design decisions are covered in Chapter 6 and the power subsystem in Chapter 7. The solar arrays rotate about the X-axis via a solar array drive assembly (SADA) and are Sun-pointing, with the +Z face remaining pointed at Mars. A +Y view of the spacecraft is shown in Figure 4-2.

Inside, there are 3 main "compartments," the top and bottom ones in a 4U volume and the middle one in an 8U volume. As seen in Figure 4-3, the +Y compartment has the batteries and power distribution unit (PDU), leaving 3U open for an additional payload, the middle hosts the

MPS-135 chemical thruster system, payload, and onboard computer (OBC), and the -Y compartment holds the BIT-3 electric propulsion system, reaction wheels, and star tracker. A sun sensor is located on each face. Propulsion subsystem design is detailed in Chapter 5, ADCS in Chapter 8, and C&DH in Chapter 9.

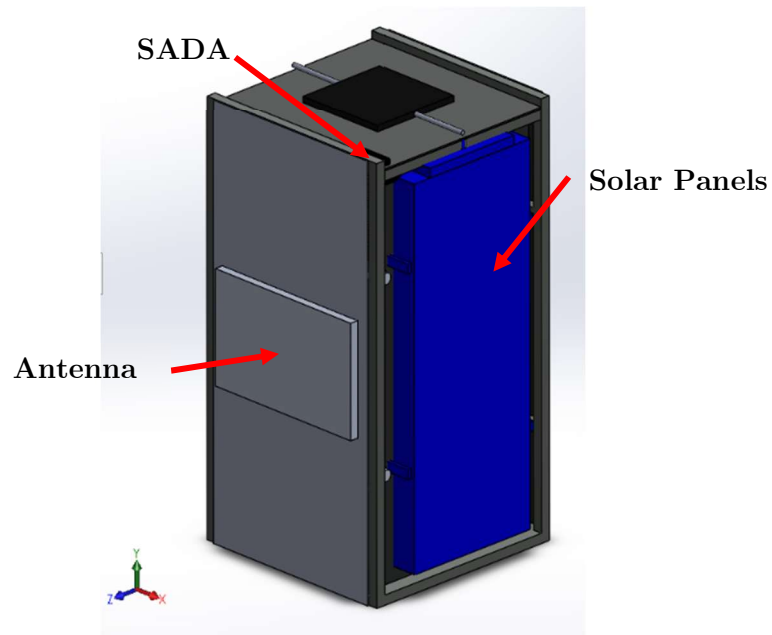


**Figure 4-1: Stowed configuration overview.**

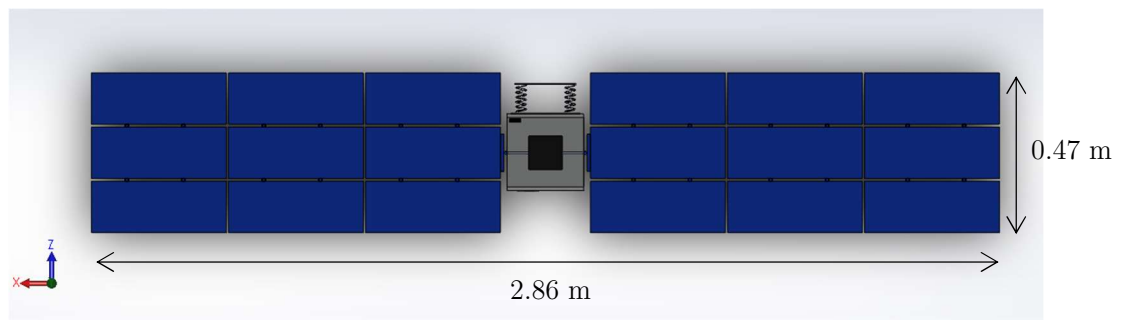


**Figure 4-2: +Y view of spacecraft depicting deployables.**

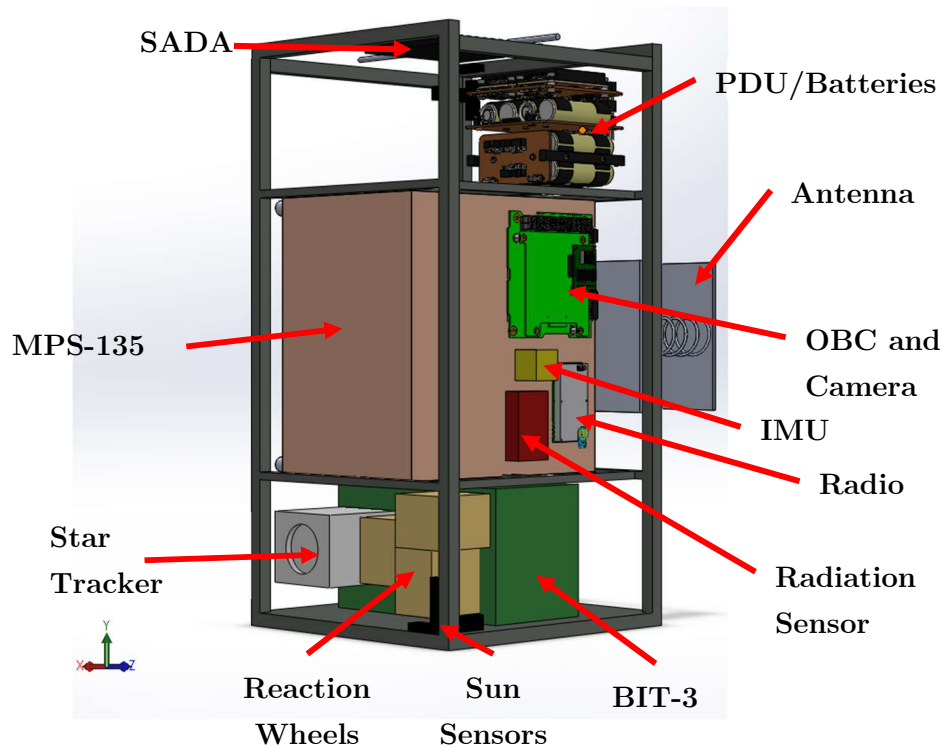


**Figure 4-3: Internal configuration.**

## 4.2 Concept of Operations

There are four identified phases of this mission: rideshare to Mars, a low-thrust transfer, an impulsive transfer, and the cyclor orbit in which science will be performed. These are depicted in Figure 4-4. The rideshare to Mars is assumed to enter a 300 km,  $0^\circ$  inclination circular orbit around Mars, where once stable, the CubeSat will be deployed from a CubeSat deployer into the same orbit; this is considered the start of the mission. For celestial geometry calculations the start date is assumed to be June 11, 2025, aligning with the arrival time of the next optimal Earth-to-Mars trajectory launch window of September 2024; this corresponds with MMX's planned early September 2024 launch and August 2025 arrival [50]. After deployment from the EXOpod, the spacecraft will deploy its solar arrays and UHF antenna. Some time for signal acquisition and power generation will occur here, followed by a checkout period.

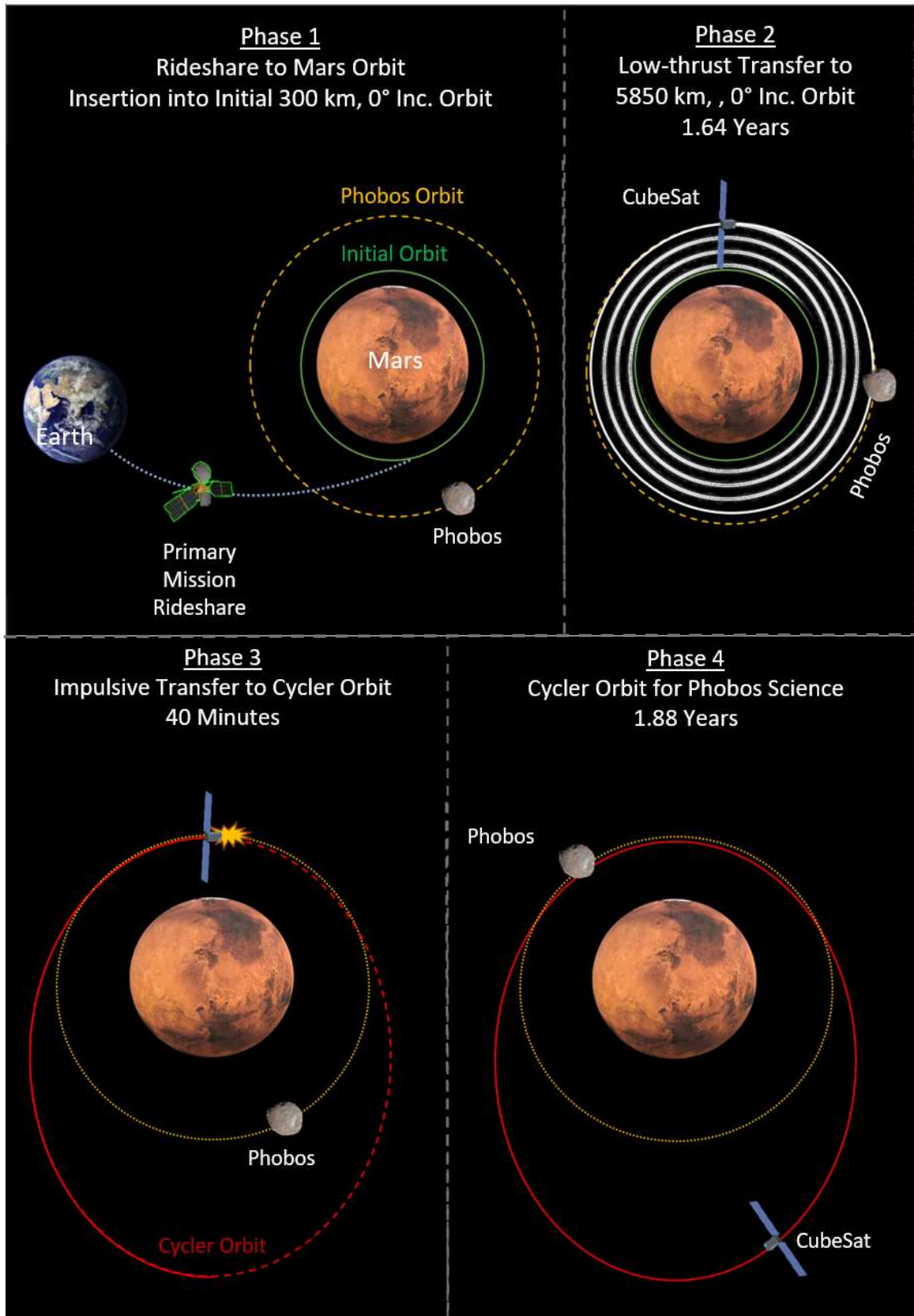


Figure 4-4: Mission concept of operations.

Once in the 300 km, 0° inclination, circular orbit, the CubeSat will begin a 1.64 year long low-thrust phase enabled by an electric propulsion system to raise the orbit to an altitude in the vicinity of the orbit of Phobos at an orbital radius of 9246 km. The high-power BIT-3 ion engine only fires when the spacecraft is in the Sun for a total of 530 days of thrust and 67 days of cruise. In this phase, there is no science performed.

At the end of the low-thrust phase, the CubeSat will perform a high delta-V impulsive maneuver to enter the final cyclor orbit. The propulsion subsystem utilizes a green monopropellant propulsion module. The spacecraft will reorient during this phase to align the thrusters and center of mass to the desired thrust vector; the solar panels will rotate the cells away from the bus to prevent impingement for the burn duration.

The final phase is the nominal science orbit which has a resonance with Phobos, providing encounters every 92 hours, and with slight orbital adjustment, has the potential to encounter Deimos every 91 hours. For this thesis, the orbit resonates with Phobos with one encounter every five CubeSat orbits, each with an orbital period of 18.4 hours. The orbit is 0° inclination with its periapsis at 9246 km and an eccentricity of 0.4497; other parameters are listed in Table 2-1. The spacecraft conducts science in this orbit for 1.88 years for a total of 179 planned encounters with Phobos that will allow imaging using a COTS 2 MP camera with a baselined return of one maximum resolution color photo per encounter, equivalent to two photos per week. Radiation data will continuously be collected in the cyclor orbit using a dosimeter, providing number of counts per 10 seconds. Orbital correction maneuvers are performed once a week with the BIT-3 thruster. The BIT-3 is also used to desaturate the reaction wheels. Each orbit, the spacecraft will have the opportunity to maintain a data rate link of 1.8 kbps - 3.2 kbps with the Electra UHF Proximity Link Payload onboard MRO for roughly 3.5 hours. Data downlink of the weekly 13.2 MB package of science data will occur for ~11 hours every week. The mission concludes December 12, 2028.



The orbital trajectory for the full 3.5 year mission was modeled in AGI's System ToolKit (STK) Version 11 and is shown in Figure 4-5; explanation of this modelling is located in Chapter 6. Throughout the mission, the spacecraft will keep the antenna inertially pointed at Mars and the solar arrays will track the Sun.

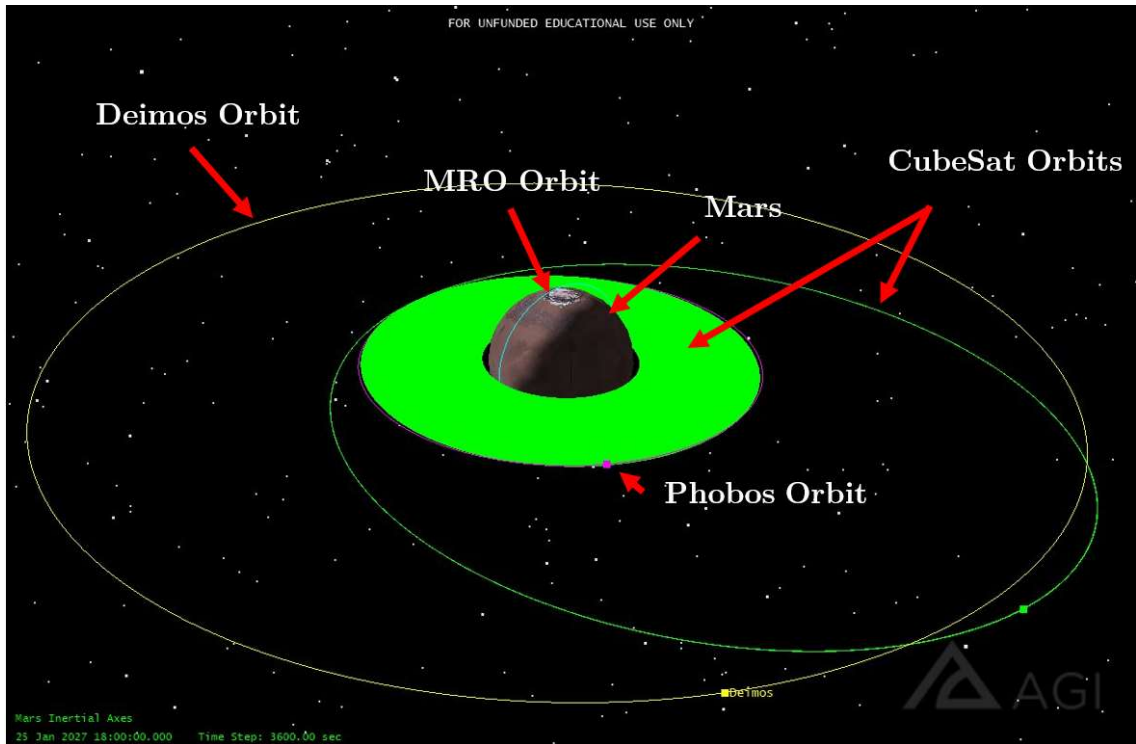


**Figure 4-5: Entire mission trajectory.**

## Chapter 5

### PROPULSION SUBSYSTEM

Though a delta-V requirement was provided along with the cycler orbit in Chapter 2, this assumed an impulsive maneuver which would require high thrust and mass systems that are not compatible with a CubeSat form factor. Trajectories were considered for different combinations of low-thrust and impulsive transfers to compare their resulting delta-V needs and select a trajectory option. This option was then used to trade chemical and electric propulsion systems. The selected subsystem solution used to continue the baseline is summarized and compared to CPCL's current and planned propulsion capabilities.

#### 5.1 Orbit Analysis

The delta-V required to transfer from the initial orbit to the cycler orbit was verified by adapting analysis tools developed in [51, 52, 53] for optimal impulsive orbital transfer, low-thrust transfer between circular orbits, and low-thrust spiral trajectories with constant periapsis to use Martian astronomical and gravitational values from [54]. It was found that the delta-V value from Table 2-1 corresponds to an impulsive maneuver. As electric propulsion is a promising system for high delta-V capable CubeSats due to size and mass constraints, delta-Vs for non-impulsive maneuvers were investigated as well; the delta-V needed for a non-impulsive spiral transfer is greater than an impulsive transfer due to constant thrust and gravitational losses, up to 1.2 times greater for a final orbital radius six times larger than the initial orbital radius [55]. An optimized low-thrust trajectory to transfer from a circular orbit to an eccentric one is outside the scope of this thesis so combinations of circular-to-circular non-impulsive, circular-to-eccentric non-impulsive with constant periapsis,

and impulsive maneuvers were analyzed with the orbit definitions used for the analysis shown in Table 5-1. Right ascension of ascending node was taken to be  $0^\circ$  as all considered orbits are coplanar. Argument of perigee is  $0^\circ$  for the “Initial” and “Phobos Circular” orbits as they have an eccentricity of 0.0; argument of perigee for “Cycler” was assumed to be  $0^\circ$  as it does not affect delta-V when transferring from a circular orbit. The combinations of analyzed maneuvers and resulting delta-Vs required for each are listed in Table 5-1 and Table 5-2.

The total delta-V required for a circular-to-circular non-impulsive, constant thrust trajectory can be approximated as the difference between the velocities of the initial and final orbits under the assumption that the eccentricity of the orbit remains approximately zero [52]. However, this calculation does not hold for a circular-to-eccentric orbit and so the delta-V for a non-impulsive, constant thrust trajectory from the “Phobos Circular” orbit to the “Cycler” orbit was calculated using the burn duration output,  $\Delta t$  in seconds, to back out the total impulse,  $I_{tot}$ , in Ns, to obtain propellant mass,  $m_p$  in kg. The propellant mass was then used to get delta-V assuming values of dry mass,  $m_0$  in kg, thrust,  $T$  in N and assumed as 0.85 mN, and specific impulse,  $I_{sp}$  in seconds assumed to be 2300 s, corresponding to a high-performance electric propulsion system. This process is summarized in Equations (5.1) - (5.3).

The delta-V results were then used in conjunction with state-of-the-art propulsion technologies to determine which trajectory options are feasible. Of the combinations listed in Table 5-2, Option 2 was not considered for this mission as it requires low-thrust trajectory optimization outside the scope of this thesis; without an accurate model of such a trajectory, propellant and power needs cannot be accurately determined. Option 1 requires a chemical propulsion system while Options 3 and 4 require a combination of chemical and electric propulsion systems. The delta-V requirements in relation to available technology performance are discussed in the next section.

$$I_{tot} = T * \Delta t \quad (5.1)$$

$$m_p = \frac{I_{tot}}{Isp * g} \quad (5.2)$$

$$\Delta V = g * Isp * \ln \left( \frac{m_0}{m_0 - m_p} \right) \quad (5.3)$$

**Table 5-1: Definition of transfer orbits considered.**

	<b>Initial</b>	<b>Phobos Circular</b>	<b>Cycler</b>
<b>Eccentricity</b>	0.0000	0.0000	0.4497
<b>Inclination (°)</b>	0	0	0
<b>Semi-major Axis (km)</b>	3696.0	9246.0	16802.9
<b>Ω (°)</b>	0	0	0
<b>ω (°)</b>	0	0	0

**Table 5-2: Transfer trajectory options and delta-Vs.**

#	Type	From	To	dV (m/s)	Total dV (m/s)
1	Impulsive	Initial	Cycler	1385	1385
2	Non-impulsive	Initial	Cycler	Requires low-thrust optimization – approx. as Non-impulsive from MRO to Phobos Circular + Non-impulsive from Phobos Circular to Cycler = 2333 m/s*	2333*
3	Non-impulsive	Initial	Phobos Circular	1252	1691
	Impulsive	Phobos Circular	Cycler	439	
4	Impulsive	Initial	Phobos Circular	1191	2272
	Non-impulsive	Phobos Circular	Cycler	1081	

## 5.2 Propulsion System Survey and Requirements

CubeSat propulsion systems listed in NASA’s 2018 State of the Art Report of Small Spacecraft Technology, were surveyed [56]. As the required delta-Vs for the considered orbits are high for a

CubeSat at greater than 1 km/s, all propulsion system types were considered despite CDS requirements regarding pyrotechnics and range safety. To narrow down the survey and maintain a focus on a near-future mission design, only systems with a TRL of 6 and above were included. These propulsion systems are shown in Table 5-3.

Utilizing a maximum propellant mass fraction of 0.3, in line with the maximum considered for Earth-escape interplanetary CubeSats in [37], the maximum delta-V each system could deliver was calculated using Equation (5.3). As none of the chemical options can provide the  $\sim 1385$  m/s required for a two-impulse maneuver from the initial orbit to the cycler orbit, Option 1 was ruled out, leaving only the combined chemical and electric propulsion options. Of Option 3 and 4, Option 3, the non-impulsive spiral to the periapsis altitude of the cycler orbit followed by an impulsive transfer to the cycler orbit has the lowest required delta-V. Therefore, chemical options capable of providing greater than  $\sim 440$  m/s and electric propulsion options capable of greater than  $\sim 1250$  m/s were traded.

**Table 5-3: Surveyed propulsion systems with TRL 6 or greater.**

Type	Product	Manufacturer	Maximum Thrust (N)	Isp (s)	TRL	Propellant
<b>Chemical</b>						
<i>Hydrazine</i>	MR-103D	Aerojet Rocketdyne	1.02E+00	224	7	Hydrazine
	MR-111C	Aerojet Rocketdyne	5.30E+00	229	7	Hydrazine
	MR-106E	Aerojet Rocketdyne	3.07E+01	235	7	Hydrazine
	1N Ariane	Ariane Group	1.10E+00	23	7	Hydrazine
	20N Ariane	Ariane Group	2.46E+01	230	7	Hydrazine
<i>Non-toxic</i>	1N HPGP	ECAPS	1.00E+00	235	8	LMP-103S
	HYDROS	Tethers Unlimited	6.00E-01	258	8	Water
	MPS-130	Aerojet Rocketdyne	1.25E+00	235	9	AF-M315E
	EPSS C1K	NanoAvionics	1.00E-01	210	9	AND
<i>Cold Gas</i>	MicroThruster	Marotta	2.36E+00	64	9	Nitrogen
	Butane Prop System	SSTL	5.00E-01	80	9	Butane
	Nanoprop GGP3	GOMSpace	1.00E-03	110	9	Butane
	POPSAT-HIP1	Micro Space	1.10E-03	43	9	Argon
	CNAPS	UTIAS/SFL	4.00E-02	40	9	Sulfur hexafluoride
	MarCO	VACCO	5.00E-02	40	9	R236fa
<i>Solid</i>	ISP 30sec Motor	Industrial Solid Propulsion	2.70E+01	187	7	HTPB
	CAPS-3	DSSP	3.00E-01	300	8	HIPEP-501A
<b>Electric</b>						
<i>Warm Gas</i>	PUC	ARFL and VACCO	5.40E-03	70	6	-
<i>Electrospray</i>	S-iEPS	MIT	7.40E-05	1160	6	Non-toxic ionic liquid
<i>Ion Engine</i>	BIT-3	Busek	9.00E-04	2300	6	Xenon-Iodine
	I-COUPS	University of Tokyo	3.00E-04	1000	9	Xenon
<i>PPT/VAT</i>	PPTCUP	Mars Space/Clyde Space	4.00E-05	655	6	PTFE
	u-CAT	GWU and USNA	5.00E-05	3000	7	Titanium
	MPACS	Busek	1.25E-03	827	8	PTFE
<i>Hall Effect</i>	BHT-200	Busek	1.30E-02	1390	8	Xenon

### 5.3 Electric Propulsion

Though electric propulsion systems can achieve very high delta-Vs, they are still limited by thruster lifetime, depending on the type of system. Taking the options that could meet the delta-V requirement, the time required to achieve 1250 m/s for the range of CubeSat bus sizes common for interplanetary mission designs was determined with results plotted in Figure 5-1. Comparing these to the lifetimes of each type of thruster, only the ion engines and hall effect thrusters fell within approximate lifetimes provided in [57] with the BIT-3 and I-COUPS just under 30000 hours and the BHT-200 well under 10000 hours.

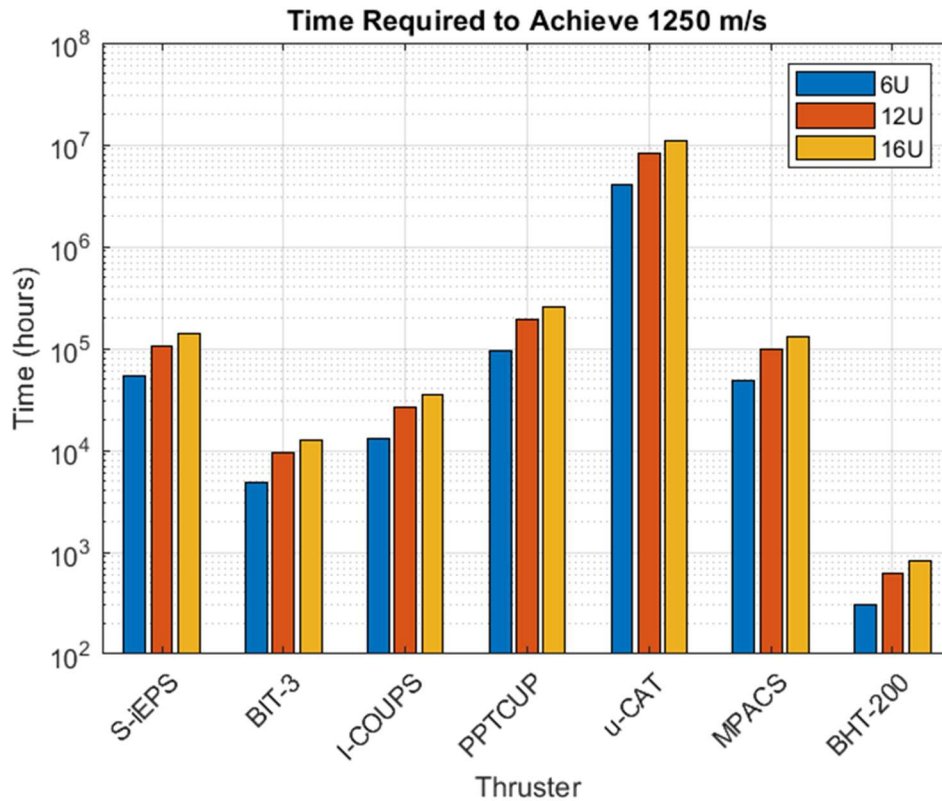


Figure 5-1: Time required for electric propulsion options to achieve 1250 m/s.

The BIT-3, I-COUPS, and BHT-200 were then traded considering the power consumption, volume of the propellant required to achieve the 1250 m/s, assuming 100 psi for the Xenon gas used in the I-COUPS and BHT-200, and dry mass of the system as the highest weighted parameters. Thrust duration and TRL were also considered, though weighted less heavily as they were all high TRL and within their thruster lifetimes. Rankings of 3 correspond to propellant volumes <1U, dry mass <1 kg, power consumption <20 W, thrust duration <2 yrs, and TRL 7-9; rankings of 1 correspond to propellant volumes >6U, dry mass >6 kg, power consumption >70 W, thrust duration >5 yrs, and TRL <5. The trade can be seen in Table 5-4 with ranking definitions listed in Appendix A. The Busek BIT-3 system performed the highest in the trade with dense solid iodine propellant and ability to reach 1250 m/s in less than two years with acceptable mass, TRL, and power consumption. and was therefore selected to continue the baseline design; key parameters of this thruster are listed in Table 5-5. Additionally, though the system is only TRL 6, it is planned to fly on two Artemis-1 missions, increasing to TRL 9 in the near future if successful. The primary drawback of this system is the 60 W needed to thrust at a level to meet 1250 m/s within the thruster lifetime; this thruster is one of the drivers of the power subsystem design as it becomes more difficult to produce as much power at Mars distance from the Sun.

**Table 5-4: Electric propulsion system trade.**

		Volume of req'd propellant at 100 psi for a 12U (U)	Dry Mass (kg)	Power (W)	Time req'd to get to 1250 m/s for a 12U (years)	TRL	Score
<i>Weights</i>		0.3	0.2	0.3	0.1	0.1	
<i>Ion Engine</i>	<b>BIT-3</b>	0.3	1.4	60	1.1	6	2.4
	<b>I-COUPS</b>	66.4	7.4	40	3.0	9	1.6
<i>Hall Effect</i>	<b>BHT-200</b>	48.6	1.1	200	0.1	8	1.6

**Legend:**  = 1       = 2       = 3



**Table 5-5: Busek BIT-3 RF Ion Thruster Parameters [58].**

<b>Propellant</b>	Iodine, solid storage
<b>Dry Mass</b>	1.4 kg
<b>Envelope</b>	180 x 88 x 102 mm (1.6 U)
<b>Propellant Load</b>	1.5 kg, expandable
<b>System Power</b>	56 - 80 W
<b>Thrust</b>	0.65 - 1.25 mN
<b>Specific Impulse</b>	2300 s
<b>Gimbal</b>	±10°

It should be noted that this thruster could achieve the estimated delta-V required for a non-optimal all non-impulsive transfer (Option 2) within the thruster lifetime with ~2.5 kg of propellant and could therefore be a viable option for future missions with robust ADCS and power systems to maintain adequate solar array pointing for the high power system. This option was not considered due to lack of accurate trajectory modelling and lower pointing requirements being more appropriate for a technology demonstration mission.

#### **5.4 Chemical Propulsion**

From the surveyed chemical propulsion options that could achieve 440 m/s, hydrazine was discarded due to its toxicity and lower TRL of 7 compared to non-toxic, or “green” propellant systems. Of the solid propellants, the ISP 30sec Motor was not considered due to its relatively high thrust which would impose greater performance requirements on the ADCS system to maintain the thrust vector and avoid tumbling; CAPS-3 was omitted due to its design, using insulated rods of propellant that would become unfeasible in mass and volume for the required delta-V.

Elimination of these systems left only non-toxic systems. Through research of the available systems, it became clear that the BIT-3 and one of the chemical systems, along with all the other subsystems in a satellite, would not fit into a 6U form factor. From this point, masses used for

performance calculations corresponded to 12U and 16U form factors (24 kg and 32 kg, respectively). The surveyed systems are modular and therefore have a set maximum impulse. This was used with Equations (5.1)-(5.3) to get the delta-V each system could deliver to these form factors. As seen in Table 5-6, none of the systems achieve the required 440 m/s. However, the MPS (Modular Propulsion System) from Aerojet Rocketdyne is available in units that can deliver up to 19360 Ns in an 8U envelope. As the MPS was the most mass and volume efficient for the provided impulse, the MPS-135-6U was selected for its ability to deliver >15900 Ns, being the smallest system to provide adequate delta-V to a 12U and 16U system, at 835 m/s and 596 m/s, respectively, considering the reduced mass from expended BIT-3 propellant; the key parameters of the MPS-135-6U are listed in Table 5-7. The performance analyses for the MPS-135 models can be found in Appendix A.

**Table 5-6: Performance parameters of surveyed chemical propulsion systems.**

	<b>Max Impulse (Ns)</b>	<b>Envelope (U)</b>	<b>Dry Mass (kg)</b>	<b>Propellant (kg)</b>	<b>dV for 12U (m/s)</b>	<b>dV for 16U (m/s)</b>
HYDROS	2151	2.3	1.87	0.74	91	68
EPSS C1K	400	1.3	1.00	0.20	17	13
MPS-130	3360	2.0	1.36	1.40	144	107

**Table 5-7: Aerojet Rocketdyne MPS-135-6U Thruster Module Parameters [59, 60].**

<b>Propellant</b>	AF-M315E
<b>Dry Mass</b>	4.3 kg
<b>Envelope</b>	~220 mm x 200 mm x 160 mm (6U with 4 protruding thrusters)
<b>Propellant Load</b>	6.9 kg
<b>System Power</b>	39 W
<b>Thrust per Thruster</b>	0.25 - 1.25 N
<b>Specific Impulse</b>	235 s
<b>Thrusters</b>	4

## 5.5 Propulsion Subsystem Summary

The delta-V requirements for the chemical and electric propulsion systems are listed in Table 5-8. Later in the configuration process, it was found that with the stowage volume of the solar panels and need to place the thruster to act through the center of mass, the MPS-135 thruster, though it provided adequate delta-V, could not fit in a 12U envelope so for the remainder of this work, a 16U bus size is baselined. The propellant mass with and without margin for a 16U form factor are provided via Equation (5.3). For the MPS-135, this is within the 6.9 kg total allowable load. The BIT-3 will require expansion; the required propellant with 20% margin is 2.14 kg, 0.64 kg over the nominal load but due to the high density of solid iodine and the tank geometry, adding this propellant adds only 7.6 mm thickness of the propellant load which was assumed could remain contained within the BIT-3 housing. The BIT-3 will complete the low-thrust transfer within a total of 530 days of thrusting.

**Table 5-8: Delta-V budget and resulting propellant masses.**

		<b>Electric</b>	<b>Chemical</b>
Required delta-V (m/s)	<i>Low-thrust</i>	1252	-
	<i>Stationkeeping</i>	50	-
	<i>Impulsive</i>	-	439
Total Per System (m/s)		1302	439
Total with 20% Margin (m/s)		1562	527
Propellant Mass (kg)		1.80	5.25
Propellant Mass with 20% delta-V Margin (kg)		2.14	6.19

## 5.6 Propulsion Subsystem Results in Relation to CPCL

CPCL has never flown propulsion systems but an electrothermal RF plasma thruster is currently under development. The 1.5U thruster is designed to provide 20 m/s delta-V to a 3U CubeSat, using gaseous Xenon stored at 3000 psi which has an Isp of 30 s. It consumes an average of 6.3 W, with

66.8 W peak power and a mass of 2.8 kg [39]. Other small satellite propulsion systems have been investigated at Cal Poly outside of CPCL such as the development of an electrospray thruster for table-top experimentation [40], which could have application as the surveyed electrospray thruster can deliver up to 110 m/s within its lifetime to a 12U CubeSat and up to 80 m/s to a 16U CubeSat. However, both the RF plasma thruster and theoretical electrospray thruster performances are too low to be applicable to this mission concept. As an example, the RF plasma thruster would require 31.5 kg of propellant to achieve the delta-V, which would be the entire bus mass, not leaving room for feed systems or other subsystems.

With the proof of the BIT-3's delta-V and thrust advantage, in-house development of an ion engine with similar capability might allow CPCL busses to fly a range of planetary and interplanetary missions. For missions with lower delta-V requirements or those with optimized low-thrust trajectories, such a system could fit in a 6U form factor, providing up to 2.5 km/s. There is precedent for ion engines developed at a university as presented in [61] where a RF ion thruster using Argon gas produced 1.78 mN of thrust with a 3786 s specific impulse; this could be a starting point for CPCL research. Additionally, the RF mechanisms in the CPCL plasma thruster could further inform this research.

## Chapter 6

### COMMUNICATIONS SUBSYSTEM

In this chapter, the communications system architectures of direct-to-Earth and Mars proximity relay architectures are explored and traded, focusing on meeting data rate mission objectives for downlink of the 13.2 MB of payload data generated each week. The link performance of the selected architecture is quantified, and the subsystem solution used to continue the baseline is summarized before comparison to CPCL’s current and planned communication capabilities.

#### 6.1 Direct-to-Earth Architecture

A direct-to-Earth (DTE) link was utilized by the MarCO CubeSats, achieving a downlink rate of 8 kbps. While this is an amazing data rate for a Mars downlink, it is one that was achieved when Earth and Mars were “close” to each other at 1.05 AU [33]. Due to the different orbital radii and periods of Earth and Mars orbits, the distance between the planets ranges from ~0.5 AU to ~2.5 AU over a two year period. To illustrate this cycle, the change in this distance over four years is shown in Figure 6-1, beginning with the launch of recent Mars-bound missions, which are timed to minimize the launch vehicle fuel required; their arrival times are also noted, occurring roughly six months after launch. This changing distance affects data rate as the space loss increases around Mars-Solar conjunction because the propagation path length increases as shown in Equation (6.1). Space loss is denoted  $L_s$  and is in dB,  $c$  is the speed of light of  $3 \times 10^8$  m/s,  $S$  is the path length in m, and  $f$  is the signal frequency in Hz.

$$L_s = 20 \log(c) - 20 \log(4\pi) - 20 \log(S) - 20 \log(f) \quad (6.1)$$

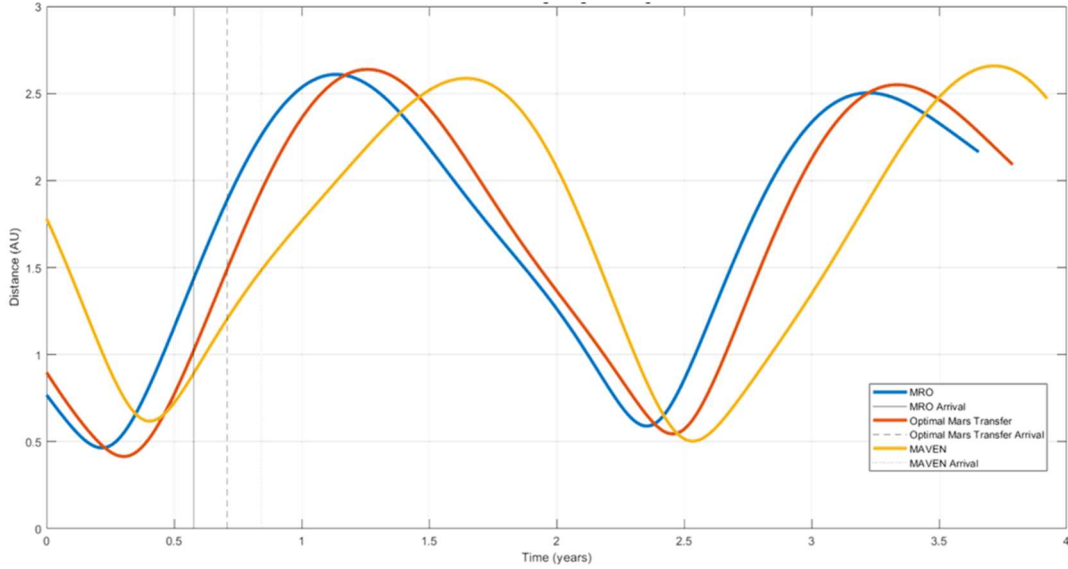


**Figure 6-1: Earth-Mars distances over time.**

The 100 bps data rate defined in the mission objectives is the driving requirement for this subsystem because it must be met throughout the mission, at up to 2.5 AU, overcoming large space loss with a constrained antenna gain due to constrained effective aperture size. A DSN ground station architecture is used, a valid assumption as ground stations, such as the ATLAS Deep Space Network (ISCN), are in development to specifically support commercial and educational small satellites providing capability similar to the DSN, and a link analysis was performed to determine the required performance of a radio and antenna and use these to trade S, X, and Ka-bands [62].

The link analysis uses RF link equations as outlined in [63]; parameters and efficiencies are assumed as in Table 6-1. As the DSN operates in X-band, S-band, and Ka-band with its 34 m and 70 m dishes with Ka-band capability only applying to the 34 m dishes, these bands were used to determine the required antenna aperture size to maintain 100 bps at 2.5 AU. The link equation, Equation (6.2), was used where  $E_b/N_0$  is the received energy-per-bit to noise-density ratio in dB,  $P$  is RF transmitter power in dBW,  $T_s$  is system noise temperature in K,  $R$  is data rate in bps, and  $k$  is Boltzman's constant,  $1.38 \times 10^{-23}$  J/K;  $G_t$ , transmit antenna gain,  $G_r$ , receive antenna gain,  $L_l$ , line

loss,  $L_s$ , space loss, and  $L_a$ , transmission path loss are in dB. Antenna gain for a parabolic dish is calculated as in Equation (6.3), where  $D$  is the antenna diameter in m,  $f$  is the signal frequency in Hz, and  $\eta$  is the antenna efficiency; this equation was used because diameter for a parabolic dish can be related to the effective diameter of planar antenna arrays using gains and dimensions of MarCO and CU-E3 reflectarrays. For example, the gain of CU-E3 is 23.3 dB which would be a 17 cm diameter dish [45]; the actual dimensions of the antenna are 20 cm x 30 cm, meaning the length of one axis is ~18% larger than the calculated dish diameter while the other axis is ~78 % larger. This roughly aligns with the MarCO gain and dimensions for a relation of ~15% larger than the calculated parabolic dish gain in one axis and ~100% larger in the other axis. These relations can be averaged to determine mass and volume figures of a deployable antenna.

$$\frac{E_b}{N_o} = P + L_l + G_t + L_s + L_a + G_r - 10\log(k) - 10\log(T_s) - 10\log(R) \quad (6.2)$$

$$G = 20\log(\pi) + 20\log(D) + 20\log(f) + 10\log(\eta) \quad (6.3)$$

As the only flight proven CubeSat radio capable of transmitting and receiving in S, X, and Ka-bands, the Iris V2.1 CubeSat Deep Space Transponder used on the MarCO mission was used for the RF power link parameter of 3.8 W [64]. As the Iris V2 uses phase shift keying (PSK) modulation, the simplest form of PSK, BPSK, was assumed.  $E_b/N_o$  can be significantly reduced through modulation coding, such as with a concatenated Reed-Solomon/convolutional error-correction code scheme, from 9.6 dB to 2.9 dB for a bit error rate (BER) of  $10^{-5}$  [63, 65]. The gain required on the CubeSat side of the link (downlink data to Earth) was determined using the parameters listed in Table 6-1 and Equation (6.2). As the DSN receiving antenna gain differs between the bands, the required transmit antenna gains are ~28 dB for S and X-band and ~34 dB for Ka-band. As space is limited on a CubeSat, antenna size is a concern; dish diameter versus resulting gain is plotted in Figure 6-2 for trading.

**Table 6-1: Link parameters used for analysis.**

Parameter	Value	Comments
S-Band Downlink Frequency, $f$	2.4 GHz	
X-Band Downlink Frequency, $f$	8.43 GHz	
Ka-Band Downlink Frequency, $f$	31.20 GHz	
Distance, $S$	2.5 AU	Maximum distance
RF Power, $P$	3.8 W	Iris Radio
Transmitter Efficiency	0.33	MarCO
System Noise Temperature, $T$	135 K	[63]
DSN Dish Diameter for S- and X- Band, $D$	70 m	DSN
DSN Dish Diameter for Ka-Band, $D$	34 m	DSN
DSN Antenna Efficiency, $\eta$	0.7	Assumed
Eb/No	2.9 dB	Coded BPSK [65]
Losses (line loss, pointing loss, random losses)	-7 dB	Assumed
Link Margin	3 dB	Typical
Data Rate, $R$	>100 bps	Requirement

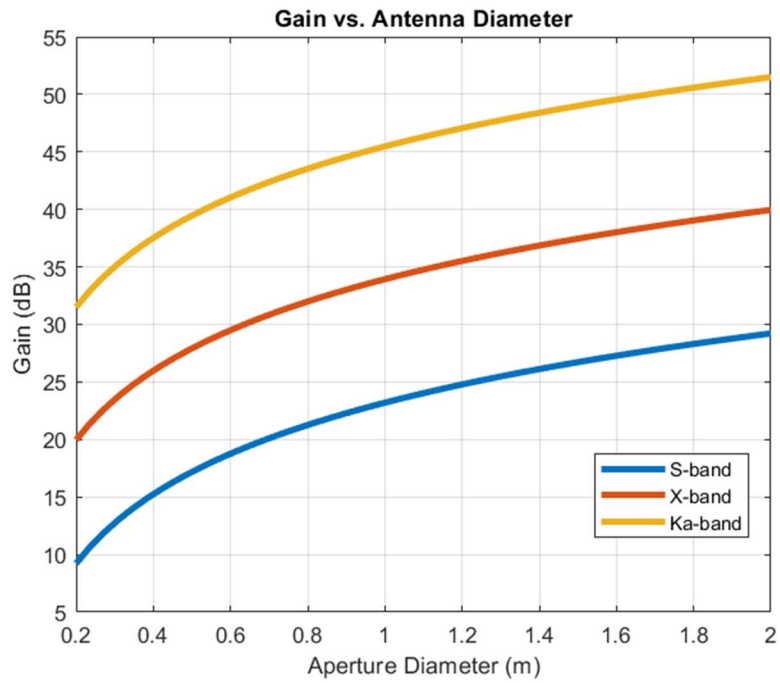


**Figure 6-2: Antenna gain versus antenna diameter for various frequency bands.**



To achieve 28 dB, a 0.5 m diameter dish is needed in X-band while a 1.8 m one is needed in S-band; in Ka-band with a 34 dB requirement, only a 0.28 m diameter is needed. For space and mass savings, Ka-band was selected to continue the DTE architecture investigation. With the selection of a band, one can look at the power and pointing requirements as well as trade antenna types. Using Equation (6.4), where  $f$  is the frequency of the signal in GHz and  $D$  is the transmitting dish diameter in m, the beamwidth was approximated to determine the pointing requirement of  $2.5^\circ$ . With no compression, pointing lock would need to be maintained for 11.2 hours to downlink one week of data in the best case scenario at 0.5 AU; at the farthest distance, times become unreasonable with one week of only radiation data taking 26 hours to downlink. Applying 25% compression only reduces these times to 8.4 hours and 19 hours, respectively.

$$\theta_{BW} = \frac{21}{f * D} \quad (6.4)$$

Despite the low return rate and long lock times, the Ka-band DTE architecture was pursued further into a survey of medium to high TRL Ka-band capable antennas. Considering complexity of antenna deployment, TRL, thermal concerns, and stowage volume, a deployable small reflectarray would be best for this architecture considering the options shown in Table 6-2. The small reflectarray, such as the one used for the MarCO mission stows flat, has been flight proven, and has simple two-step hinge deployments. Its gain is limited by keeping the folds to one direction for a maximum area of  $\sim 0.6 \text{ m}^2$ , or three times the area of the largest face of a 6U or 12U CubeSat. With the increased area comes thermal considerations as it is additional metal surface area exposed to solar irradiance, compared to a patch array or mesh reflector.

**Table 6-2: Antennas considered for high gain DTE, adapted from [33, 66].**

	Volume	TRL	Aperture/ Gain	Deployment	Thermal Concerns	Cost	
	0.2	0.1	0.3	0.2	0.1	0.1	1
<b>Patch Array</b>	~0.1U	9	<0.06 m <sup>2</sup>	Simple	None	Low	2.4
<b>Small Reflectarray</b>	~0.1U	9	~0.18 m <sup>2</sup>	Simple	Some	Low	<b>2.6</b>
<b>Large Reflectarray</b>	>0.5U	4-5	~1.0 m <sup>2</sup>	Complex	Some	Medium	2.1
<b>Mesh Reflector</b>	~1.5U	9	>0.20 m <sup>2</sup>	Complex	None	Medium	2.1

**Legend:**  = 1       = 2       = 3

As the ground segment is not limited by power, the uplink can be achieved with an X-band patch antenna with a gain of at least 6 dB (minimum gain commercially available) can be used to close the link. A summary of the parameters for the DTE communications subsystem architecture option is presented in Table 6-3 [67]. A major drawback of the DTE architecture is that it assumes significant DSN (or similar ground station) resource usage, which besides requiring long lock times at farther Earth-Mars distances, would be costly and in-high demand by the industry [68]. This DTE architecture would be best suited for a mission that must maintain communication with Earth during interplanetary travel and at Mars; for a mission that begins at Mars it is more reasonable to investigate the resources already present for a relay, decreasing the required capability of the CubeSat communication and ADCS subsystems.

**Table 6-3: Summary of Ka-Band DTE architecture parameters.**

Parameter	Value	Comments
Transmit Frequency, $f$	31.2 GHz	Ka-band
Satellite Transmit Antenna	Deployable reflectarray ~0.33 m x 0.53 m (0.28 m effective diameter)	Rectangular approximation using MarCO and CU-E3 reflectarray gain and dimensions
Radio RF Power	3.8 W	Iris Radio
Radio Power Consumption	12.6 W Receive, >30.8 W Transmit	Iris Radio
Radio Mass	1 kg	Iris Radio
Radio Volume	0.5 U	Iris Radio, may be larger for thermal control
Downlink Rate	~100 bps - 2.6 kbps	
Uplink Rate	~5 kbps - 133 kbps	
Satellite Receiving Antenna	Patch antenna	
Receive Frequency, $f$	7.15 GHz	
Ground Station	DSN 70 m Dish X-band, DSN 34 m Dish Ka-band	

## 6.2 Relay Architecture

As a direct-to-Earth architecture would require a long lock for downlink with a major ground station resource, a tight pointing requirement, large deployable antenna, and high power consumption, a relay architecture was explored. As mentioned, there is precedent for some theoretical CubeSat missions to leverage existing communications resources at Mars. The Mars Reconnaissance Orbiter and Trace Gas Orbiter both possess the Electra Proximity Link Payload which has UHF transceivers and a nadir-pointing, low gain, omnidirectional quadrifilar helix UHF antenna [69]. Using the Electra radio gain of 0 dB and half-duplex RF power of 7 W with an assumed efficiency of 85%, the required performance of a UHF radio on the CubeSat was determined [69]. The nominal link was designed around periapsis of the cycloidal orbit as this is when the CubeSat is the closest to MRO which is in a 300 km altitude polar orbit around Mars. This portion of the orbit is shown in Figure 6-3. The mission trajectory was modelled in STK using the initial orbit values defined in

Table 5-1 and using the Astrogator package to simulate a 1.64 year low-thrust transfer using BIT-3 performance parameters of thrust and specific impulse. A target sequence was implemented to perform an impulsive maneuver using MPS-135 performance values of thrust and specific impulse to insert the CubeSat into the cyclor orbit with the desired eccentricity of 0.4497. This orbit was then propagated for 1.88 years. True anomaly and position of the spacecraft in the cyclor orbit portion of the trajectory were calculated and output by STK. The Pythagorean Theorem was used with CubeSat position and an MRO altitude of 300 km at the poles to find an average slant range through the close approach. It was determined that from a true anomaly of  $277^\circ$  to  $86^\circ$ , the CubeSat is within a  $\sim 13500$  km slant range assuming the geometry shown and within a  $\sim 9950$  km slant range at periapsis, taking roughly 3 hours and 40 minutes to traverse this  $169^\circ$  close approach.

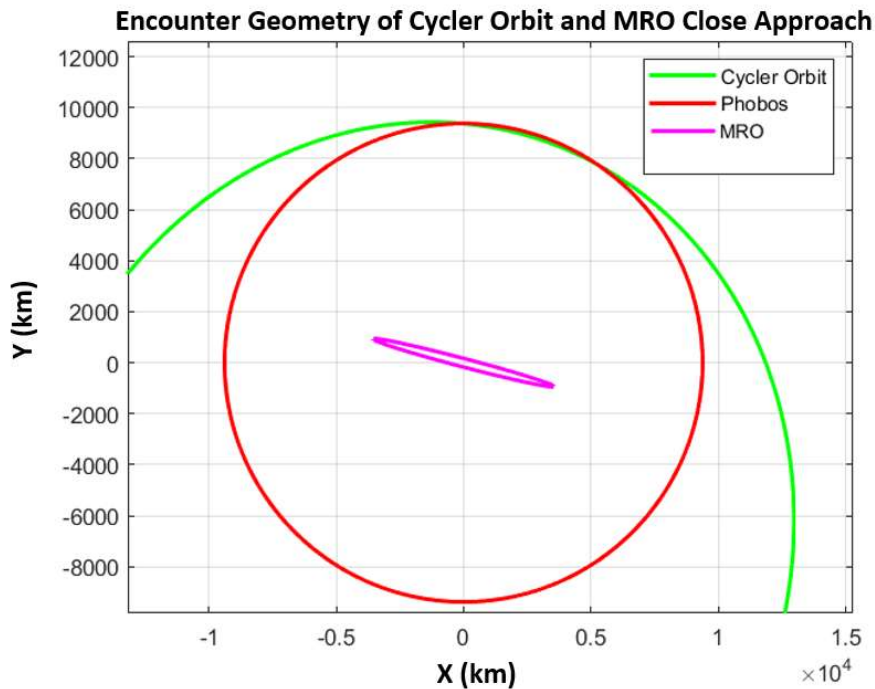


**Figure 6-3: Encounter geometry of cyclor orbit and MRO for link analysis.**

As the relay link architecture has less space loss and UHF requires less pointing due to a larger beamwidth, it is easier to achieve higher performance and so just meeting the 100 bps requirement can be done with an omnidirectional antenna on the CubeSat, though it would require long transmit times to MRO. Therefore, for this architecture, it was desired to maximize the link capability to reduce the Electra utilization that would theoretically also be in use by other orbiters. A survey of UHF radios and antennas show there is interest in but little actualization of high-performance UHF systems as they traditionally consist of ~1 W RF transmit power radios and omnidirectional whip antennas. These components would close the link according to the 100 bps mission objective but it would have low throughput throughout the orbit, not meeting the objective of downlinking one week of data within three downlink opportunities.

Therefore, the 2018 NASA State of the Art Report on Small Satellites was used to survey high TRL UHF components, listed in Table 6-4. From the survey, the Lithium-1 Radio from Astronautical Development LLC was selected due to providing the highest RF power at 2.5 W and a TRL of 9, having flown on RAX-1 and 2, MCubed, and CSSWE missions [70].

**Table 6-4: Surveyed UHF radios considered for relay architecture.**

Product	Manufacturer	TRL	RF Power	Modulation	Power Usage
Lithium-1 Radio	Astronautical Development LLC	9	2.5 W	FSK, GMSK	<10.0 W
VUTRX Radio	AAC-Clyde	9	2.0 W	GMSK, ADSK	3.0-7.0 W
UHF Transceiver Type II	Endurosat	9	1.0 W	OOK, FSK, GMSK, GFSK	>1.4 W
NanoCom Ax100 Radio	GomSpace	8	1.3 W	GFSK/GMSK	4.0 W

For the antennas, only 0 dB, omnidirectional antennas are commercially available, having maximum RF outputs of ~1 W. UHF patch antennas have been developed, however, these are made

on a custom basis and so few specifications are available. Therefore, to achieve high gain with flight heritage, while providing concrete mass and volume parameters, a deployable UHF loop antenna such as the one used on MarCO was chosen. This antenna's beam pattern and dimensions have been characterized in [35], allowing for a more informed baseline design regarding mass budgets, pointing requirements, and concept of operations. The parameters used in the link analysis are shown in Table 6-6. The link is conservative as the same system noise temperatures were used for uplink and downlink, using an assumed 243 K; this is on the higher end for estimated Mars CubeSat relay links which range from 216 to 258 K [71, 72]. The radiation profile of the antenna shows 2.5 dB at  $\pm 30^\circ$  from the boresight and 5 dB at the boresight. Using maximum and minimum slant ranges, MRO was determined to be up to  $15^\circ$  to  $20^\circ$  from the boresight; combined with the radiation profile, the gain on the UHF antenna was taken to be 3.5 dB. This is the worst-case gain as MRO could pass through the beam center for some orbits. As the Li-1 uses FSK/GMSK coding schemes, the  $E_b/N_0$  was found possible to be reduced to 2.9 dB from 9.6 dB if pre-coded using the same concatenated Reed-Solomon/convolutional error-correction code scheme applied to the DTE architecture [65]. The Electra payload specifications do not mention accepted coding schemes so it was assumed that the transceivers would be compatible; GMSK signals can be decoded by a QPSK receiver at the DSN as shown by the ExoMars TGO [73].

As the beamwidth of UHF is much larger and the nominal downlink occurs at periapsis, the pointing requirements becomes  $10^\circ$  to maintain MRO within the beamwidth. Additionally, the UHF radio consumes less SWaP than the Iris Radio. This architecture can provide data rates from 1.8 kbps to 3.2 kbps, shown in Figure 6-4, for 3.5 hours each orbit throughout the mission, resulting in a higher average data rate than the DTE architecture. With this link, the data rate was integrated to determine downlink time during periapsis. Using the sizes of packets for one week of radiation data ("Rad"), low resolution 100 x 100 pixel black-and-white ("Lo") thumbnails and high resolution 1632 x 1232 pixel black-and-white ("Hi BW") or full color images ("Hi"), and applying compression rates from 0% to 20%, the number of passes needed to downlink the data package was

calculated with results shown in Figure 6-5. The constraint to be able to downlink one week of data in three passes, baselined to be two high resolution color images and continuous radiation data (Table 3-2), is satisfied by the current link with <3% compression. Some compression ability is available through the camera chip; however, the amount is unspecified. Nevertheless, the needed compression value is reasonable as launched CubeSats, such as the 3U Phoenix from Arizona State University, have achieved 20% data compression [74].

**Table 6-5: Relay link parameters.**

Parameter	Value	Notes
CubeSat Transmit Frequency, $f$	390 MHz	UHF
Relay Transmit Frequency, $f$	450 MHz	UHF
Max Distance, $S$	13,500 km	Slant range ~1.75 hrs on either side of perigee
Min Distance, $S$	10,000 km	Slant range at perigee
System Noise Temp., $T$	243 K	Estimates for Mars relay range from 216-258 K
CubeSat RF Power, $P$	2.5 W	Lithium-1 Radio
CubeSat UHF Gain, $G_t$	3.5 dB	MarCO, 2.5 dB $\pm 30^\circ$ from boresight, 5 dB at boresight
Relay Antenna Gain, $G_r$	0 dB	Electra, quadrifilar helix
Relay RF Power, $P$	7 W	Electra
Eb/No (no coding)	9.6 dB	Lithium-1 GMSK
Eb/no (coding)	2.9 dB	Lithium-1 GMSK, theoretical performance
Link Margin	3 dB	Typical
Losses	-7 dB	Assumed

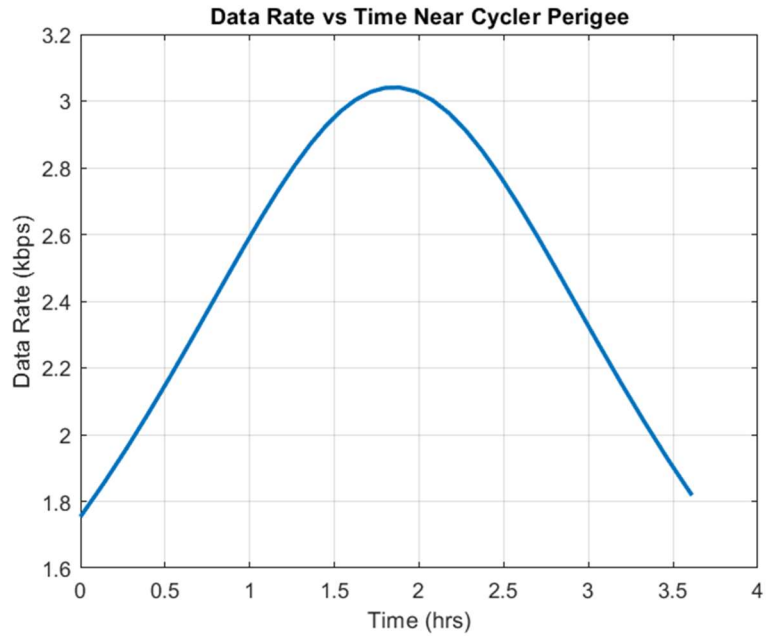


Figure 6-4: Data rate change through the 3.5 hr pass near cyclor periapsis.

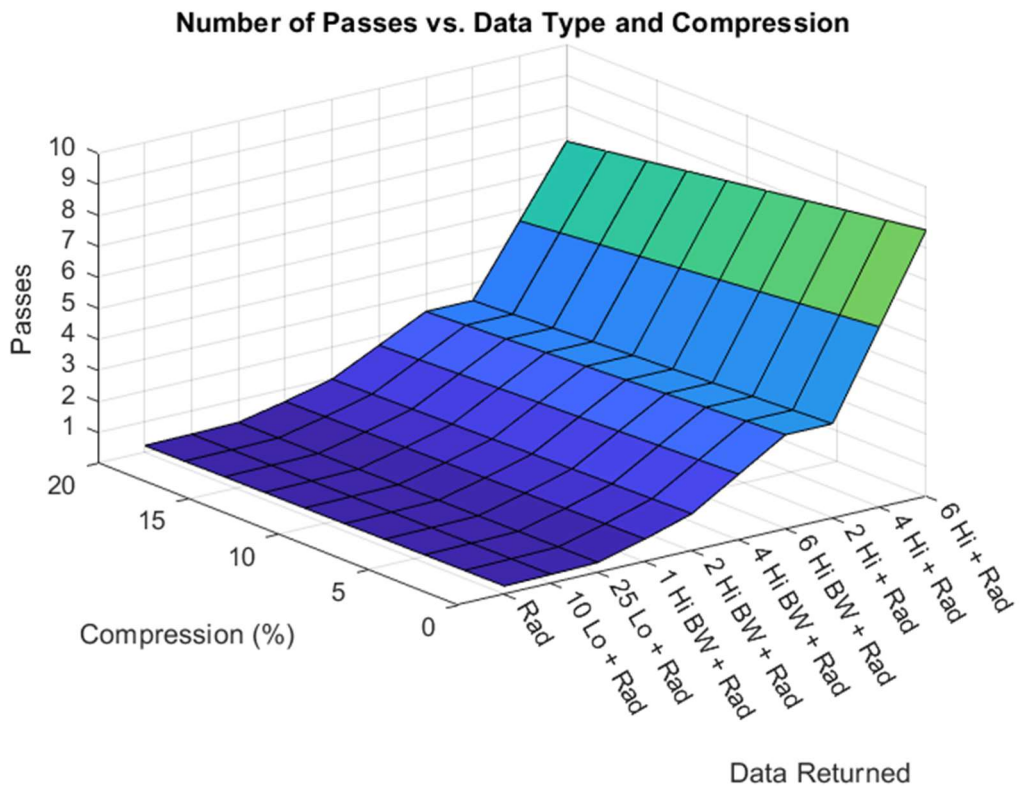


Figure 6-5: Number of MRO passes needed to downlink various data packets with varying compression levels.



The repeated passes also allow more opportunity for either downlinking more data if time allows, breaking up downlink intervals into shorter times, or re-downlinking data if corrupted. Yet another advantage of a relay architecture is that literature suggests a movement towards more relay capable satellites as we begin building a Mars telecommunications system that could support human exploration [71]. As landers and rovers utilize UHF, it can be assumed that the relay orbiters will support this band. A summary of the parameters for the communications subsystem architecture option is listed in Table 6-6.

To illustrate the increased performance of higher frequency bands for potential future Martian relay resources, an additional link analysis was performed using a proposed but cancelled X-band capability of the Electra radio that also featured a steerable 30 dB X-band antenna. If a 12 dB patch antenna and the Iris Radio RF power of 3.8 W were used, the data rate at periapsis would increase five times to ~15.8 kbps.

**Table 6-6: Summary of UHF relay architecture option parameters.**

Parameter	Value	Comments
Satellite Transmit Frequency, $f$	390 MHz	
Satellite Antenna	Deployable UHF antenna, 0.5 U stowed	MarCO
Satellite Radio RF Power, $P$	2.5 W	Iris
Satellite Radio Power Consumption	10 W max	Li-1
Satellite Radio Mass	52 g	Li-1
Satellite Radio Volume	0.02 U	Li-1
Downlink Rate	~1.8 kbps - 3.2 kbps	
Uplink Rate	~1.4 kbps - 6.7 kbps	
Satellite Receive Frequency, $f$	450 MHz	
Relay Antenna Gain, $G_r$	0 dB	Electra
Relay RF Power, $P$	7 W	Electra

A comparison of DTE and relay architectures is shown in Table 6-7. Due to the power and mass savings of >20 W and >1kg, pointing requirement relaxed from 2.5° to 10°, and more feasible resource utilization, the relay architecture was used to continue the baseline design. Detailed link budgets for both architectures are included in Appendix B.

**Table 6-7: Comparison of UHF Relay and DTE Ka-band architectures.**

	<b>Max Satellite Input Power</b>	<b>Data Rate</b>	<b>Resource Feasibility</b>	<b>Radio Mass/Volume</b>	<b>Antenna</b>	<b>Pointing Req.</b>
UHF Relay	10.0 W	~2500 bps average	Existing relays for this purpose	52 g/ 0.02U	Single burn wire deployment	10.0°
DTE Ka-Band	30.8 W	100 bps-2600 bps variable over years	DSN congestion	1.2 kg/ 0.5U	Multiple hinge deployment	2.5°

### 6.3 Communications Subsystem Results in Relation to CPCL

The flight proven CPCL UHF communications board includes a transmitter, receiver, filtering, and amplifiers for 1 W RF transmit power. This radio could be used for the mission concept but would require antenna gain of 7.5 dB to maintain the same link as the standard CPCL antenna is an omnidirectional, deployable Nickel-Titanium dipole antenna with a peak gain of 2.15 dB. The Cal Poly ground station is equipped with three UHF stations with 80-100 W RF amplification power, 24 dB gain arrayed Yagi antennas to achieve data rates up to 38.4 kbps in LEO with FSK/GMSK modulation schemes. An X-band ground station and transceiver are under development within CPCL. As the dish is expected to be 2.4 m in diameter and using the 70 m dish in X-band was a difficult link to close, this would not be sufficient for the studied case. The X-band transceiver on the other hand could prove very useful if other Mars satellites carried an X-band relay; developing

X-band capability will also be useful for near Earth interplanetary missions, such as was proposed for the CPCL lunar mission concept [19].

## Chapter 7

### POWER SUBSYSTEM

With the selection of an electric propulsion comes a need for power generation  $>60$  W for the propulsion system alone, becoming more difficult at Mars than at Earth due to the additional 0.5 AU distance from the Sun. The power system must provide power to the spacecraft throughout the duration of the mission and remain power positive while in eclipse to maintain its attitude and thermal requirements. This chapter will cover the derivation of requirements for power generation and storage from defined power modes, component sizing, and component selection. The selected subsystem solution used to continue the baseline is summarized and compared to CPCL's current and planned power subsystem capabilities.

#### 7.1 Power Consumption Requirements

The power subsystem shall be able to supply power to the CubeSat throughout various operational modes in all orbit phases. The operational modes were separated into three mission segments, the low-thrust phase, the impulsive burn to insert into the cycler orbit, and cycler orbit. These different phases result in different power requirements, needing strategic duty cycling to balance the size of the power system between the high-power electric propulsion system and the lower power cycler orbit. As they provide the most power constraining cases the baseline must be designed to, the worst-case eclipses were used in battery and array sizing. The power consumption of selected components is listed in Table 7-1. Note that the selection of these components was an iterative process and will be discussed in other chapters; the power consumption values are taken from product data sheets unless otherwise noted as assumed values.

**Table 7-1: Power consumption of selected components.**

	Quantity	Standby Power (W)	Average Power (W)	Peak Power (W)
<b>Propulsion</b>				
BIT-3 Ion Engine	1	1.000*	60.000	60.000
MPS-135 Thruster	1	-	-	-
<i>Catalyst Bed Heater</i>	4	0	7.000	7.000
<i>System Heater Power (avg)</i>	1	0	10.000	10.000
<i>Valve Power</i>	4	0	0.250	0.250
<b>Communications</b>				
UHF Radio	1	0.200	10.000	10.000
<b>Payload</b>				
Camera	1	0	0.125	0.140
Radiation Sensor	1	0	0.070	0.070
<b>CDH</b>				
OBC	1	0.400	0.400	0.400
OBC Daughterboard	1	0.300	0.300	0.300
<b>ADCS</b>				
Reaction Wheels	3	0.100	0.300	1.800
Sun Sensor	6	0*	0.038	0.050
IMU	1	0.003	0.350	0.368
Star Tracker	1	0*	1.000	1.500
<b>Power System</b>				
Power Board	1	1.000	3.000	3.000
BPX Battery Pack	1	0.064	0.064	0.064
BP4 Battery Pack	1	0.030	0.030	0.030
ACU	1	0.329	0.329	0.329
PDU	1	0.600	0.600	0.600
SADA	1	0.500	1.000	1.000
<b>Thermal</b>				
BPX Heater	1	0*	3.500	6.000
Other Heaters	1	0*	36.500	36.500

*\*Assumed*

The breakdown of power consumption for the three phases is shown in Table 7-2. In the low-thrust phase, the BIT-3 ion engine requires a continuous 60 W; as this is a large power draw for a CubeSat, the thruster will only be on in the Sun in order to reduce the solar panel area which adds mass and volume. This reduces solar panel area because less power is required in eclipse and therefore requires fewer batteries that need to be charged while in the Sun. As the in-Sun power required during the low-thrust transfer is the highest of all phases, only essential components

remain on to prevent over production of power in other phases. The heaters are off in-Sun due to the large thermal dissipation from the BIT-3 that can act as a heater to the batteries and other components. In eclipse, the BIT-3 was assumed to have a standby power of 1 W as it turns on and off repeatedly. As the eclipse times during the low-thrust regime are short, it was assumed that there would be no communications, so the radio is in receive-only mode. The solar panel tracker is also in standby mode in eclipse as it does not need to track, and the battery heaters are on due to the removal of the BIT-3 heat dissipation. The impulsive transfer power requirements fall between the requirements of the low-thrust and cycler phases so if those two phases are power positive, the impulsive transfer will be as well.

**Table 7-2: Power consumption modes throughout mission.**

Phase	Low-Thrust Transfer		Impulsive Transfer	Cycler Orbit					
Modes	Eclipse (W)	Sun (W)	Transfer (W)	Eclipse (W)	UHF Uplink (W)	UHF Downlink (W)	Science (W)	Standby (W)	Orbit Maintenance (W)
<b>Frequency</b>	-	-	Once	0-9/Week	1/Week	1/Week	2/Week	-	1/Week
<b>Duration</b>	52 mins (Worst-case)	5.7 hrs (Worst-case)	40 mins	97 mins (Worst-case)	<10 mins	11 hrs	<1 hr	~135 hrs (Worst-case)	4.7 hrs (Worst-case)
<b>Propulsion</b>									
BIT-3	1.0	60.0	1.0	1.0	1.0	1.0	1.0	1.0	54.5
MPS-135	0.0	0.0	39.0	0.0	0.0	0.0	0.0	0.0	0.0
<b>Communications</b>									
UHF Radio	0.2	10.0	0.2	10.0	10.0	10.0	0.2	0.2	0.2
<b>Payload</b>									
Camera	0.0	0.0	0.0	0.0	0.0	0.0	0.1	0.0	0.0
Rad. Sensor	0.0	0.0	0.0	0.1	0.1	0.1	0.1	0.1	0.0
<b>CDH</b>									
OBC	0.7	0.7	0.7	0.7	0.7	0.7	0.7	0.7	0.7
<b>ADCS</b>									
Rxn Wheels	0.9	0.9	0.9	0.9	0.9	0.9	0.9	0.3	0.9
Sun Sensors	0.2	0.2	0.3	0.2	0.2	0.2	0.2	0.2	0.2
IMU	0.4	0.4	0.4	0.4	0.4	0.4	0.4	0.0	0.4
Star Tracker	1.0	1.0	1.0	1.0	1.0	1.0	1.0	1.0	1.0
<b>Power System</b>									
Power Board	3.0	1.0	3.0	3.0	3.0	3.0	3.0	3.0	3.0
Battery Packs	0.1	0.1	0.1	0.1	0.1	0.1	0.1	0.1	0.1
ACU	0.3	0.3	0.3	0.3	0.3	0.3	0.3	0.3	0.3
PDU	0.6	0.6	0.6	0.6	0.6	0.6	0.6	0.6	0.6
SADA	0.5	1.0	0.5	1.0	1.0	1.0	1.0	1.0	1.0
<b>Thermal</b>									
BPX Heater	3.5	0.0	0.0	3.5	3.5	3.5	3.5	3.5	3.5
Other Heaters	0.0	0.0	0.0	Needs Revision, see Chapter 12	36.5	36.5	36.5	36.5	0.0
<b>Mode Power (W)</b>	<b>12.4</b>	<b>76.2</b>	<b>48.0</b>	<b>22.8</b>	<b>59.3</b>	<b>59.3</b>	<b>49.6</b>	<b>48.5</b>	<b>66.4</b>

## 7.2 Sizing the Solar Panels

To size the solar panels, required power generation for components that are on in the Sun as well as charging the batteries for eclipse need to be taken into account along with solar cell degradation, temperature effects, and power system inefficiencies. To determine the amount of power the solar arrays must provide in sunlight, Equation (7.1) was used where  $P_e$  is power in W required in eclipse,  $T_e$  is time in eclipse in seconds,  $X_e$  is efficiency of the path from the solar array through the batteries to the components; similarly,  $P_d$  is power required in Sun,  $T_d$  is time in the Sun,  $X_d$  is efficiency of the path from the solar array to the components. To calculate the additional solar array area needed to account for losses and degradation, the beginning of life power generation in W/ m<sup>2</sup>,  $P_{BOL}$ , is calculated using Equations (7.2) and (7.3) where  $\eta$  is the solar cell efficiency,  $P_s$  is the incident solar irradiance at Mars which is 607.8 W/m<sup>2</sup> which was assumed constant for this analysis;  $I_d$  is the inherent degradation due to temperature of the cells,  $\beta$  is the worst case beta angle, the angle between the Sun vector and the normal of the cell face which varies as the orbit plane moves around the Sun. Then, end of life power generation per area,  $P_{EOL}$ , can be calculated using Equation (7.4) where  $t$  is the mission lifetime in years. Finally, required array area in m<sup>2</sup>,  $A$ , is determined using Equation (7.5).

$$P_{SA} = \frac{\left(\frac{P_e T_e}{X_e} + \frac{P_d T_d}{X_d}\right)}{T_d} \quad (7.1)$$

$$P_0 = \eta P_s \quad (7.2)$$

$$P_{BOL} = P_0 * I_d * \cos(\beta) \quad (7.3)$$

$$P_{EOL} = (1 - 0.25)^t P_{BOL} \quad (7.4)$$

$$A = P_{SA} / P_{EOL} \quad (7.5)$$



The in-Sun power consumption plus battery charging for eclipses in the low-thrust phase are what the solar panels must be sized for. To obtain  $T_e$ , the eclipse times for the low-thrust regime over the 1.6 year transfer were obtained using reported eclipses corresponding to the trajectory modelled for the duration of the mission using STK's Astrogator package (explained in Chapter 6). The eclipse durations over the mission vary as Mars orbits the Sun and the CubeSat's orbit is raised; the low-thrust phase eclipse durations are shown in Figure 7-1 and those during the cyclor orbit phase in Figure 7-2.

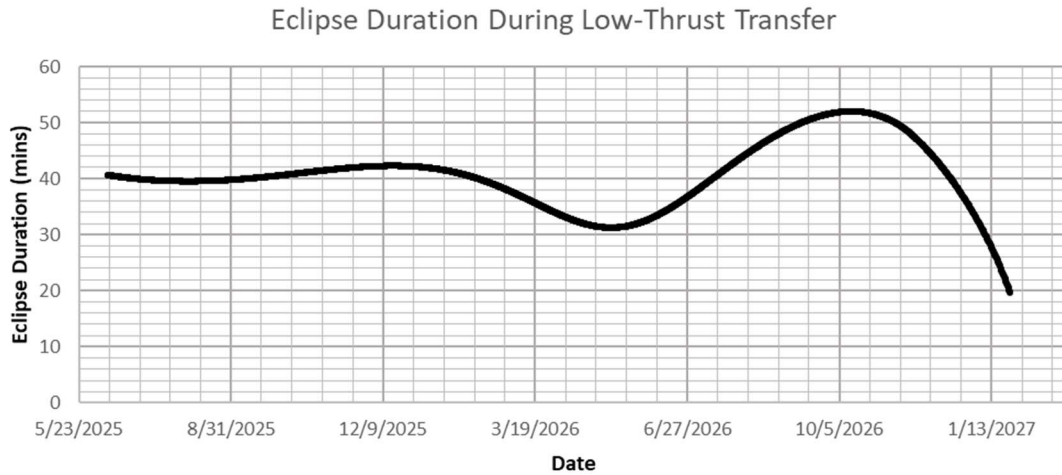


**Figure 7-1: Eclipse duration during low-thrust transfer.**

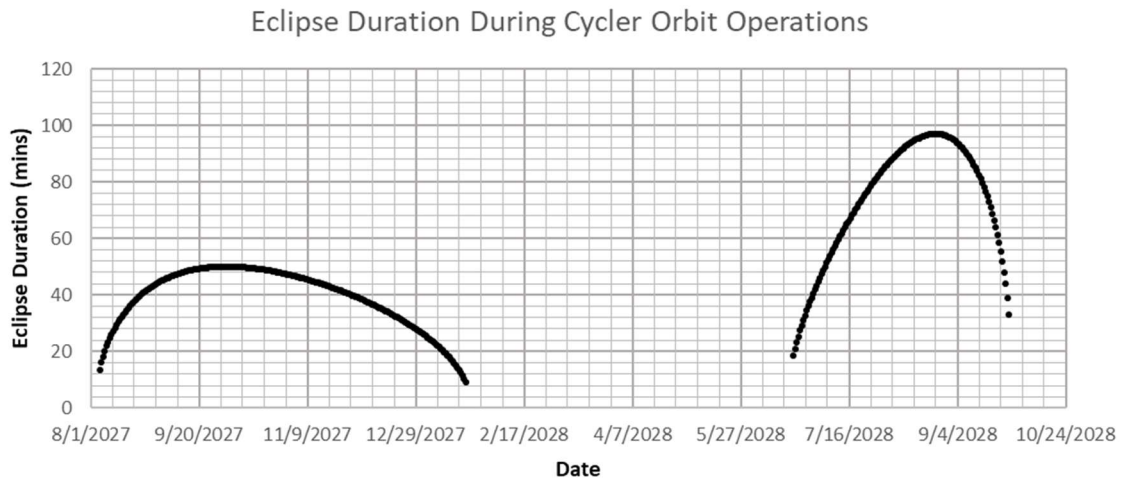


**Figure 7-2: Eclipse duration during cyclor orbit.**

From Table 7-2, the power needed in the Sun is 76.2 W, which results in 91.4 W power consumption with 20% margin. The power required in eclipse was taken to be 12.4 W plus 20% margin for a total of 14.9 W that the batteries must provide for the maximum eclipse time of 52 mins; from STK, it was determined that this maximum eclipse time occurs when the spacecraft period is 6.60 hrs, making the time in the Sun 5.73 hrs. The efficiencies,  $X_e$  and  $X_d$ , were assumed to be 0.65 and 0.85, respectively, to correspond to direct energy transfer power regulation [75]. To reduce array size as there is no cost constraint, Spectrolab 30.7% efficient NeXT Junction (XTJ) Prime solar cells were used. Inherent degradation was assumed to be 0.88, the high end of temperature degradation as the solar panels are expected to remain cool as discussed in Chapter 12 [75]. The worst-case beta angle for Mars is  $25.19^\circ$  due to Mars' obliquity of the ecliptic and the mission lifetime is 3.5 years. The resulting required solar array area is  $0.82 \text{ m}^2$ . Using Spectrolab's standard rectangular cell with an area of  $27 \text{ cm}^2$ , this is 303 solar cells [76]. If a less efficient, potentially more cost-effective cell were used such as the 28.4% efficient UTJ SpectroLab solar cells, this goes up to 328 cells, which based on the CubeSat form factor, could add an additional folding panel, increasing stowage size and mass. Using the same process for the cycler orbit phase, with a maximum eclipse of 97 minutes, leaving 20.0 hrs in the Sun, a required eclipse power of 22.8 W and a maximum sunlit power of 66.4 W results in a  $0.72 \text{ m}^2$  solar panel area to achieve 20% margin; as this is less than the panel area for the low-thrust transfer, the CubeSat will be power positive in the cycler orbit phase. A summary of solar panel sizing parameters and results is listed in Table 7-3.

**Table 7-3: Solar panel sizing parameters and results.**

	<b>Low-Thrust</b>	<b>Cycler</b>
<b>Eclipse Time</b>	0.87 hrs	1.62 hrs
<b>Sun Time</b>	5.73 hrs	20.00 hrs
<b>Sun Power with 20% Margin</b>	91.4 W	79.7 W
<b>Eclipse Power</b>	14.9 W	27.4 W
<b>Solar Panel Area</b>	0.82 m <sup>2</sup>	0.72 m <sup>2</sup>
<b>Number of Cells Assuming SpectroLab 27 cm<sup>2</sup> Cells</b>	303 cells	269 cells

Current deployable CubeSat form factor solar panels are designed for high power Earth-orbiting or lunar missions which are on par with the power required for this mission but due to the distance from the Sun, require a much larger area. The maximum power producing commercially available arrays are from MMA Design, the company that provided MarCO’s solar arrays, providing up to 112 W BOL at Earth. The array features two wings, each with two deployments in one axis and one in the other axis for a total of four deployments per wing. Therefore, the arrays for this mission were configured by extrapolating the design of MMA Design’s existing arrays, using the stowage height and mass of existing arrays to determine approximately how much mass and volume each additional panel and fold adds. Additionally, the number of cells per panel was increased from 14 (two rows of seven cells on a 20 cm x 30 cm panel) to 18 (two rows of nine cells on a 20 cm x 40 cm panel) due to the longer side length available on a 16U form factor assuming use of the 27 cm<sup>2</sup> XTJ cells. Due to the need for the BIT-3 to remain aligned along the velocity vector during the low-thrust transfer and power generation needs to remain constant throughout the sunlit portion of the orbit, the solar panels need to be able to track the Sun without shadowing from the bus, rotating about an axis perpendicular to the velocity vector and the Mars-pointing axis, requiring a solar array drive assembly (SADA). Assuming the configuration shown in the top of

Figure 7-3 with two wings each consisting of nine 2 x 9 cell panels and extrapolating the MMA 6U variant deployment strategy (pictured in the bottom of Figure 7-3) in which the panels unfold along the X-axis before the side panels unfold in the Z-axis to include an additional panel, the wings can be stowed to a height of 3 cm each. Note that four of the panels need not be fully populated to achieve the required 303 cells. This panel area could be populated to provide more power and margin or removed to reduce mass.

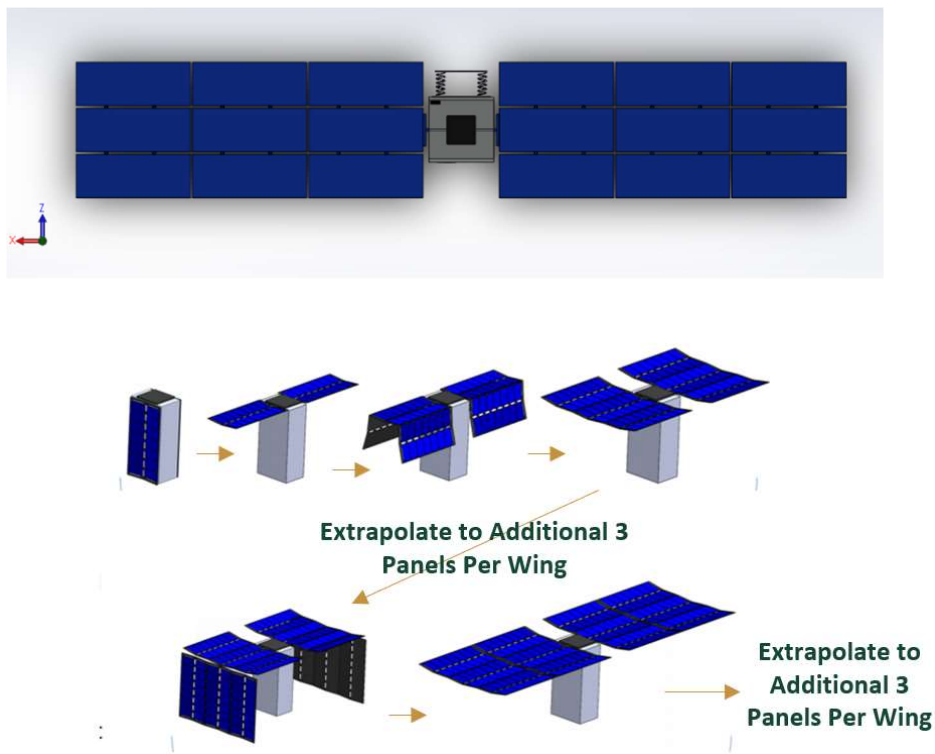


**Figure 7-3: Deployed configuration (top) and proposed folding strategy for MMA arrays (bottom) [77].**

### 7.3 Sizing the Batteries

To determine battery capacity in Wh, Equation (7.6) was used, where  $T_e$  is eclipse time in hrs,  $P_e$  is power required in eclipse in W,  $\eta$  is PDU efficiency, and  $DOD$  is depth of discharge. The eclipse time was determined from STK and power required taken from the power budget in Table 7-2;

PDU efficiency was assumed to be 95%. DOD was assumed using a worst case DOD value corresponding to the number of expected charge/discharge cycles for the mission, determined to be 4393 cycles from the STK eclipse analysis, which is 40% for Lithium-ion batteries [75].

$$C = \frac{T_e * P_e}{\eta * DOD} \quad (7.6)$$

Using the eclipse times and power required in eclipse for the low-thrust phase and cycler orbit phase, the energy storage capacity required is 33.9 Wh and 118.3 Wh, respectively, including 20% margin. Therefore, the batteries must be sized for cycler orbit phase. However, because the 118.3 Wh is only required for eight orbits and only 25 orbits are above 115.0 Whr of required energy storage, it was assumed communications could be avoided for this 0.6% of eclipses. A summary of the battery sizing parameters and results are listed in Table 7-4.

**Table 7-4: Battery sizing parameters and results.**

	<b>Low-Thrust</b>	<b>Cycler</b>
<b>Eclipse Time</b>	0.87 hrs	1.62 hrs
<b>Eclipse Power with 20% Margin</b>	14.9 W	27.4 W
<b>Energy Storage Capacity</b>	33.9 Wh	118.3 Wh

A survey of battery technology available was performed, again pulling state-of-the-art products covered in NASA’s Small Spacecraft Technology Report; these are listed in Table 7-5. A high specific energy is desirable as a higher energy density reduces mass. Lithium-ion batteries are the higher performing of the surveyed options and have flight heritage. As they were the highest performing and are designed for CubeSat application featuring stackable electronics and built-in

heaters, the GomSpace NanoPower BP4 and BPX were baselined. The BP4 has 38.5 Wh energy storage and the BPX has 77 Wh; using the stackable interface, these can be combined to obtain a total of 115.5 Wh. With the BPX in a 4S-2P configuration and the BP4 in a 4S-1P, the battery capacity is 5.2 Ah and 2.6 Ah respectively, corresponding to a output battery voltage of 14.8 V [78, 79].

**Table 7-5: Surveyed battery technology [56].**

Product	Manufacturer	Specific Energy (Wh/kg)	Cell Type	TRL
40Whr CubeSat Battery	AAC Clyde	119.0	Li-Polymer	9
BAT-100	Berlin Space Technologies	58.1	Li-Fe	9
BP-930s	Canon	132.0	4 18650 Li-ion cells	9
COTS 18650 Li-ion Battery	ABSL	90.0-243.0	Sony, Molicell, LG, Sanyo, Samsung	8
NanoPower BP4	GomSpace	143.0	Li-ion	9
NanoPower BPX	GomSpace	154.0	Li-ion	9

#### **7.4 Power Management and Distribution System Selection**

To manage the power flow from the solar arrays and batteries to components, a power management and distribution (PMAD) system is needed. This system regulates and converts voltages and protects against overcurrent events that could damage components. Power distribution systems were surveyed from NASA’s 2018 Small Spacecraft Technology Report. Of the surveyed systems, many were sized for 1U-3U missions or for satellites larger than 27U. Of the remaining systems, few were commercially available and had available data sheets. Therefore, due to its flight proven status and compatibility with the baselined NanoPower BPX and BP4 battery packs, the GomSpace NanoPower P60 Dock was chosen. The standard configuration for this dock includes an Array Conditioning Unit (ACU) and Power Distribution Unit (PDU). It is a high capacity power supply, compatible with a the battery output voltage of 14.8 V [80, 81, 82].

## 7.5 Power Subsystem Summary

A summary of the power subsystem including the solar arrays, batteries, and PMAD unit is listed in Table 7-6, with mass and volume being used to inform configuration in Chapter 10. As the system is sized for the high-power low-thrust phase, there is excess power during the cycler orbit. This design allows for ~13 W to ~38 W of power to be available to an additional payload during the cycler orbit phase, corresponding to orbit maintenance and standby modes, respectively. If not used for the payload, this excess power becomes heat that will need to be managed which could be done by rotating the solar panels away from the Sun or could be leveraged as a heater. As the thermal subsystem was investigated last, the batteries are not sized for the additional heater power required in the worst cold case cycler orbit eclipse. Possible solutions maintaining the current design are discussed in Chapter 12.

**Table 7-6: Power subsystem summary.**

<b>Required Solar Panel Area</b>	0.82 m <sup>2</sup>
<b>Required Energy Storage</b>	118.3 Whr
<b>Battery Mass</b>	0.76 kg
<b>Battery Volume</b>	0.51 U
<b>Battery Capacity</b>	115.5 Whr
<b>Solar Cells</b>	XTJ 30.7%, rectangular 27 cm <sup>2</sup>
<b>Solar Panel Configuration</b>	Dual single-axis articulated wings; 18 2 x 9 cell panels
<b>Solar Panel Mass</b>	1.50 kg per wing
<b>Solar Panel Stowed Volume</b>	3.63 U
<b>PMAD Mass</b>	0.19 kg
<b>PMAD Volume</b>	0.07 U

## 7.6 Power Subsystem Results in Relation to CPCL

Solar cells used on CPCL busses have all been body mounted and include SpectroLab's UTJ and TASC cells (28.3% and 27% efficient, respectively) and the baselined XTJ cells. Deployable

hinged solar arrays will be necessary to achieve the required power and as CPCL has only done deployments of antennas not utilizing hinges, this would be a new area of expertise to develop. Battery packs have utilized COTS batteries including Rose Lithium-ion 4400 mAh with 4 1S-2P packs stacked for a total of 65 Wh at 3.7 V (ExoCube), and more recently Tenergy 2600 mAh Lithium-ion batteries with a nominal voltage of 4.2 V for a total of 37.4 Wh (ADE) [49]. The electrical power system control board is part of the CPCL System Board, providing regulated 3.3 V and 5 V and providing protection circuitry for charging and discharging of the batteries. Not much development is needed here as use of COTS batteries and custom battery brackets has been proven capable in interplanetary environments as shown by MarCO. However, the power subsystem needs to be designed to handle the higher voltage due to the large solar arrays and the mixture of high power and low power commercial components resulting in various input and output voltages. To account for the higher power throughput, distribution, and variation in voltages, a redesign of the battery board will be required.



## Chapter 8

### ATTITUDE DETERMINATION AND CONTROL SYSTEM

As a spacecraft performing thrust maneuvers over a significant period of time, requiring continuous large amounts of power, and needing to maintain a communications link to downlink data, this mission requires an active attitude determination and control system to point solar arrays, an antenna, and thrusters. The spacecraft will also have to perform orbit maintenance maneuvers which require knowledge of the satellite's attitude to create the desired thrust vector. In this chapter, the pointing requirements are derived to determine required sensor performance and reaction control capability needed to counteract orbital perturbations. The selected subsystem solution used to continue the baseline is summarized and compared to CPCL's current and planned ADCS capabilities.

#### 8.1 Attitude Control Requirements

For this mission, attitude control requirements will come from pointing knowledge and accuracy and disturbance rejection; these values come from counteracting orbital perturbations, pointing the antenna at Mars, and pointing the solar arrays at the Sun. For pointing the antenna, it was assumed that it would remain inertially pointed, with the pointing requirement derived from the beamwidth of the antenna. For the selected UHF antenna, this beamwidth is  $\pm 30^\circ$ . In order to maintain the link, the pointing requirement is  $10^\circ$ , as derived in Chapter 6. As power generation is a driver due to the electric propulsion system and the solar panels are assumed to maintain pointing for maximum power generation, the allowable angle the panels are off Sun-pointing in addition to the worst-case Mars-Sun beta angle loss before consuming the 20% margin in the power budget was determined. Using Equation (8.1), where  $P_i$  is required power without margin,  $P_m$  is required power with 20%

margin in W, and  $\theta$  is the angle between the normal of the solar arrays and incident solar rays in degrees, the angle to consume 20% of the margin in the most power stringent mission phase was determined.

$$\theta = \cos^{-1}\left(\frac{P_i}{P_m}\right) \quad (8.1)$$

For the required pre-margin power of 76.2 W and 91.4 W with 20% margin, the maximum off-Sun pointing is 33.5°. In the worst-case beta angle of 25.2°, the maximum allowed off-pointing becomes the difference of the two at 8.3°. The BIT-3 can gimbal, controlling the thrust vector within ±10° in two directions; therefore, the spacecraft’s attitude must be known within 10° in order to use the gimbal to maintain the thrust vector direction. The camera has a wide field of view at 194° x 142°, imposing less strict pointing than the antenna and solar panels. Even applying the recommended optical instrument pointing requirement from [75] as 10% of the swath width, this is still greater than the antenna and solar panel pointing requirements at 14.2°. Considering these pointing requirements, the tightest is the 8.3° derived from the solar array pointing; this is the minimum accuracy that will be required by attitude sensors. Table 8-1 summarizes the required pointing accuracies of the antenna, solar array, BIT-3, and camera.

**Table 8-1: Required pointing accuracy for components.**

<b>Component</b>	<b>Pointing Requirement</b>
<b>UHF Antenna</b>	10.0°
<b>Solar Array</b>	8.3°
<b>BIT-3</b>	10.0°
<b>Camera</b>	14.2°

## 8.2 Attitude Sensors

To be able to determine the spacecraft attitude, the following sensors can be used: sun sensors, magnetometers, horizon sensors, and star trackers. For the required accuracy of  $8.3^\circ$ , sun sensors, magnetometers, and horizon sensors were investigated. Magnetometers are not applicable as Mars does not have a global magnetic field but rather multiple weak local fields [83]. Though Mars will be taking up a large portion of the field of view of the spacecraft, horizon sensors operate by using IR horizon radiance models of a planet's atmosphere to trigger. These are commercially available for Earth but would require modification and use of a Mars radiance model which would differ significantly due to the difference atmospheric compositions, density, and height of Mars' atmosphere [84]. Additionally, these sensors are calibrated for a specific altitude; the altitude in the low thrust phase is constantly increasing and the altitudes in the initial orbit and cycler orbit differ; horizon sensors can therefore not be considered for the studied case. For course attitude determination, this leaves sun sensors. Sun sensors are cost-effective and low power, allowing use of multiple units on various spacecraft faces and can provide accuracy ranging from  $0.005^\circ$  for fine sensors to  $3^\circ$  for coarse [75]. From the survey of NASA's report on small satellite state of the art sun sensors, the coarse analogue of the New Space Systems Fine digital sun sensor, the NCSS-SA05, was chosen due to its TRL of 9, documented radiation tolerance, and low mass. Full sky coverage can be achieved with one of these sensors on each face of the CubeSat, for a total of 6 sun sensors [84, 85]. The specifications of this sensor are listed in Table 8-2. A major drawback of sun sensors is that they are not useful in eclipse. In eclipse, the remaining options for attitude determination are gyroscopes (or when combined with an accelerometer, an inertial measurement unit (IMU)) and star trackers. Gyroscopes provide relative data, measuring angular rotation from an initial reference; they cannot provide an absolute reference. A gyroscope can be added as a complement to sun sensors to maintain knowledge of the spacecraft's attitude through eclipse. Gyroscopes are also subject to drift bias over time. Drift bias is characterized and specified by the

manufacturer but can still cause errors over a long period of time. A common practice to augment a gyroscope’s high frequency measurements is to include a star tracker for low frequency measurements to correct for this drift over time [75]. This was the method adopted for this mission. Surveying the high TRL gyroscopes and star trackers showed similar mass, power, and performance for all. For selection of star tracker, the MAI-SS Space Sextant was chosen due to its high radiation tolerance. Though it has higher performance than required, it is only 150 g more massive than the lowest accuracy option for roughly the same power consumption [86, 87]. For the gyroscope, the lowest mass TRL 9 option for a 3-axis MEMS gyroscope was chosen. This was the ADIS16405 IMU from Analog Devices, which also includes an accelerometer [88]. The performance and physical parameters of the selected attitude sensor suite are listed in Table 8-2.

**Table 8-2: Physical and performance parameters of selected ADCS components.**

<b>Sensor Type</b>	Star Tracker	Sun Sensor	IMU
<b>Sensor Name</b>	Maryland Aerospace MAI-SS Space Sextant Star Tracker	New Space Systems NCSS-SA05	ADIS16405
<b>Quantity</b>	1	6	1
<b>Mass</b>	0.282 kg	0.005 kg	0.016 kg
<b>Volume</b>	0.250 U	0.002 U	0.027 U
<b>Power</b>	1.000 W	0.038 W	0.350 W
<b>Accuracy</b>	0.008 deg	0.500 deg	0.007 °/s

### **8.3 Reaction Control Actuation**

In orbit, the CubeSat will experience solar radiation pressure, gravity gradients, and drag during the low thrust phase. These external forces cause torques on the spacecraft that need to be counteracted to maintain an attitude and need to be quantified to size a reaction control system. In addition to counteracting perturbations, a reaction control system is needed to slew to maintain a communications link. Worst cases were assumed for the following analyses due to the various regimes over a long mission duration. Internal disturbance torques due to sources such as thruster

misalignment, reaction wheel friction, dynamics of the solar panels, and thermal effects were assumed negligible due to the small size of the CubeSat.

To determine the torque created about the center of mass due to solar radiation pressure, Equation (8.2) was used where  $\phi$  is the solar constant at Mars which is  $608 \text{ W/m}^2$  (calculated in Chapter 1),  $c$  is the speed of light which is  $3 \times 10^8 \text{ m/s}$ ,  $A_s$  is sunlit area in  $\text{m}^2$ ,  $q$  is the reflectance factor,  $C_{ps}$  is the center of pressure in m,  $CM$  is the location of the center of mass in m, and  $\varphi$  is the Sun incidence angle in degrees. The reflectance factor was assumed to be 0.6, an average between the highly reflective bus and the highly absorptive solar panels [75]. For the worst-case solar pressure case defined here, the sun incidence angle is  $0^\circ$ .

$$T_s = \frac{\phi}{c} A_s (1 + q) (C_{ps} - CM) \cos(\varphi) \quad (8.2)$$

To determine the torque created due to gravity gradients, Equation (8.3) was used where  $\mu$  is Mars' gravitational constant of  $42828 \text{ km}^3/\text{s}^2$ ,  $r$  is orbital radius in km,  $I$  is the inertia of the spacecraft in  $\text{km}^2$ , and  $\theta_g$  is the moment of inertia imbalance between the inertially pointing axis and the local vertical in degrees.

$$T_g = \frac{3\mu}{2r^3} |I_z - I_x| \sin(2\theta_g) \quad (8.3)$$

To complete the perturbational analysis, the drag encountered during the low-thrust phase was determined using Equation (8.4), the aerobraking drag model to determine the density in  $\text{kg/m}^3$ ,  $\rho$ , of the atmosphere at an altitude of 7 km and above, and Equation (8.5) to determine the torque due to drag [89]. In Equation (8.4),  $h$  is the altitude in m; in Equation (8.5),  $C_d$  is the drag coefficient,  $A_r$  is the cross sectional area in the ram direction in  $\text{m}^2$ ,  $V$  is the spacecraft's orbital velocity in m/s, and  $C_{pa}$  is the center of aerodynamic pressure in m. As the drag is most significant during the low-

thrust phase,  $V$  can be determined by Equation (8.6), the velocity of an object in a circular orbit where  $\mu$  is Mars' gravitational constant and  $r$  is the orbital radius in km. The drag coefficient was assumed to be 2.0, the lower end of the common drag coefficients of spacecraft [75].

$$\rho = \frac{0.699 * \exp(-0.00009 * h)}{0.1921 * (-23.4 - 0.00222 * h + 273.1)} \quad (8.4)$$

$$T_d = 0.5 * \rho * C_d * A_r * V^2 * (C_{pa} - CM) \quad (8.5)$$

$$V = \sqrt{\frac{\mu}{r}} \quad (8.6)$$

These disturbances together form a total disturbance torque,  $T_{tot}$ . The torque that the reaction control system must reject is  $T_{tot}$  in N, plus 20% margin. In order to calculate these disturbances, the configuration of the spacecraft needs to be known to obtain sunlit and ram areas as well as the moment of inertia matrix, center of mass, and center of pressure. Though this process was initially done using estimates from other deep space CubeSat designs and updating values as the design progressed, the analysis presented here is of the final design. The center of mass and inertia matrix were determined using the SolidWorks Mass Properties tool after ensuring all components were modelled with the correct mass properties corresponding to Table 10-2. The discussion of the center of mass and inertias will be presented in Chapter 10.

Here, the resulting values relevant to determining ADCS component requirements are presented with axes corresponding to the presented CAD models of the baseline with the origin at the rail corner where the -X, -Y, and +Z faces meet. Two deployed configurations were identified that result in the largest cross-sectional ram and sunlit areas and therefore worst-case drag and solar radiation pressure disturbance torques, one in which the solar panel surface is flush with the +Y face of the CubeSat and one in which they are rotated 90° about the X-axis (referred to as the “perpendicular” case). The mass and area properties of both cases were analyzed in SolidWorks

using the Mass Properties tool (this methodology is explained in Chapter 10) with the results listed in Table 8-3; there is not a significant difference between the configurations in terms of center of mass and inertia with 1 mm difference in the X-axis center of mass location and 0.056 kg·m<sup>2</sup> difference in moments of inertia about the X and Y axes.

**Table 8-3: Mass and area properties of deployed configurations.**

	<b>Flush</b>	<b>Perpendicular</b>
Center of Mass	[0.115 0.232 0.107] m	[0.116 0.232 0.107] m
Principal moments of inertia at CM	$\begin{bmatrix} 2.284 & 0 & 0 \\ 0 & 1.973 & 0 \\ 0 & 0 & 0.574 \end{bmatrix} kg * m^2$	$\begin{bmatrix} 2.340 & 0 & 0 \\ 0 & 1.917 & 0 \\ 0 & 0 & 0.574 \end{bmatrix} kg * m^2$
Maximum Center of Pressure displacement from CM	[0.002 0.00 0.006] m	~ [0.00 0.203 0.007] m
Maximum ram area	1.191 m <sup>2</sup>	0.051 m <sup>2</sup>
Maximum sunlit area	1.191 m <sup>2</sup>	1.243 m <sup>2</sup>

To obtain the maximum disturbance torque, the 300 km initial orbit altitude in the low-thrust phase was used for drag and gravity gradient disturbances. As the gravity gradient torque is caused by an offset of the inertially pointing axis, in this case the Z-axis, and the local vertical, causing a torque about the Z or Y-axis, the Z and X components of the principal moment of inertia are used in the calculation as the Z-axis is the minimum principal axis and will therefore result in the greater difference; the “flush” case was used as this would result in the maximum inertia difference. The angle of offset was taken to be 1° as the moments of inertia are well balanced [75]. For drag area, 1.19 m<sup>2</sup> was used as it is the larger of the considered configurations; for sunlit area for solar radiation pressure, 1.24 m<sup>2</sup> was used. For the maximum solar radiation pressure, the difference between the center of pressure and the center of mass corresponding to the largest area was used which was the “perpendicular” case. Similarly, the difference in center of pressure and mass used for drag was the one corresponding to the largest ram direction, the “flush” case. The resulting

worst-case disturbance torques are listed in Table 8-4. These disturbance torques are on the order expected for a small satellite considering the orbit altitude and low-density of the Martian atmosphere [75].

**Table 8-4: Worst case disturbance torques.**

<b>Solar Radiation Pressure</b>	8.16 x 10 <sup>-7</sup> Nm
<b>Drag</b>	2.18 x 10 <sup>-9</sup> Nm
<b>Gravity Gradient</b>	7.59 x 10 <sup>-8</sup> Nm
<b>Total</b>	8.89 x 10 <sup>-7</sup> Nm
<b>Total with 20% Margin</b>	1.07 x 10 <sup>-6</sup> Nm

Another consideration is the slew rate that must be achieved to maintain the communications link. This rate was determined by using STK to find the flight path angle range of the spacecraft during the period of time the spacecraft is within 13000 km slant range of MRO corresponding to the “close approach” of the CubeSat as explained in Chapter 6; this was determined to be 46° over 3 hours and 40 mins. Therefore, the maximum required slew rate is 0.003 °/s. The torque required to achieve this slew rate is dependent on the spacecraft’s inertia about the slew axis. To calculate this torque, Equation (8.7) is used, where  $\theta$  is the slew angle in radians,  $I$  is the inertia about the slew axis in kg-m<sup>2</sup>, and  $t$  is the slew time in seconds.

$$T = \frac{4\theta I}{t^2} \quad (8.7)$$

For a 46° slew over 3 hours and 40 mins, with the Z-axis as the slew axis, the required slew torque is 9.66 x 10<sup>-9</sup> Nm. As the total disturbance torque with margin and the slew rates are within the range of reaction wheel control at much less than 1 Nm and <0.05 °/s, these were baselined as



the reaction control actuator [75]. The primary parameters for sizing reaction wheels are the maximum required slew torque and the total momentum storage to counteract disturbance torques. Momentum storage requirements for reaction wheels,  $h_{mom}$  in Nms, can be approximated using Equation (8.8) which integrated the total disturbance torque,  $T_{tot}$ , over the orbital period in seconds,  $P$ . This equation is an approximation and assumes the maximum torque builds up over a quarter of an orbit and so 0.707 is the root mean square average of a sinusoidal function [75].

$$h_{mom} = \frac{T_{tot} * P * 0.707}{4} \quad (8.8)$$

Using  $1.07 \times 10^{-6}$  Nm as the worst-case torque with margin and the maximum period of all phases, which occurs in the cycler orbit, the required momentum storage was calculated to be 0.0125 Nms. The derived reaction wheel requirements are a torque rating of at least  $1.07 \times 10^{-6}$  Nm and momentum storage capacity of 0.0125 Nms; these requirements are summarized in Table 8-5.

**Table 8-5: Derived reaction wheel performance requirements.**

<b>Disturbance Rejection Torque with Margin</b>	$1.07 \times 10^{-6}$ Nm
<b>Slew Torque with Margin</b>	$1.16 \times 10^{-8}$ Nm
<b>Momentum Storage with Margin</b>	0.0125 Nms

A survey of reaction wheels for CubeSats showed these requirements are within commercially available component capability. Of these, Sinclair Interplanetary offers 10 to 60 mNms capacity reaction wheels with TRLs of 9 that are designed to tolerate 20 krad while maintaining low mass and power. The RW-0.03 wheel was chosen as a baseline as its nominal momentum storage satisfies the momentum capacity requirement and provides torque from 0.5 to 2 mNm. To have 3-axis

stabilization, which is required to point the arrays and antenna while resisting perturbations, 3 reaction wheels are required at a minimum, one in each axis, though more can be added for redundancy. The specifications of the chosen wheel are summarized in Table 8-6. The momentum can be dumped by the BIT-3 whose  $\pm 10^\circ$  gimbal at a distance of 227 mm from the center of mass can impart a moment of 0.148 to 0.193 mNm for power inputs ranging from 54 to 60 W. Using the lower power consumption, a saturated momentum wheel with 0.04 Nms can be dumped in 26 minutes. Alternatively, the MPS-135 thrusters can be used with a moment arm of  $\sim 10$  cm; at 0.25 N, the reaction wheels can be fully desaturated in 1.6 s. Depending on the mission phase and available power, the appropriate desaturation method can be chosen.

**Table 8-6: Baselined reaction wheel performance and physical parameters.**

<b>Reaction Control Actuator</b>	Sinclair Interplanetary RW-0.03
<b>Momentum</b>	0.03 Nms nominal, 0.04 Nms peak
<b>Torque</b>	0.5 mNm at 0.04 Nms, 2 mNm at 0.02 Nms
<b>Mass</b>	185 g
<b>Volume</b>	0.1 U
<b>Power</b>	0.1 W at 0.01 Nms, steady state 0.3 W at 0.04 Nms, steady state

#### **8.4 ADCS Subsystem Results in Relation to CPCL**

ADCS system designs have included magnetometers and magnetorquers with solar angle sensors. Sinclair reaction wheels have interfaced with the CPCL System Board vis I<sup>2</sup>C connection. Lab ADCS software has been implemented to perform Sun ephemeris calculations, reference frame conversion, and references to magnetic field models with a Kalman Filter to determine attitude and body rates. For position, software uses an orbital propagator and TLE uploaded from the ground station; drivers for the reaction wheels and magnetorquers have also been developed. The CPCL

ADCS software has been successfully flown in ExoCube which possessed both passive stabilization using gravity gradient booms and active control using reaction wheels [18]. Star tracker software, designed to be used with COTS cameras, has been developed by students in collaboration with CPCL. The performance of the commercially available star trackers is much higher than required for this concept, adding unnecessary SWaP consumption. Further development of an in-house star tracker could reduce SWaP for missions with lower sensor accuracy requirements.

The primary actuators used by past CPCL missions would not apply to this mission concept; magnetorquers, such as those used by IPEX would not prove useful as Mars' gravitational field is weak [18]. Gravity gradient booms, successfully implemented on ExoCube and on ExoCube II which has not yet launched, only allow pointing in the local vertical with limited maneuverability and the stabilizing torques decrease with the cube of the orbit radius, making it ineffective in the cyclor orbit even if other pointing requirements were not applied. Necessary for this mission concept, reaction wheels will likely be needed on capable missions in higher Mars orbit, either to point for communications such as in the relay or DTE architectures explored, point solar arrays, or track objects for science purposes. There is precedent for university development of low-cost reaction wheels for small satellites as outlined in a student project from George Washington University [90]; this could serve as a starting point for CPCL investigation.

## Chapter 9

### COMMAND AND DATA HANDLING SUBSYSTEM

To process commands, control the spacecraft's subsystems, and store data after science phases until data can be downlinked, a C&DH system is needed. The main considerations for determining the C&DH system are memory storage and interfaces. Much of the performance of a C&DH computer is dependent on the implemented software which is out of the scope of this thesis. Memory storage is important in case of loss of communications so that science data can be sent once a link is established without loss of data. As the C&DH system will be controlling all other subsystems, it needs to be fault tolerant, especially to radiation, which can cause logic flips. In this chapter, memory storage requirements will be derived, and commercial processors traded. The selected subsystem solution used to continue the baseline is summarized and compared to CPCL's current and planned C&DH subsystem capabilities.

#### 9.1 Memory Storage

Per the objective to be able to store four weeks of data, the memory storage must be able to store seven days of radiation data and images from two Phobos passes. The radiation sensor records 119 bytes per minute which results in 9,596,160 bits per week or ~1.2 MB. The 2 MP camera has a maximum resolution of 1632 x 1232 pixels. A black-and-white image has 1 byte/pixel while a color image pixel has 3 B. Taking a single-color high resolution image per pass as the minimum requirement, the C&DH system must store 96,509,952 bits of image data per week, or ~12 MB. For four weeks, the total data storage required is at least ~53.1 MB, or 63.4 MB with 20% margin.

Estimating code storage is not as straightforward as data as it depends on the software used. As a minimum, the MarCO onboard computer (OBC) system was used to determine the memory

needed for code storage and execution. MarCO used an AstroDev LLC MSP430F2618 OBC with 128 kB of flash storage and 8 kB of RAM. These can be taken as a minimum for non-payload data storage as MarCO was autonomous in that it determined its attitude and maintained a trajectory from Earth to Mars; according to [75], ADCS code is the largest contributor to source code line count and therefore code memory. This can be analogous to the long-term attitude determination and control autonomy that will be required of this mission concept to perform orbital maneuvers and control its attitude.

Most high TRL systems that were surveyed surpassed these minimum storage requirements for data and code causing the trade to come down to mass and power. The surveyed TRL 9 systems are listed in Table 9-1. The ISIS OBC was chosen due to its high storage capacity in RAM, 4 GB of data storage which in SD card format can be reduced or expanded as needed and has sufficient flash memory for code. None of the OBC systems had physical radiation mitigation, though the large code capacity of the ISIS OBC allows for EDAC algorithms to be implemented in addition to the included watchdog timers for fault detection. This computer also features a range of interfaces including general purpose input/output pins (GPIO), UART, and an image sensor interface, facilitating compatibility with a range of components. The performance and physical parameters of the selected OBC are summarized in in Table 9-2.

**Table 9-1: Surveyed C&DH systems [56]**

<b>Product</b>	<b>Manufacturer</b>	<b>TRL</b>	<b>RAM</b>	<b>Flash Memory (Data)</b>	<b>Flash Memory (Code)</b>	<b>Power (W)</b>	<b>Mass (g)</b>
Nanomind A712D	GomSpace	9	2 MB SRAM	4 MB	4 MB	0.3	55
ISIS OBC	ISIS	9	64 MB DRAM	4 GB (SD cards) 256 kB FRAM	1 MB	0.4	100
Q5, Q6, Q7	Xiphos	9	768 MB SRAM	64 GB (microSD cards)	128 MB	1.0	32
NanoMind A3200	GomSpace	9	32 MB DRAM	128 MB	512 KB	1.0	24

**Table 9-2: Baselined C&DH system summary.**

<b>Selected OBC</b>	ISIS OBC [91]
<b>Processing RAM</b>	64 MB
<b>Code Memory</b>	1 MB Flash
<b>Data Memory</b>	4 GB (2 2 GB SD cards), 256 kB FRAM
<b>Mass</b>	0.1 kg
<b>Volume</b>	0.1 U
<b>Power</b>	0.7 W

## **9.2 Command and Data Handling Subsystem Results in Relation to CPCL**

CPCL uses an in-house System Board, which has been commercialized as the Tyvak Intrepid Board, with 32 MB memory for critical flight software storage, a microSD for data storage, and 300 mW in highest power state. Flight software (FSW) has included controlling and responding to radio, data logger, ADCS, and system managers for processes including transmitting data, processing incoming commands, storing and exporting data, activating ADCS and gathering

position, attitude, and body rates; for CPCL missions, ~90% of software is reused. As new drivers for the baselined components will need to be developed, less software will be able to be reused. Where possible, more autonomy, onboard processing, and error detection and correction to protect against radiation effects should be considered in development.

## Chapter 10

### SPACECRAFT CONFIGURATION

The primary driver of the configuration is the objective to adhere to a CubeSat specification and in turn be compatible with standard deployers. As previously mentioned, there are few published standards of larger CubeSat deployers (12U+). The EXOpod from EXOlaunch was the only available detailed specification for 16U. During the propulsion subsystem design, it was found that the systems needed to achieve the delta-V would not fit into a 12U form factor. This was due to interference of the solar panels and the required placement of the propulsion modules to act through the center of mass. Increasing the form factor to a 16U allows the solar panels to become longer and therefore store thinner by removing a folded panel and hinge on each wing. Though the smaller cross section of the 16U is the same as a 12U (~20 cm x 20 cm), thinning the solar panel stowage allows the propulsion modules to fit within the center of this bus. Increasing the length of the bus by 1U also allows more room for a payload. Care in configuration also needs to be taken to ensure that after deployment and propellant expenditure the center of mass remains in a favorable location for orbit transfers and maintenance maneuvers. The EXOpod 16U specification, configuration process, and resulting baseline configuration will be presented in this chapter. The baseline configuration will then be compared to CPCL's current and planned structure sizes and mechanisms. This chapter also includes mass and volume budgets as well as a discussion of the payload hosting capabilities of the baseline.

#### 10.1 EXOpod 16U Specification

The EXOpod specification states that many of the general requirements of the CubeSat to be deployed are provided in the CDS Rev 13. However, the EXOpod deployer allows the CubeSat to



exceed some of the constraints of the CDS. An example is the nearly double usable volume that is allowed between the CubeSat rails and the walls of the deployer; the CDS allows 6.5 mm while EXOpod allows 11.2 mm. CubeSat features can be any shape and size within the envelope but cannot exceed the envelope. The EXOpod also allows extra usable tuna can volume that extend into the springs of the deployer. An additional constraint is the rails must be hard anodized Aluminum 7075, 6061, 5005 and/or 5052 to prevent cold welding and rail surface degradation due to vibration during launch.

Figure 10-1 shows the EXOpod's allowable dimensions in relation to the rails; it also shows the tuna can dimensions in relation to the main bus structure with axes corresponding to the presented CAD models. The gray and yellow portions are usable volume while red denotes the rails which contact the deployer. The maximum CubeSat dimensions for a 16U are listed in Table 10-1. The specification states the maximum mass for a 16U is 24 kg, however, CDS Rev 14 allows up to 2 kg per U. Therefore, the specification was primarily used for spatial dimensions. Maximum allowable mass was assumed to 32 kg as it is more realistic to get a waiver for mass than for a custom deployer volume and/or shape. Tuna cans were not utilized for this design, but their detailed dimensions are included in Appendix C.

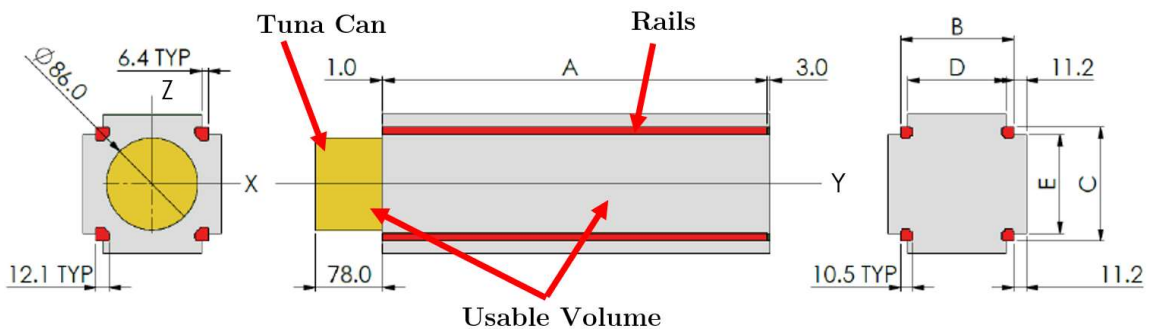


**Figure 10-1: Maximum allowable outer dimensions for CubeSats launched in an EXOpod with additional dimensions listed in Table 10-1 [26].**

**Table 10-1: EXOpod Allowed Maximum Dimensions with Axes Referring to Figure 10-1 [26].**

<b>Dimension</b>	<b>Letter on Figure 10-1</b>	<b>Value</b>
<b>CubeSat Rail Length (Y)</b>	A	454.00 mm
<b>CubeSat Rail Length (X)</b>	B	226.30 mm
<b>CubeSat Rail Length (Z)</b>	C	226.30 mm
<b>Maximum Space Between Rails (X)</b>	D	213.50 mm
<b>Maximum Space Between Rails (Z)</b>	E	213.50 mm
<b>Number of Tuna Cans</b>	-	5
<b>Distance Between Tuna Cans</b>	-	126.30 mm
<b>Maximum Distance Between CG and Geometric Center</b>	-	20.00 mm
<b>Rail Parallelism</b>	-	0.05 mm
<b>Surface Roughness</b>	-	1.60 $\mu\text{m}$

## 10.2 Mass Budget

During the configuration process, mass is important to consider as some components are more massive than others, having a greater effect on the location of the center of mass and resulting moments of inertia about it. Taking all the components selected through the processes explained previously, mass and volume of each were taken from data sheets and summed as shown in Table 10-2.

Some components did not have data sheets or required extrapolation from existing data from models. The antenna mass and volume were determined from a 4% volume figure provided in a description of the MarCO reflectarray antenna and scaled to the size of the UHF deployable antenna [33, 35]. The propellants and ISIS daughterboard have no volume as they are included in the dimensions of the thrusters and OBC, respectively. The solar panel mass was taken from the eHAWK 27AS112 data sheet, which utilizes the selected SpectroLab XTJ cells, with listed energy per mass ranging from 97 to 121 W/kg for standard to high performing systems [92]. As the solar

panel design was extrapolated from these systems, an average of the standard and high-performance systems was used to scale to the panel size, which is sized to allow 324 cells (but with only 303 populated). The ratio of the designed panel wattage to the eHAWK panel wattage at Earth is  $324 \text{ W}/112 \text{ W}$ , or 2.9. Multiplying this ratio by the average of the masses of the eHAWK 27AS112 panels results in a mass of 3 kg total, or 1.5 kg for each wing. Harnessing was assumed to be 1.1 kg using the mass predictions for a planetary mission in [75], which suggests using 21% of dry mass to estimate the power system including harnessing. Using this estimate for a 23.1 kg dry mass and subtracting the power system mass leaves 0.9 kg, or 1.1 kg with 20% margin. The density of Al6061,  $2700 \text{ kg/m}^3$ , was used to obtain mass estimates of bus panels assuming a 3 mm thickness for radiation shielding (explained in Chapter 11); these masses will be less considering the cutouts for thrusters, camera, and star tracker. The structure mass and volume were obtained using the published mass of the ISIS 16U bus including a primary and secondary structure; the volume was obtained from the density of the structure [91].

The propulsion system mass and volume fractions seem quite large for a CubeSat at ~46% and 50%, respectively, but for the propulsive capabilities the satellite possesses, it scales with other satellites. It is difficult to compare the propulsion subsystem mass and volume fractions to standard satellite missions, such as those listed in [75], due to the CubeSat scale; a planetary mission is listed as an 11% expected mass fraction. As propulsion is not common in CubeSats yet, only MarCO and some mission concepts such as MARIO from Politecnico di Milano are available for comparison. MarCO, for example, had a 40 m/s delta-V capable cold gas system used only for trajectory correction maneuvers that used 33% of the volume and 30% of the mass [93, 28]. The MARIO design, with a combined chemical and electric propulsion system for a standalone Earth-escape to Mars mission has a propulsion subsystem designed for a total 445 m/s delta-V with a mass fraction of ~50 % and volume of ~66 % [94]. Slight mass reduction could be done by not filling the MPS-135 to its full 6.9 kg capacity as only 6.2 kg including 20% margin is required; this was not implemented in this design but could be investigated in further iterations.

**Table 10-2: Mass and volume budget (U = 1000 cm<sup>3</sup>).**

	Quantity	Mass/ Unit (kg)	Total Mass/ Component (kg)	Volume/ Unit (U)	Total Volume/ Component (U)
<b>Propulsion</b>					
BIT-3	1	1.40	1.40	1.60	1.60
<i>Propellant</i>	1	2.14	2.14	-	-
MPS-135	1	4.30	4.30	6.00	6.00
<i>Propellant</i>	1	6.90	6.90	-	-
<b>Communications</b>					
UHF Radio	1	0.05	0.05	0.02	0.02
UHF Antenna	1	0.25	0.25	0.57	0.57
<b>Payload</b>					
Camera	1	0.05	0.05	0.02	0.02
Radiation Sensor	1	0.03	0.03	0.02	0.02
<b>CDH</b>					
OBC	1	0.08	0.08	0.11	0.11
<i>OBC Daughterboard</i>	1	0.02	0.02	incl.	incl.
<b>ADCS</b>					
Reaction Wheels	3	0.19	0.56	0.10	0.30
Sun Sensors	6	0.01	0.03	0.00	0.01
IMU	1	0.02	0.02	0.03	0.03
Star Tracker	1	0.28	0.28	0.25	0.25
<b>Power System</b>					
Power Board	1	0.08	0.08	0.03	0.03
BP4 Battery Pack	1	0.26	0.26	0.18	0.18
BPX Battery Pack	1	0.50	0.50	0.33	0.33
ACU	1	0.05	0.05	0.03	0.03
PDU	1	0.06	0.06	0.01	0.01
Solar Panel	2	1.50	3.00	1.81	3.63
SADA	1	0.18	0.18	0.07	0.07
Harnessing	1	1.10	1.10	0.75	0.75
<b>Thermal</b>					
Heaters	1	0.10	0.10	0.07	0.07
Heat switches	3	0.10	0.30	0.00	0.01
Thermal straps	3	0.18	0.54	0.06	0.18
MLI	1	0.10	0.10	0.00	0.00
<b>Structure</b>					
8U Panel, 3 mm thick	4	0.43	1.73	0.16	0.64
4U Panel, 3 mm thick	2	0.22	0.43	0.08	0.16
Structure	1	2.25	2.25	0.83	0.83
Radiation shielding	1	0.19	0.19	0.07	0.07
<b>Total</b>			<b>26.98</b>		<b>15.86</b>

### 10.3 Configuration Process

A custom structure using EXOpod's allowable rail dimensions and relations was created in SolidWorks with a simple support structure that breaks the bus into two 4U platforms and one 8U platform. Where available, the manufacturer-provided CAD models of selected components were used, else datasheet specifications were used to create boxes of outer dimensions; all components were placed into an assembly to determine possible configurations within the structure envelope. Each component was inspected to ensure the correct mass properties corresponding to Table 10-2 were applied to obtain estimations of the center of gravity location and moments of inertia.

A major driver of the configuration after the envelope is the need to place the propulsion systems such that they act through the center of mass as an offset would induce an unwanted moment. This is complicated by the inclusion of two different propulsion units that will be used at different phases of the mission. Because the BIT-3 is used for a long period of time (1.6 years during the low thrust phase), plume impingement on the solar panels is a concern. To avoid this, the BIT-3 was placed at the bottom of the structure, directing the ion exhaust away from the solar arrays. Placing the electric propulsion system at the bottom of the structure only leaves the center of the structure as a viable spot for the MPS-135. It is especially important for this thruster to be aligned with the center of mass as it has a higher thrust and greater moment arm, at up to 2.5 N at 10 cm from the center of mass, having the potential to induce tumbling though exact alignment is not necessary at this stage as all components were assumed to have uniform density for this first iteration, an assumption that will need to be revisited as the model is refined. With the stowage thickness of the solar panels and the maximum height past the rails being 11.2 mm, the solar panels extend beyond the rails into the bus by 18.8 mm. With the specified dimensions of the MPS-135, this leaves one orientation of the thruster. The solar panels were placed such that a single SADA placed on the face opposite the BIT-3 could articulate them about a single axis. This axis needs to be perpendicular to the BIT-3 thrust axis to prevent panel shadowing while maintaining inertial

pointing of the UHF antenna. The radio is placed close to the antenna to reduce line loss and mass of harnessing.

Interfaces between components were identified to guide the placement of other components which had no constraints other than thermal concerns, reducing harnessing, and maintaining contiguous space for an actual payload; the interface diagram, referred to as an N2 diagram, is included in Appendix D. Placement of components must be balanced to keep the center of mass near the geometric center. The batteries were placed close to the solar arrays in the +Y 4U platform to keep the wiring between them as short as possible, reducing harnessing mass. The reaction wheels and star tracker were placed in the -Y compartment, opposite the batteries to balance the mass about the geometric center of the bus with the star tracker orientation allowing view of the stars by facing away from Mars. The reaction wheels are oriented such that each is aligned with a principal axis. The remainder of components, circuit boards, sensors and payload, were placed in the space between the MPS-135 and bus wall; they are concentrated on one side to allow harnessing to route through the other to the components in the bottom compartment. The IMU is placed to align with the axes of the center of mass. Having the payload and IMU close to the OBC reduces data harness length. The placement of the lightweight sun sensors has a negligible effect on the center of mass and inertia; they were placed in groups of three in order to consolidate their harnessing and such that one is on each face of the bus. These could require relocation if the solar panels obscure too much of the field of view or glint into the sensor, affecting reading accuracy; these effects would need to be further investigated for actual configuration of the sensors. As the exact flyby geometry at Phobos was outside the scope of this thesis, the camera may require relocation to another face as well. Like the sun sensors, the low mass of the camera makes it able to be moved; alternatively, cameras could be added to multiple faces. The internal configuration described is depicted in Figure 10-2.

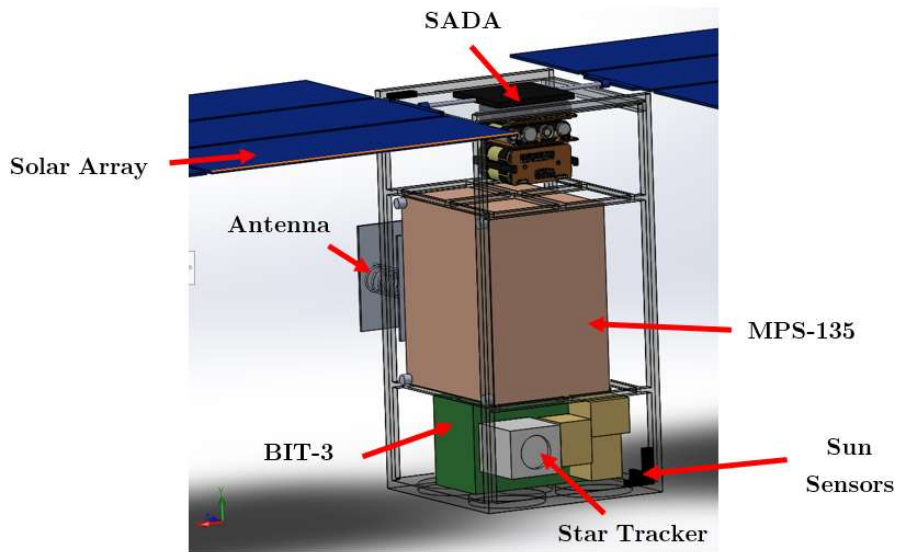
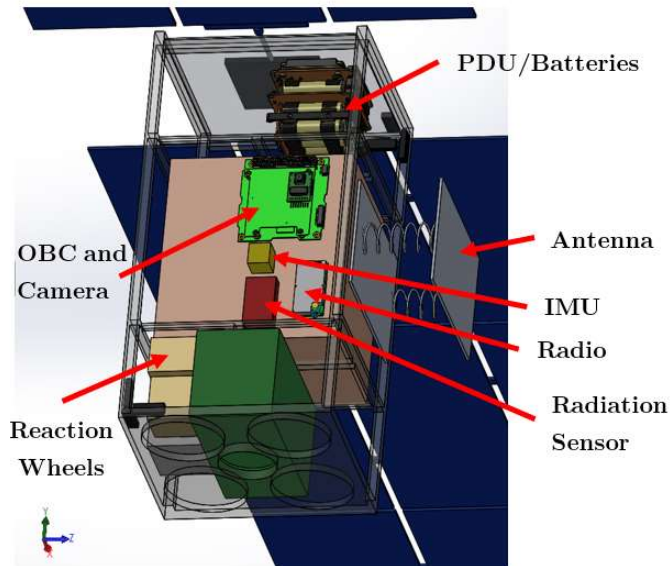


**Figure 10-2: Internal configuration.**

#### 10.4 Configuration Results

There are two resulting configurations: stowed and deployed. The stowed configuration is designed to fit into the EXOpod deployer envelope while the deployed configuration is designed to be the configuration through the duration of the mission. The deployed configuration involves deployment

of solar panels and a UHF antenna. For figures in this chapter, note that the four -Y face tuna can cutouts are to illustrate where additional volume could be added; only the center circle is a through cut. The origin is at the rail corner where the -X, -Y, and +Z faces meet. Though an ISIS structure was used for a mass estimate, a custom bus structure was created to fit the EXOpod dimensions. A customized structure will be needed for this concept as selected components, though in CubeSat form factors, are greater than 1U requiring inner compartments with supports to be shaped to the component placement required for the mission.

#### **10.4.1 Stowed**

The baselined configuration, shown in Figure 10-3, was verified through inspection to comply with the envelope dictated by EXOpod which is summarized in Figure 10-1 and Table 10-1. As shown in the dimensioned drawing of Figure 10-4, the volume extending beyond the rails, which were set to the typical 10.5 mm square, is 11.2 mm. The maximum rail length is 454.0 mm, the outer distance between rails in the perpendicular plane is 226.3 mm. The inner distance between rails is 205.3 mm which is less than the maximum allowed 213.5 mm. The maximum offset of the center of mass is equal to the maximum allowed at 20.0 mm. The center of mass and inertia about the center of mass in the stowed configuration are listed in Table 10-3.



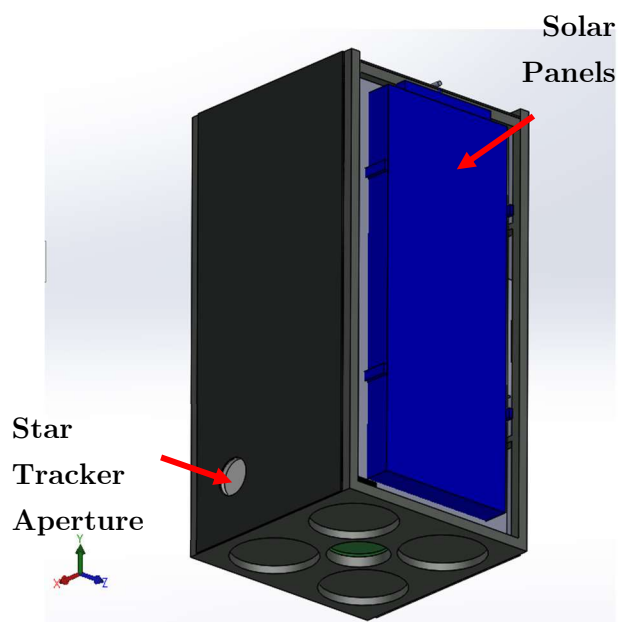
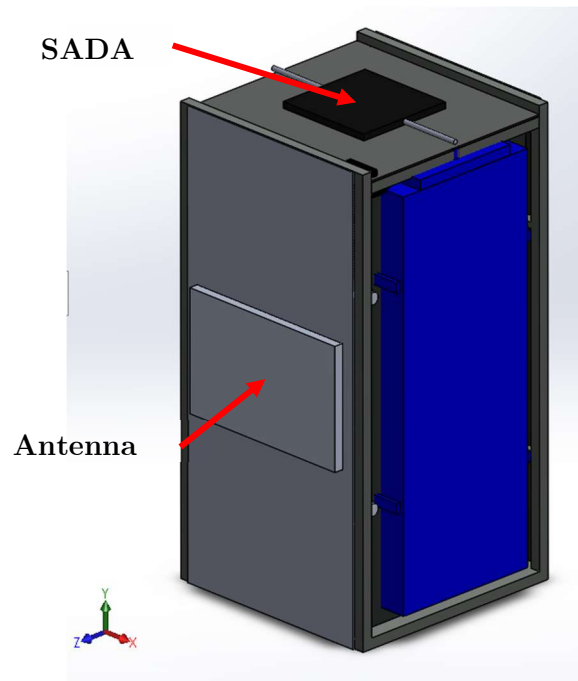
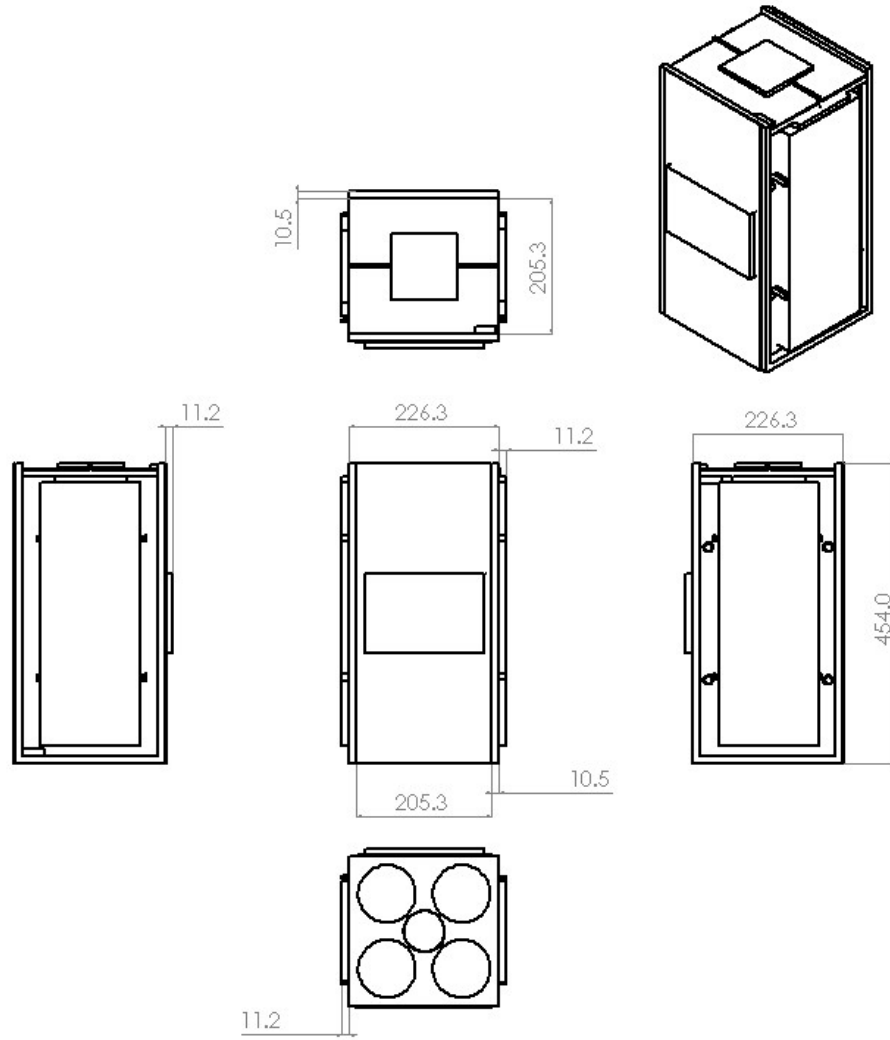


Figure 10-3: Stowed configuration.



**Figure 10-4: Stowed configuration showing compliance with EXOpod deployer specification. Dimensions are in mm.**

**Table 10-3: Mass properties of the stowed configuration.**

	Inertia ( $\text{kg}\cdot\text{m}^2$ )			CG (mm)	CG-Geometric Center Offset (mm)
	X	Y	Z		
X	0.42	0	0	118.78	5.28
Y	0	0.19	0.02	207.05	-19.95
Z	0	0.02	0.44	-111.49	2.01

### 10.4.2 Deployed

After exiting the CubeSat deployer, the solar panels need to deploy to begin generating electrical power to begin the low-thrust phase. The UHF antenna also must deploy to establish communications with the MRO Electra Proximity link. This configuration is shown in Figure 10-5 and Figure 10-6. The solar panel deployment reveals the MPS-135 thrusters, camera, and two of the sun sensors. As the solar panels have a large area and mass, the change in moment of inertia and center of mass was of concern directly after deployment. These were investigated in SolidWorks with the Mass Properties tool with results listed in Table 10-4. As expected, the inertia about the Y and Z-axes increased due to the solar array deployment. The center of mass moved closer to the geometric center of the bus, with a maximum offset of ~8 mm. The X and Z-axes have a slight offset, which could be a concern during the low-thrust phase as the BIT-3 thrusters perpendicular to the X-Z plane in the geometric center of the bus.

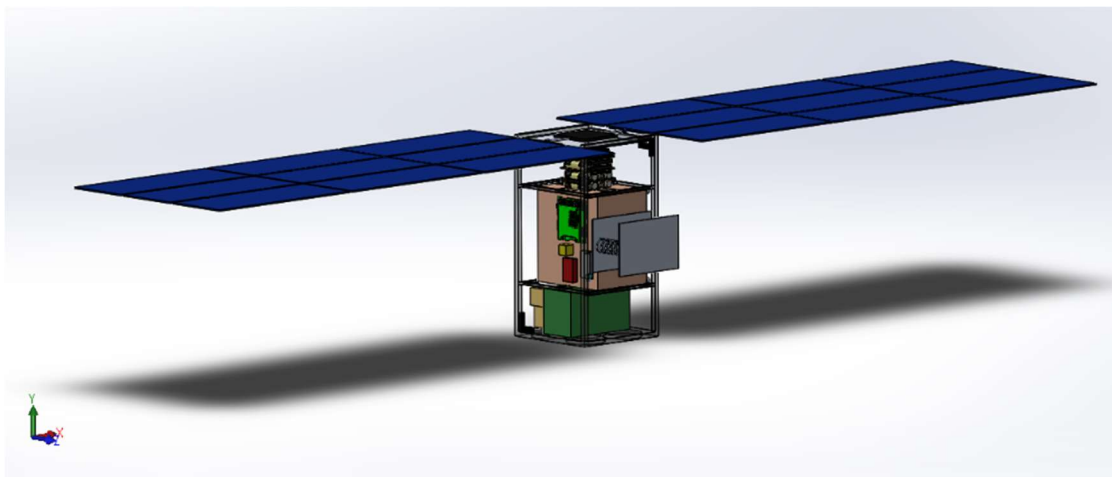


**Figure 10-5: Deployed configuration showing relative interior configuration.**

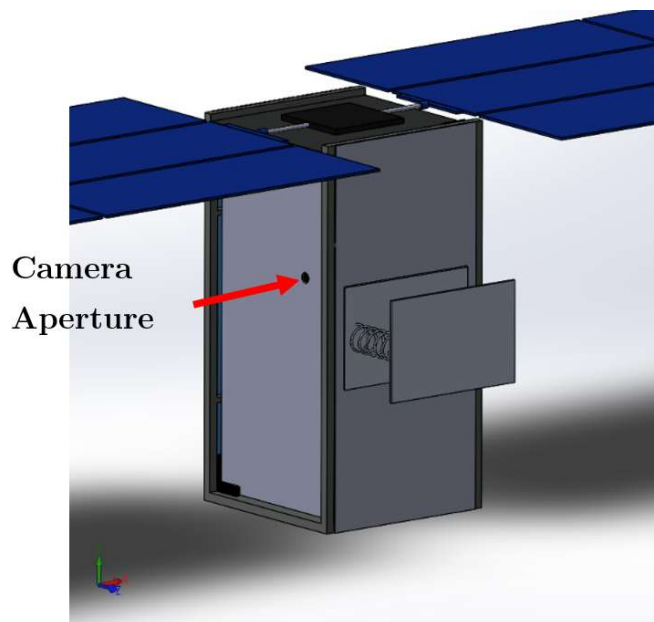
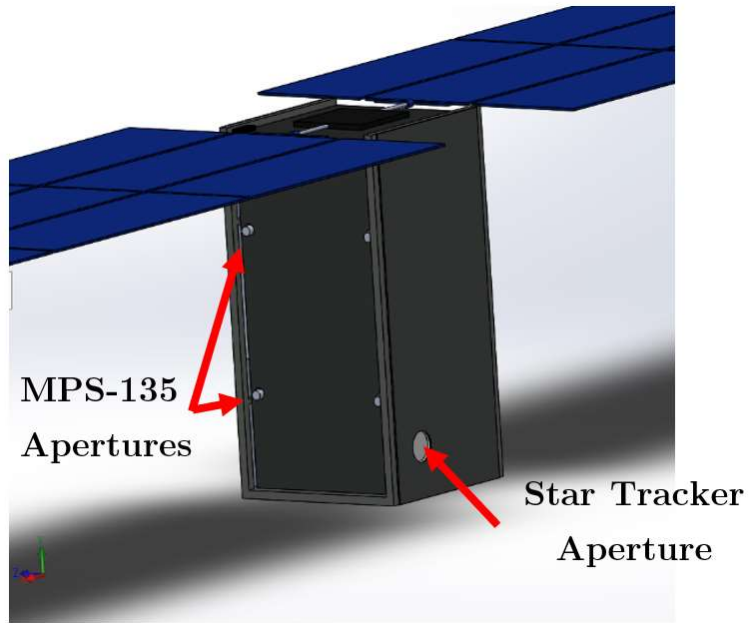


**Figure 10-6: Deployed configuration showing side panels with apertures.**

**Table 10-4: Post-deployment mass properties.**

	Inertia (kg·m <sup>2</sup> )			CG (mm)	CG-Geometric Center Offset (mm)
	X	Y	Z		
<b>X</b>	0.59	-0.01	0	118.76	5.26
<b>Y</b>	-0.01	1.98	0.02	235.13	8.13
<b>Z</b>	0	0.02	2.29	-111.16	2.34

At the end of the low-thrust phase, a significant amount of mass will have been expended. This is of concern as the MPS-135 must act through the center of mass to maintain stability. The resulting mass properties were investigated, accounting for the loss of 1.7 kg of propellant expended through the low-thrust phase; these are listed in Table 10-5. The reduced mass of the BIT-3 unit does not have a large effect on the inertia as it is aligned with the geometric center of the bus in two axes but does result in a ~1 cm shift up of the center of mass in the Y-axis. This does result in the thruster unit acting ~2 cm off the center of mass in the Y-axis though with the four thruster configuration, if this remains an issue after design iteration, the thrust level can be proportionally adjusted on individual thrusters to prevent inducing a moment during the impulsive orbit transfer.

**Table 10-5: Post-low thrust phase and pre-impulsive transfer mass properties.**

	Inertia (kg·m <sup>2</sup> )			CG (mm)	CG-Geometric Center Offset (mm)
	X	Y	Z		
<b>X</b>	0.54	-0.01	0	119.14	5.64
<b>Y</b>	-0.01	1.98	0.02	246.65	19.65
<b>Z</b>	0	0.02	2.24	-111.03	2.47

The final major change in mass properties during the mission is the expenditure of ~5.25 kg of fuel during the impulsive transfer. Maintaining a geometrically centered center of mass is important

for the cycler orbit for the performance estimates of the ADCS components to hold. This final configuration was investigated in the same manner as the other configurations with results listed in Table 10-6. Again, there is little change in the moments of inertia at  $<0.05 \text{ kg}\cdot\text{m}^2$ , as the thruster system is geometrically centered in the bus. The center of mass shifts up  $\sim 3 \text{ cm}$  in the Y-axis though this is not an issue as the BIT-3 used for orbit corrections acts through the X-Z plane, which the center of mass is centered in with a maximum offset of  $\sim 4 \text{ mm}$  as shown in Figure 10-7. The Y-axis shift is within the estimate of maximum center of pressure and center of mass used for the solar radiation pressure torque, having an 18 cm offset compared to the  $\sim 20 \text{ cm}$  that was used as explained in Chapter 8, Table 8-3.

**Table 10-6: Cycler orbit mass properties.**

	Inertia ( $\text{kg}\cdot\text{m}^2$ )			CG (mm)	CG-Geometric Center Offset (mm)
	X	Y	Z		
X	0.49	-0.01	0	114.96	1.46
Y	-0.01	1.95	0.02	253.62	26.62
Z	0	0.02	2.2	-110.04	3.46

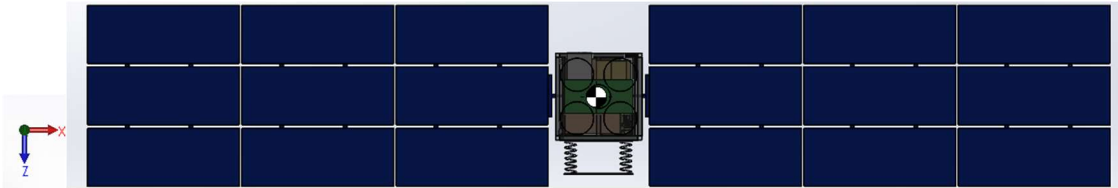


**Figure 10-7: Center of mass aligning with BIT-3 thruster.**

### 10.5 Bus as a Payload Host

As a bus provider, CPCL provides a bus to host customer payloads. A consideration of this configuration was to allow mass and volume for an additional payload. While there are alternatives, this design allows a 3U “L” shaped payload compartment at the top of the bus and a 0.5U x 2U

compartment at the bottom of the bus, for a total of 4U available volume. With the addition of payloads, it would be necessary to reconfigure components to maintain a balanced satellite. A possible option, depending on the properties of the payload, is to move the battery module to -Y compartment to open the entire +Y compartment of the bus for an uninterrupted 4U platform. Moving the batteries could have the added benefit of reducing heater needs as the BIT-3 generates up to 17.5 W of heat and could be leveraged to keep the batteries warm.

As for mass, the bus total is 27.0 kg or 32.4 kg with 20% margin. Including the margin, the bus total is just over the 32 kg limit for a 16U CubeSat. However, it may be possible to obtain a waiver on a case by case mission, and more feasibly than a waiver for a deviation in volume envelope as it would not require a custom deployer. Additionally, mass estimates used were conservative and there are opportunities for reduction such as not filling the MPS-135 to capacity. Under the assumption of a strict 32 kg maximum, there is no mass available to the payload as the bus is 400 g above the allowed mass. If accepting a lower mass margin for the bus, 10% for example, 2.3 kg is available to a payload. A summary of the SWaP results for the baseline is listed in Table 10-7 with power values from Chapter 7.

**Table 10-7: Baseline SWaP summary.**

	<b>Bus Total</b>	<b>Available to Payload</b>
<b>Mass</b>	27 kg 29.7 with 10% margin	2.3 kg
<b>Volume</b>	16U	4U
<b>Power</b>	111 W EOL	13 W – 38 W

## **10.6 Configuration Results in Relation to CPCL**

The largest structure CPCL has produced is a 3U for ExoCube and ExoCube-II with most missions being 1U [18]. A larger bus size will be required for a planetary mission; work is being done to

develop a 6U A6061-T6 structure for the CPCL lunar concept [19]. Beginning with the structural design of a 6U or 12U could prove beneficial before moving to a 16U structure as these will be in demand for Earth orbiting missions and could be stacked such as with ExoCube in which two 1U structures were attached to either side of a 1U chamber. There will not be a “one structure fits all” design as the large bus size invites an array of missions and requirements. However, it may be possible to create a primary structure with a customizable secondary structure or vice-versa to reduce development and testing time. Side panels will need to be custom made according to the mission as sensor apertures and placement will vary and a mission with lower radiation exposure can save mass by having thinner panels. For missions with propulsion modules, structure designs will need to include centered through-holes that are outside of the 1U domain (hole centered in a 4U face), requiring curved supports that have not been developed at CPCL yet.

This mission concept calls for two deployments, the solar arrays and the antenna. CPCL has experience with deployments of whip antennas and gravity gradient booms. These mechanisms utilize a simple burn wire made of “fishing line” heated with a resistive circuit. The antenna deploys from its own spring energy while the booms also utilized a hinge. Depending on how the solar arrays are sourced and if they are custom made for the concept’s form factor, CPCL may need to further develop hinge capability for the interface between the SADA rotor and wing mounts where the panels fold to the sides of the bus. Considerations here are material properties such as strength and stiffness as the solar arrays will flex, thermal distortions, susceptibility to cold welding, and locking mechanisms. Securing the solar arrays can be likened to ExoCube’s booms, using burn wire at the bottom of the panels; as the solar panels are kilograms more massive than the booms, a stronger wire may need to be used to withstand the launch environment. The baselined antenna design, outlined in [35], is spring actuated, needing only a burn wire. The burn wire material should be thoroughly tested for longevity as it must hold for the ~6 month cruise duration; if it were to fail inside the deployer, the CubeSat would likely become jammed, compromising the entire mission.



CPCL deployers include a flight 1U to 3U P-POD and a currently in development 6U interplanetary ISP-POD. The ISP-POD has planned capability to communicate with the CubeSat after deployment, receiving >100 Mb from the CubeSat using an omnidirectional antenna. The deployer can then relay that data to the primary spacecraft to be relayed to an Earth ground station. The P-POD has flight heritage that can be applied to the ISP-POD in terms of mechanical design. As the ISP-POD is not large enough for a 16U and the industry is trending towards larger CubeSats for missions beyond the moon, it would be worth investigating the cost of developing a 12U deployment system, as this could also house two 6Us. As the 16U form factor is less common and doesn't break into common form factors (four long or flat 4Us, two 8Us, or one 12U and one flat 4U), it could be more applicable to make a deployer that could be adapted between 12U and 16U but that is primarily designed for 12Us.

## Chapter 11

### RADIATION CONSIDERATIONS

With GCRs fluxes generally known as explained in Chapter 2, taking the rate as 40.4 mrad/day, the total ionizing dose (TID) from GCRs for a 3.5-year mission is 51.6 rad. For solar particle radiation, because ranges of radiation data were available at different points in time for various levels of shielding the expected radiation dose was modelled using ESA's SPENVIS software. The models used were Rosenqvist et al. (2005, 2007) for solar particle fluences and CREME-6 for solar particle fluxes for all ions. The solar particles flux was modelled for the full 3.5-year mission using the start and end date specified in the concept of operations. This was then applied to the SHIELDOSE-2 ionizing dose model that determines the TID in silicon for various thicknesses of finite aluminum slab shields, analogous to a CubeSat side panel.

The analysis was broken into two parts, a circular orbit at 4624 km (the average of the initial and final circular orbital radii) for 1.64 years and the cycloidal orbit for 1.88 years. The dates used for these analyses correspond to the dates in the concept of operations. The results of this analysis are shown in Figure 11-1 and Figure 11-2. These were used to determine the side panel thickness on the CubeSat. For 3 mm shielding, the TID for the first phase is 3.7 krad and the second phase is 4.2 krad for a total of 7.9 krad through the mission.

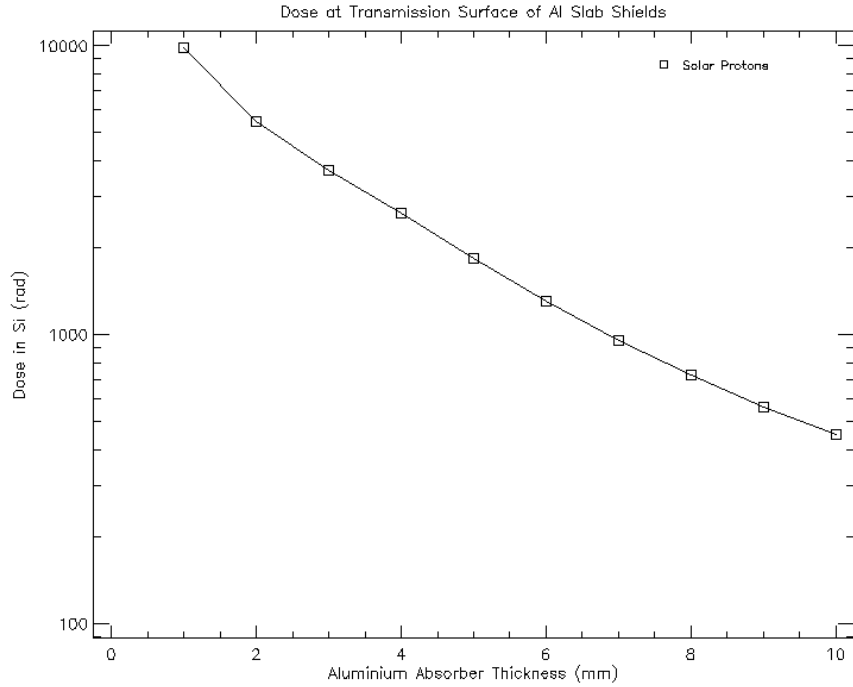


**Figure 11-1: Total ionizing dose in silicon for 1.64 years exposure in a 4624 km altitude, 0° inclination circular orbit.**

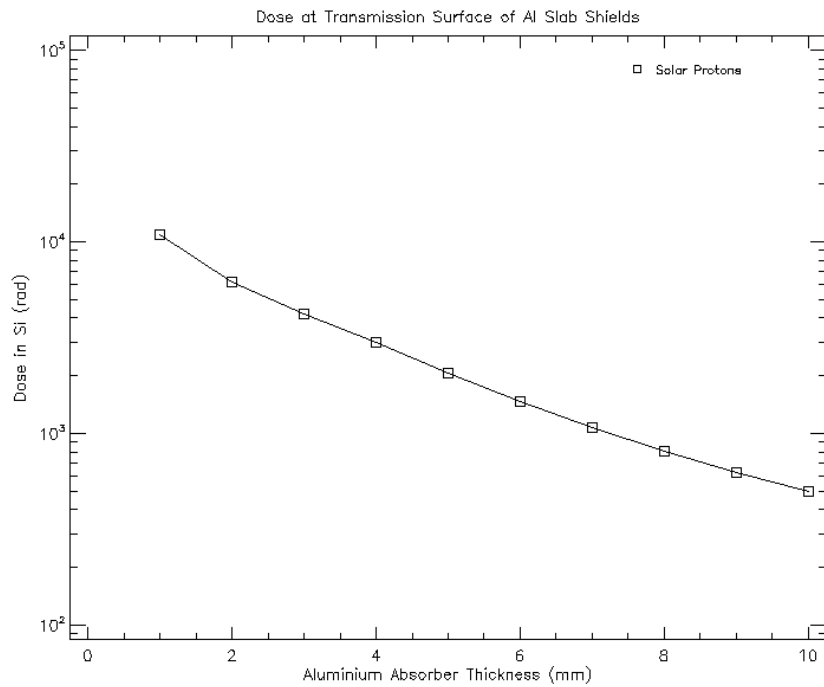


**Figure 11-2: Total ionizing dose in silicon for 1.88 years exposure in the cyclor orbit.**

Component selection throughout the design placed preference on radiation tolerant devices where possible but these are still not very common as they go against the CubeSat COTS philosophy. The components that did have specified radiation tolerances are listed in Table 11-1.

**Table 11-1: Radiation tolerances of selected components where provided by manufacturer.**

<b>Component</b>	<b>Radiation Tolerance (krad)</b>
Sinclair Interplanetary Rxn Wheels RW-0.03	20 [86]
New Space Systems Sun Sensor NCSS-SA05	Comparable model is 10 krad [85]
Maryland Aerospace Space Sextant Star Tracker	75 [87]
Honeybee SADA	10 [95]
GomSpace P60 System (incl. ACU and PDU)	20 [80, 81, 82]
SkyFox Labs PiDose	<10 [48]

Applying 3 mm aluminum panels to all sides reduces TID to components inside the bus to ~8 krad. Configuration of various components applies additional shielding to other components; for example, the MPS-135 thruster is a large metal housing that can protect the electronics and payload next to it from one direction. To shield the OBC, IMU, and radio to the maximum accepted COTS tolerance of 3 krad requires an additional 3 mm of shielding. Applying this to the five faces not protected by the MPS-135 results in an additional mass of ~190 g with the OBC requiring 150 g, the radio requiring 25 g, and the IMU 13 g.

For the rated components, all are within the expected TID but the placement of the SADA and multiple sun sensors in the modelled CubeSat are outside of the shielding of the panels. The +Y panel that has the SADA attached to it could easily be moved to above the SADA with the connection to the solar panels emerging from within the bus in order to keep the 10 krad rated SADA within the anticipated 8 krad exposure shielding. As the SADA and top panel are

comparable masses, swapping placement of these would not affect previous analyses. The same issue and resolution applies to the 10 krad rated sun sensors; as explained in Chapter 10, these can be moved without significantly affecting mass and inertia properties and so could be placed inside of the bus with apertures cut in the side panels.

## Chapter 12

### THERMAL PROTECTION SYSTEM

Due to the various mission phases and corresponding power modes, the thermal subsystem must be able to handle a range of thermal conditions from the large heat dissipation during the low-thrust transfer to the cooler cyclor orbit that has lower heat dissipation and experiences less IR heating from Mars. In this chapter, the thermal requirements of the selected components are used to work towards a thermal protection system design that works for the two distinct mission phases, identified as the “hot” and “cold” cases. Despite being one of the major design drivers, the presented subsystem design was not able to keep components within their operational temperatures due to the interactions of the heat load duty cycles and orbital regimes. Recommendations on how to close the design are provided and preliminary findings are compared to CPCL’s current and planned thermal subsystem capabilities.

#### 12.1 Thermal Requirements

Each component, the physical properties of which are listed in Table 12-1, has an operational and survival temperature range. Components’ survival temperatures were assumed to be the same as their operational temperatures as many data sheets only provided operational temperatures. Each component has an internal heat generation which differs when the component is on or off; this heat needs to be dissipated. The required temperature range and internal heat generation for each component, listed in Table 12-2, were obtained from data sheets when available. For non-specified heat generation, a conservative 10% efficiency was applied to the average electrical power consumption except for the radio where 40% efficiency was applied according to the datasheet’s input and output power. As is customary in lumped thermal analyses, thermal properties such as

material and specific heat capacity ( $C_p$ ) were taken to be bulk properties. Components with mixed makeup were assumed to be aluminum for this preliminary analysis.

**Table 12-1: Component physical and material specifications/assumptions.**

Component	Dimensions (mm)			Material	Mass (kg)	$C_p (\frac{J}{kg \cdot K})$
	X	Y	Z			
BIT-3	180	88	102	Aluminum	3.54	921.10
MPS-135	160	200	200	Aluminum	11.20	921.10
Batteries/PDU	87	87	92	Lithium-Ion	0.95	960.00
Radio	10	33	65	Aluminum	0.05	921.10
Antenna	180	150	5	Aluminum	0.25	921.10
Camera	31	31	12	Aluminum	0.05	921.10
Radiation Sensor	53	32	14	Aluminum	0.03	921.10
OBC	96	90	12	Aluminum	0.10	921.10
Star Tracker	55	65	70	Aluminum	0.28	921.10
Reaction Wheels (each)	50	50	40	Aluminum	0.19	921.10
Sun Sensors	33	11	6	Aluminum	0.01	921.10
IMU	23	23	24	Aluminum	0.02	921.10
SADA	100	100	7	Aluminum	0.18	921.10
Solar Panels (each wing)	948	1371	5	GaAs, Aluminum	1.50	921.10
Structure	230	230	450	Aluminum	2.25	921.10

**Table 12-2: Component operating temperature ranges and internal heat generation.**

	Operating Temperature Range (°C)		Low-thrust Phase Average $Q_{int}$ (W)	Cycler Phase Average $Q_{int}$ (W)
	Min.	Max.		
BIT-3	-10	45	17.50	1.00
MPS-135	-10	45	0.00	0.00
Batteries/PDU				
Charging	0	45	0.40	0.40
Discharging	-20	60		
Radio	-30	70	6.00	6.00
Antenna	-100	100	0.00	0.00
Camera	0	50	0.00	0.01
Radiation Sensor	-30	60	0.00	0.01
OBC	-25	65	0.63	0.63
Star Tracker	-40	80	0.10	0.10
Reaction Wheels (each)	-40	70	0.03	0.03
Sun Sensors	-25	70	0.01	0.01
IMU	-40	105	0.04	0.04
SADA	-30	85	0.10	0.10
Solar Panels (each wing)	-150	110	0.00	0.00

## 12.2 Determining the Thermal Load

In space, the primary modes of heat transfer are radiation and conduction. For the overall spacecraft, the only external heat input is radiation. Therefore, the heat exchanges for space environment thermal analysis are direct solar radiation, planetary albedo, planetary infrared (IR) emission, and spacecraft IR heat emittance, and spacecraft surface-to-surface IR [23]. Free molecular heating and charged particle heating were omitted as the spacecraft is only briefly in Mars orbit low enough to experience these heating sources associated with drag as evidenced by the low drag torque in Chapter 8 and there are no significant radiation belts around Mars. Total spacecraft temperature was found using the heat balance equation in Equation (12.1) which states that in thermal equilibrium, heat input and output are equivalent. Heat inputs are solar radiation, denoted  $\dot{Q}_{solar}$ ,



planetary IR as  $\dot{Q}_{IR,planet}$ , planetary albedo as  $\dot{Q}_{albedo}$ , and internal heat generation as  $\dot{Q}_{int}$  with output being spacecraft IR emission,  $\dot{Q}_{IR,emit}$ .

$$\dot{Q}_{solar} + \dot{Q}_{IR,planet} + \dot{Q}_{albedo} + \dot{Q}_{int} - \dot{Q}_{IR,emit} = 0 \quad (12.1)$$

Direct solar radiation,  $\dot{Q}_{solar}$  in W, is calculated by Equation (12.2) where  $\alpha_s$  is solar absorptance of the irradiated material,  $F_{sun \rightarrow S/C}$  is the view factor between the Sun and spacecraft surface,  $\theta_s$  is the angle between the normal of the spacecraft face and the ecliptic plane in degrees, and  $A$  is the area of the irradiated material in m<sup>2</sup>;  $I_s$  is solar irradiance in W/m<sup>2</sup>. For a maximum heating approximation,  $\theta_s$  was set to 0°;  $I_s$  at Mars is 607.8 W/m<sup>2</sup>.

$$\dot{Q}_{solar} = I_s \alpha_s F_{sun \rightarrow S/C} \cos(\theta_s) A \quad (12.2)$$

Solar radiation reflected off of a planet and absorbed by the spacecraft, albedo, is given by Equation (12.3) where  $\rho_a$  is the planetary bond albedo, taken to be the maximum for Mars at 0.28, and  $G$  is an albedo specific view factor for a flat plate determined by Equation (12.4) in which  $r$  is the distance between the plate and center of the celestial body and  $R_{planet}$  is the radius of the planet, both in km [23].

$$\dot{Q}_{albedo} = I_s G \rho_a \alpha_s A \quad (12.3)$$

$$G = \left( \frac{r}{R_{planet}} \right)^{-2} \left( 1.488 - 0.1730 \ln \left( \frac{r}{R_{planet}} \right) \right) \quad (12.4)$$

Infrared radiation emitted by a celestial body,  $\dot{Q}_{IR,planet}$ , is given by Equation (12.5) where  $\sigma$  is Stefan Boltzmann's constant,  $5.67 \times 10^{-8} \text{ W} \cdot \text{m}^{-2} \cdot \text{K}^{-4}$ ,  $\epsilon_{IR}$  is the emissivity of the celestial body

(0.95 for Mars),  $F_{planet \rightarrow S/C}$  is the view factor between the planet and spacecraft,  $T_{planet}$  is the temperature of the planet (210 K for Mars), and  $\varepsilon_{S/C}$  is the emissivity of the spacecraft that here acts as the IR absorptance according to Kirchoff's law of thermal radiation [23, 96]. Finally, the spacecraft emits IR heat to its surroundings, given by  $\dot{Q}_{IR,emit}$  in Equation (12.6) where  $F_{S/C \rightarrow space}$  is the view factor between the spacecraft surface and space and  $\varepsilon_{S/C}$  is the IR emissivity of the spacecraft surface. Except for the calculated albedo view factor, all view factors were assumed to be 1.

$$\dot{Q}_{IR,planet} = \sigma \varepsilon_{IR} \varepsilon_{S/C} F_{planet \rightarrow S/C} T_{planet}^4 A \quad (12.5)$$

$$\dot{Q}_{IR,emit} = \sigma \varepsilon_{S/C} F_{S/C \rightarrow space} T_{S/C}^4 A \quad (12.6)$$

### 12.3 Initial Analysis

A steady state lumped thermal analysis was performed in MATLAB using Equations (12.1) – (12.6) to determine the bus temperature for the “hot case” which was identified as when the spacecraft is in the 300 km Mars orbit with the BIT-3 on in the Sun. For an initial estimate, the  $Q_{int}$  values from Table 12-2 were summed for a total internal heat generation of 32.2 W in a bus size of 230 mm x 230 mm x 450 mm with an aluminum finish ( $\alpha = 0.09$ ,  $\varepsilon = 0.03$ ); the solar panels were considered thermally isolated from the bus due to the small mount size. Assuming one large face is perfectly facing Mars for maximum albedo and IR exposure and the opposite face is Sun-pointing, the bus temperature was 187 °C. Radiative coatings would be needed to dissipate the heat. Changing the optical properties of the Sun-facing side, an area of 0.10 m<sup>2</sup>, to a white radiator (Z93,  $\alpha = 0.17$ ,  $\varepsilon = 0.92$ ) reduces the average temperature to ~20 °C. Using this temperature as the bus structure temperature and considering only radiative heat transfer, the entire inside of the structure and all components exteriors were assumed to be coated in black paint (Ebanol C Black,  $\varepsilon = 0.73$ ) to determine the heat transferred to the internal components; the surface areas of components from

Table 12-1 were used to calculate component temperatures for altitudes ranging from the initial 300 km orbit to the final low-thrust phase orbit altitude of 9246 km. These results are shown in Figure 12-1; the slight decrease in temperature is due to the decreasing view factor of Mars IR and planetary albedo. While most components are within their operational temperatures, the radio and BIT-3 are outside of theirs, at  $\sim 80^\circ\text{C}$  and  $\sim 15^\circ\text{C}$  higher than allowed, respectively, indicating that conduction methods will be needed to route excess heat out as radiation from their surface area is not enough. Therefore, a model was created in Thermal Desktop to better account for the geometries between components, conduction paths to radiators, and eclipses.

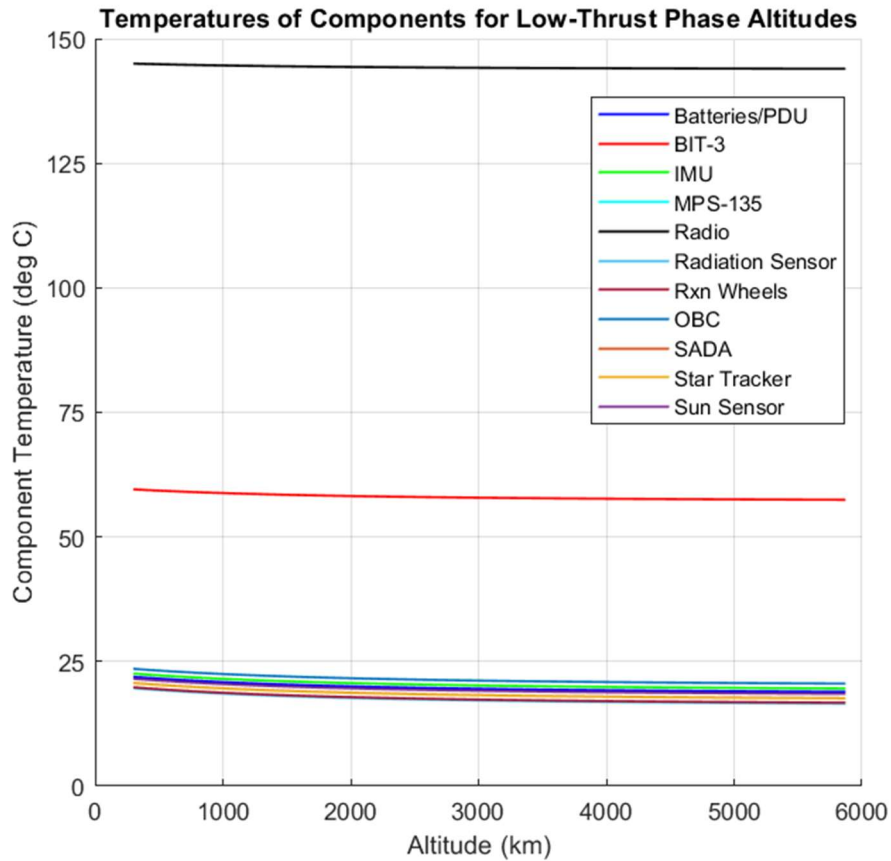


Figure 12-1: Resulting component temperatures for initial thermal analysis.

## 12.4 Thermal Desktop Model

Two cases were set up in Thermal Desktop, the initial orbit at 300 km in the low-thrust phase and the cycler orbit with planetary heating rates set to Mars. The model geometry treated the structure as a thin shell rectangular prism. Conductance paths were added between components and the structure to simulate mounting with screws. Aluminum was the primary material used for these connections but due to concerns about the BIT-3 heating the nearby reaction wheels and star tracker, these were thermally isolated from the thruster using low-conductance Delrin connections. The radiators were also thermally isolated from the bus structure using Delrin. The heat loads from Table 12-2 were applied, with the BIT-3 turning off in eclipse during the hot case, reducing the heat load to 1 W; this heat load was constantly 1 W in the cold case. The solar panels were set to track the Sun for both orbits. Optical coatings were applied as listed in Table 12-3. For this analysis, the SADA was moved to just inside the bus interior as mentioned a possibility in Chapter 11.

**Table 12-3: Thermal finishes utilized [23, 97].**

Surface Finish	$\alpha_s$	$\epsilon_{IR}$	Locations
Zerlouts Z-93 White Paint	0.17	0.92	Bottom bus panel around face of BIT-3
GSFC Black Silicate MS-94 Paint	0.96	0.89	All interior structure surfaces, all components except otherwise noted
ATN Blue Solar Cells	0.86	0.85	Solar cells
Bare Aluminum	0.09	0.03	Exterior bus panels, non-cell solar panel sides, reaction wheel housing, radiation sensor, antenna
Barium Sulfate with Polyvinyl Alcohol	0.06	0.88	Space-facing side of BIT-3, radiators
MLI (Kapton Outer Cover w/ 8 layer Aluminized Mylar interior)	--	0.01	SADA, BIT-3

The results of the hot case are shown in Figure 12-2 with post processing results from the hottest point in the orbit in Figure 12-3. All components, save the BIT-3, are within their operating temperate ranges. The BIT-3 was connected to three dedicated radiators, one on the antenna face,

and one on each solar panel stowage face, as well as the entire bottom of the bus for a total of 0.33 m<sup>2</sup>. Despite this, the BIT-3 exceeds its maximum operating temperature for half of the orbit by up to 35 °C. The theoretical radiator area that should be able to dissipate 17.5 W at ~80 °C is an additional 0.023 m<sup>2</sup>, which would require covering another face of the bus in optical coating. This was attempted but little change was observed, likely due to the external heating environment. This issue should be further investigated. Research into phase change materials for averaging the BIT-3 temperature extremes should be conducted as the calculated radiator area exceeds realistic application considering imager and sensor apertures that would reduce body-mounted area. Deployable radiators could also be a viable mitigation but add additional mass in deployment mechanisms and would increase surface area that contributes to solar radiation pressure and drag perturbations.

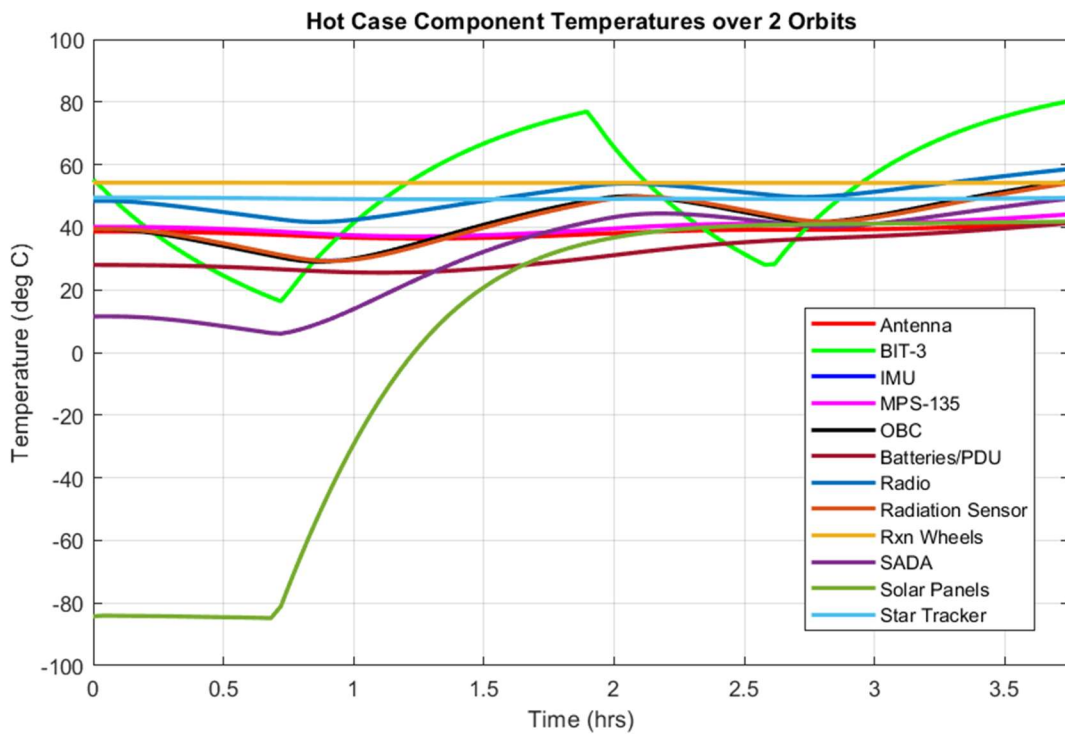


**Figure 12-2: Hot case component temperature Thermal Desktop results over two orbits.**

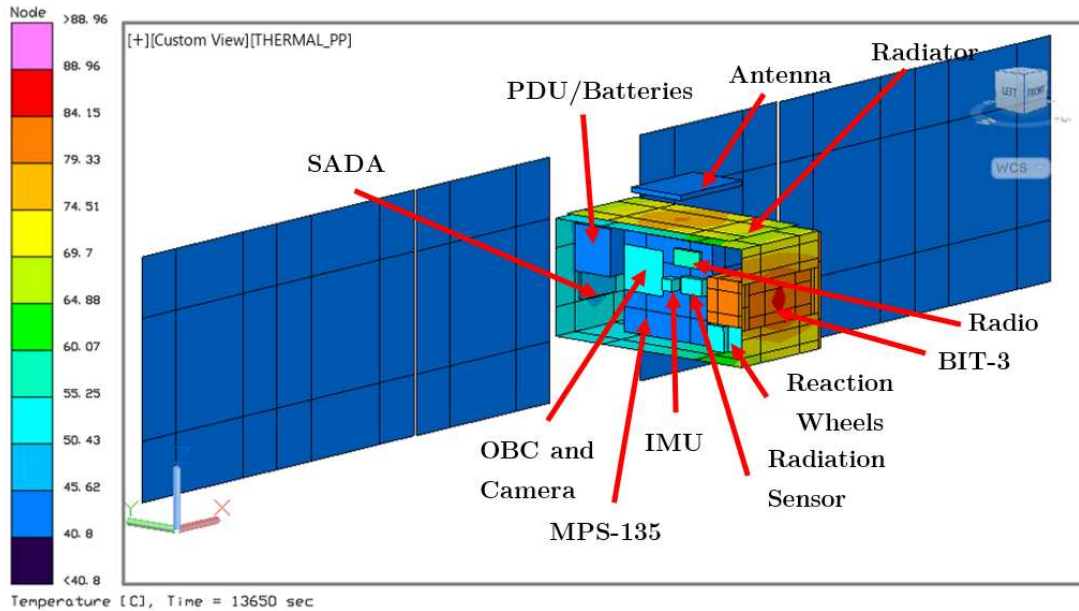


**Figure 12-3: Hot case component temperature post-processing Thermal Desktop results at hottest point in orbit.**

For the cold case, a large source of heat, the BIT-3, is removed for much of the mission. Having the BIT-3 remaining connected to the large radiators in this phase causes the thruster to fall extremely below its operating range which is problematic as it is still needed for station keeping maneuvers and reaction wheel desaturation. The other interior components also begin to fall below their thresholds due to the heat leaching BIT-3. To reduce the heat loss to space, it was assumed that the BIT-3 became thermally isolated from the three side radiators; this could be done through use of paraffin heat switches such as the Starsys Pedestal Switch with a mass of only 100 g [23]. Despite covering some components in MLI, their internal heat generation was not sufficient, and heaters were required. The GomSpace battery packs already have a 3.5 W heater; 0.5 W was added for the OBC, 1 W for the SADA, and 35 W for the BIT-3. The results of the cold case with these added heaters are shown in Figure 12-4 with post processing results from the coldest point in the orbit in Figure 12-5; all components are within their operational temperature limits. This is a large amount of heater power required that was not explicitly accounted for as part of the power budget

due to the thermal analysis being performed last without chance for iteration. However, the power subsystem was sized to support BIT-3 maneuvers at a power of 66 W with the power for other phases being much lower (12 – 23 W) and so there is plenty of power to provide this heat input through this phase; phase change materials could store this heat for distribution in eclipse where batteries are not sufficient. Further investigation should include determining how often this high heater power is required and if it can be done in duty cycles. If possible, duty cycles would be preferable as it would leave more power available to an additional payload in the science phase; including phase change materials could also facilitate this approach.

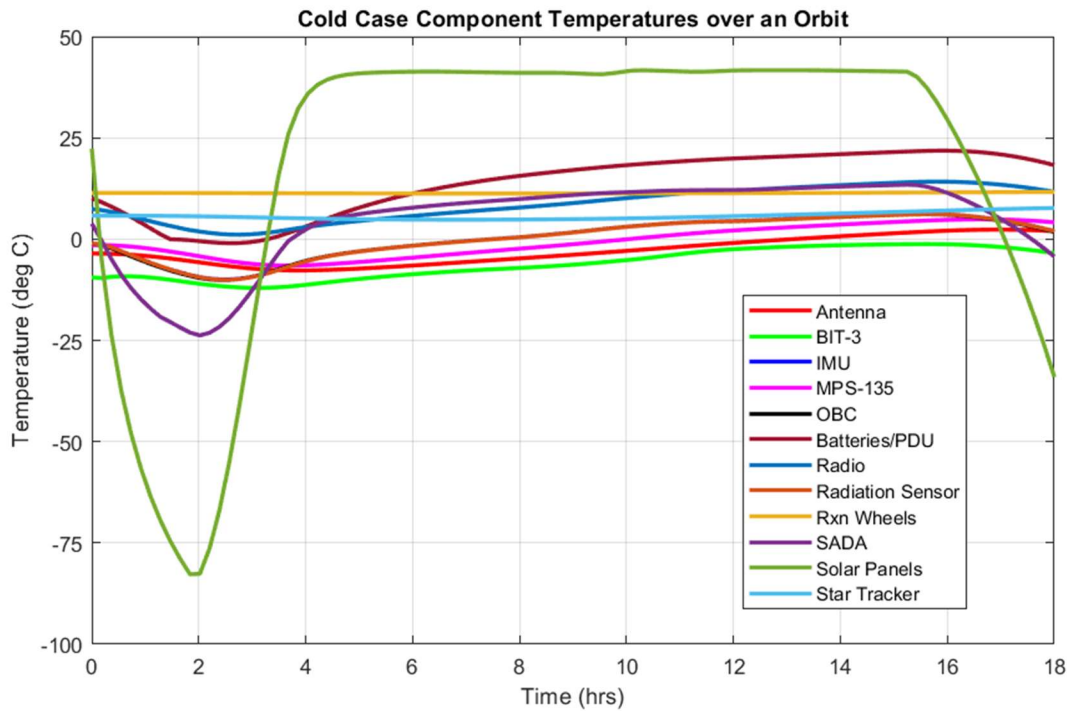


**Figure 12-4: Cold case component temperature Thermal Desktop results over an orbit.**

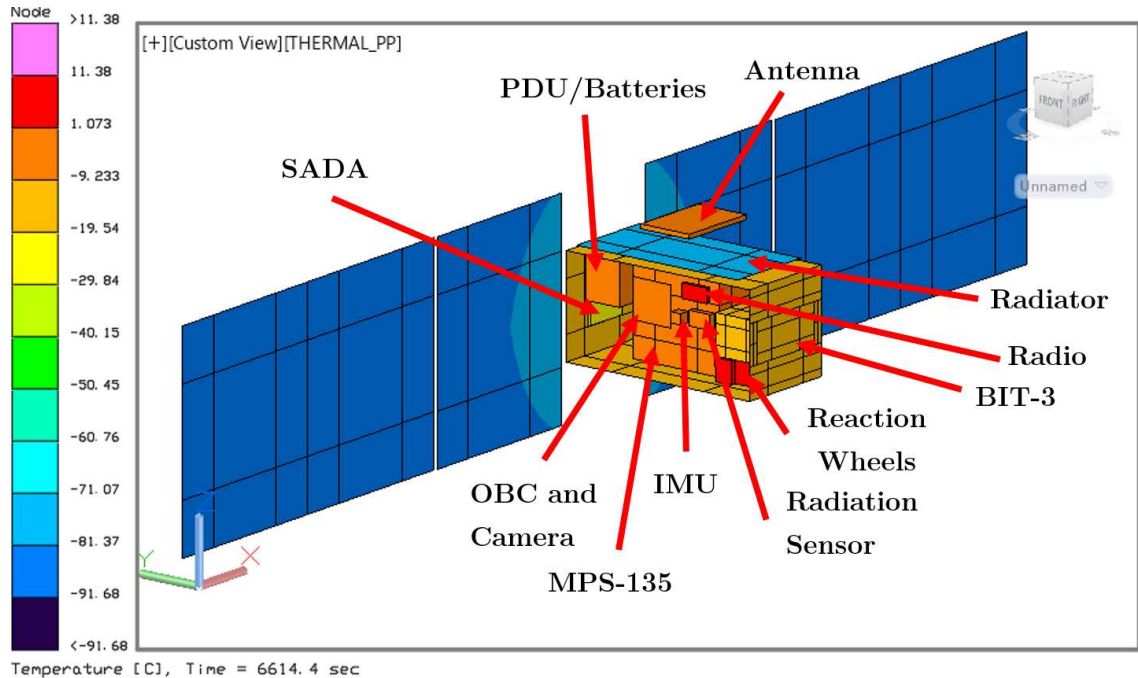


**Figure 12-5: Cold case component temperature post-processing Thermal Desktop results at coldest point in orbit.**

## 12.5 Thermal Subsystem Summary and Needed Work

This thermal protection system presented needs to be further developed as it does not meet the requirements for some components in the “hot” case and requires 40 W of heater power in the “cold” case of the mission. Implementing radiators to cool the BIT-3 did bring the temperature down towards operational limits which implies that a solution is feasible. Multiple Artemis-1 missions are utilizing the BIT-3 in a smaller form factor with a higher environmental thermal load at ~1 AU so those designs should be examined as that information becomes available. Though not a complete design, this analysis shows that simple radiative mitigations are not sufficient for the range of thermal environments encountered on this mission. Passive control approaches are more appropriate than active due to the power constraints from an already large power subsystem so the mitigations utilized for the results presented include optical coatings, radiators, and heat switches; heaters were added for thermal control in the cold case. These mitigations and their implications



are summarized in Table 12-4. Many technologies used on larger spacecraft such as louvers, deployable radiators, and composite heat straps are in development for small spacecraft [56]. Due to the range of environments encountered in this mission, one of these techniques will likely be required to create an effective thermal subsystem design.

**Table 12-4: Mitigations applied to the presented model.**

<b>Mitigation</b>	<b>Comments</b>	<b>Mass</b>
Optical surface finishes	See Table 12-3	Negligible due to small surface area
Heaters	Applied to batteries/PDU, OBC, SADA, and BIT-3 and on during cold case for a total of 40 W	~100 g using 6Ω Kapton Polyimide flex heaters from [98]
MLI	Calculated effective emissivity of 0.01	< 100 g
Radiators	3 dedicated to BIT-3 on +X, -X, and +Z faces, 1 on the -Y face for a total 0.33 m <sup>2</sup> ; implies use of heat straps	Spacecraft side panels can act as radiators for no additional mass; assuming 30 cm length of 1 cm x 2 cm thick copper straps, ~540 g
Heat switches	Needed to isolate BIT-3 from radiators during cold case	~300 g
Low conductivity standoffs	Delrin for thermally isolating reaction wheels, star tracker, and radiators from the bus structure	Screw replacement, accounted for in structure mass

## 12.6 Thermal Subsystem Results in Relation to CPCL

No CPCL flight mission to date has utilized thermal optical coatings or heaters as the thermal environment in LEO for a small object with low heat generation is relatively stable, resulting in temperatures typically within COTS specifications. CPCL exteriors to date have been black, sometimes anodized, aluminum with most surface area covered by solar cells. Circuit boards are conformal coated to distribute heat within the board and these have been spaced using low conductivity spacers. With the exploration into higher propulsive capabilities for missions beyond LEO, it will become necessary to control for the resulting thermal loads. CPCL has the advantage

of having multiple thermal vacuum testing facilities on site where research into implementing these methods could be rapidly conducted. Promising mitigation methods such as deployable radiators and louvers require hinge mechanisms, which were recommended in Chapter 10, though additional research would be needed for how high thermal loads across these would affect their performance. Other areas of development include heaters and MLI which could be developed and tested in-house. Phase change materials should be considered for designs; a heat sink could be easily produced and tested at Cal Poly but heat switches are better left as COTS due to their complex inner mechanisms.

## Chapter 13

### SUMMARY OF RECOMMENDATIONS TO CPCL

The Cal Poly CubeSat Lab has flight experience in Earth-orbiting CubeSats. Throughout this thesis, known lab capabilities for each subsystem were discussed and recommendations were made on what capabilities should be improved or researched based on the required performance of each for the Phobos-Deimos mission concept. These surveyed current and proposed capabilities of the lab as well as the applicable university research performed outside CPCL are in no way an exhaustive list. Similarly, the baseline the recommendations are based off are mission specific despite selecting a mission intended to generalize what is needed for an interplanetary mission. However, through determining what is required for the baseline, subsystem designs and performances that would be useful for other types of missions were encountered and commented on. Current CPCL capability and experience, subsystem baseline performance, and recommendations to reconcile these differences are summarized in Table 13-1. As this facet of the aerospace industry is rapidly evolving, the Artemis-1 CubeSats will shed more light on required performance and execution as these missions become operational and undergo more detailed analysis and testing [19]. For reference, the Artemis-1 manifested CubeSats are listed in Appendix E.

**Table 13-1: Summary of CPCL capability, baseline results for mission concept, and recommendations.**

<b>Subsystem</b>	<b>Current Capability/ Experience</b>	<b>Baselined for Phobos-Deimos Cycler Mission Concept</b>	<b>Recommendation from Baseline and Design Process</b>
<b>Propulsion</b>	<ul style="list-style-type: none"> <li>• 1.5U electrothermal RF plasma thruster providing 20 m/s delta-V to a 3U in development</li> <li>• University research into electrospray thrusters</li> </ul>	<ul style="list-style-type: none"> <li>• RF ion thruster capable of providing 1250 m/s low thrust</li> <li>• Green monopropellant system providing 440 m/s high thrust</li> </ul>	<ul style="list-style-type: none"> <li>• Electric propulsion required for high delta-V missions in a CubeSat form factor</li> <li>• For more orbital flexibility, ion thrusters should be developed</li> <li>• Advanced orbital trajectory design to optimize propellant usage</li> </ul>
<b>Communications</b>	<ul style="list-style-type: none"> <li>• UHF 1W Transceiver</li> <li>• NiTi omnidirectional whip antennas</li> <li>• X-band deep space transceiver in development</li> </ul>	<ul style="list-style-type: none"> <li>• Relay architecture</li> <li>• UHF 2.5 W transceiver</li> <li>• 5 dB peak gain deployable loop antenna</li> <li>• GMSK encoding for reduced Eb/No</li> </ul>	<ul style="list-style-type: none"> <li>• Higher RF amplification power for UHF</li> <li>• Higher gain UHF antennas</li> <li>• X-band radio development is useful as it will likely be compatible with future Mars relay resources</li> <li>• Encoding performance should be improved</li> </ul>
<b>Ground Station</b>	<ul style="list-style-type: none"> <li>• UHF ground stations</li> <li>• X-band in development</li> </ul>	<ul style="list-style-type: none"> <li>• Relay architecture puts ground station into relay hosts' discretion</li> <li>• MRO Electra Proximity Link payload used as "ground station" with omnidirectional receiver</li> </ul>	<ul style="list-style-type: none"> <li>• X-band ground station would facilitate testing of a deep space radio</li> </ul>
<b>Power</b>	<ul style="list-style-type: none"> <li>• Body mounted solar arrays (UTJ, XTJ, TASC)</li> <li>• COTS Li-ion batteries up to 65 Whr</li> <li>• In-house battery board</li> </ul>	<ul style="list-style-type: none"> <li>• Deployable solar arrays with XTJ cells for 111 W EOL power generation</li> <li>• 12 Li-ion batteries for 115.5 Whr total capacity</li> <li>• PDU with configurable voltage output</li> <li>• ACU capable of high voltage solar input</li> <li>• 14.8 V battery output voltage</li> </ul>	<ul style="list-style-type: none"> <li>• Flexible array technology should be investigated as it matures as this would alleviate the stowage constraints encountered in this design</li> <li>• A more capable battery board and PDU will be needed to handle higher voltage and a diverse voltage inputs/outputs</li> </ul>
<b>ADCS</b>	<ul style="list-style-type: none"> <li>• Magnetometers</li> <li>• Sun sensors</li> <li>• Star tracker algorithm for use with COTS camera</li> <li>• IMU</li> </ul>	<ul style="list-style-type: none"> <li>• 6 coarse sun sensors</li> <li>• Star tracker</li> <li>• IMU</li> </ul>	<ul style="list-style-type: none"> <li>• Star tracker development should be continued as it greatly improves the capability of any mission and would remedy the lack of magnetometer usage</li> </ul>

			<ul style="list-style-type: none"> <li>In-house sun sensor thermal and radiation tolerance should be investigated</li> </ul>
<b>Actuators</b>	<ul style="list-style-type: none"> <li>Magnetorquers</li> <li>Gravity gradient booms</li> <li>COTS reaction wheel</li> </ul>	<ul style="list-style-type: none"> <li>3 30-mNs reaction wheels desaturated by either thruster system</li> </ul>	<ul style="list-style-type: none"> <li>Reaction wheels may be able to be produced in-house if high machining precision can be achieved</li> </ul>
<b>C&amp;DH</b>	<ul style="list-style-type: none"> <li>In-house System Board</li> <li>64 MB SRAM</li> <li>Reusable FSW with support for custom FSW</li> <li>Payload interface board</li> <li>MicroSD storage</li> </ul>	<ul style="list-style-type: none"> <li>1 MB flash code storage</li> <li>64 MB RAM</li> <li>4 GB data storage, SD card format</li> </ul>	<ul style="list-style-type: none"> <li>Attention to EDAC software development to mitigate radiation effects</li> <li>FSW development for autonomy as communication will be sparser, reducing operator control to investigate and correct anomalies</li> </ul>
<b>Structure</b>	<ul style="list-style-type: none"> <li>1U and 3U support structure and side panels</li> <li>Proposed 6U structure</li> </ul>	<ul style="list-style-type: none"> <li>16U</li> <li>Supports designed for components larger than 1U (up to 6U)</li> <li>Curved regions for centered thruster exhaust</li> </ul>	<ul style="list-style-type: none"> <li>Development of 12U bus as less propulsion heavy missions would fit this form factor and encounters same structural issues (curved through holes) as a 16U</li> <li>6U should be developed first, extrapolated to 12U</li> <li>If mission needs require, 12U can be extrapolated to 16U</li> <li>Experience in custom support design</li> </ul>
<b>Mechanisms</b>	<ul style="list-style-type: none"> <li>Fishing line burn wire</li> <li>Hinge for gravity gradient boom</li> </ul>	<ul style="list-style-type: none"> <li>Minimized stretch burn wire for long-term stowage (~6 months) for solar panels and antenna</li> <li>Spring actuation for antenna</li> <li>Potential hinge between SADA and solar panels if not supplied and integrated by manufacturer</li> </ul>	<ul style="list-style-type: none"> <li>Burn wire qualification for long-duration missions</li> <li>Hinges for deployables with attention to stiffness, strength, and thermal properties</li> </ul>
<b>Radiation</b>	<ul style="list-style-type: none"> <li>Typical LEO exposure within COTS tolerance</li> </ul>	<ul style="list-style-type: none"> <li>3 mm shielding on all bus faces</li> <li>Additional 3 mm shielding for OBC, radio, and IMU</li> </ul>	<ul style="list-style-type: none"> <li>Radiation exposure modelling considering interior geometry</li> <li>EDAC software development</li> <li>Use of radiation tolerant parts were cost/mass allows depending on mission duration</li> </ul>
<b>Thermal</b>	<ul style="list-style-type: none"> <li>Typical LEO exposure within COTS tolerance</li> <li>Conformal coating on PCBs</li> </ul>	<ul style="list-style-type: none"> <li>Patch heaters</li> <li>Optical coatings</li> <li>0.33 m<sup>2</sup> radiators with heat straps and heat switches dedicated to</li> </ul>	<ul style="list-style-type: none"> <li>Radiator development</li> <li>Optical coating application experience</li> <li>Advanced thermal modelling experience</li> </ul>

	<ul style="list-style-type: none"> <li>• Low-conductivity spacers between PCBs</li> </ul>	<p>electric propulsion system</p> <ul style="list-style-type: none"> <li>• MLI</li> <li>• Low-conductance standoffs</li> </ul>	<ul style="list-style-type: none"> <li>• Investigate phase change materials such as heat sinks and heat switches</li> <li>• MLI could be made and tested in-house</li> </ul>
<b>Deployers</b>	<ul style="list-style-type: none"> <li>• P-POD (1U-3U)</li> <li>• ISP-POD (6U) in development with radiation mitigation and proximity relay capability</li> </ul>	<ul style="list-style-type: none"> <li>• 16U EXOpod with additional tuna can space available</li> </ul>	<ul style="list-style-type: none"> <li>• 12U or 16U with ability to modify to one or the other as these form factors can also house 6Us which are increasing in popularity</li> <li>• Relay capability should be further developed as this could decrease dependence on existing relay resources at Mars</li> </ul>
<b>Mission Operations</b>	<ul style="list-style-type: none"> <li>• Repeated passes and no/low pointing requirements do not require autonomy</li> <li>• Frequent ground intervention</li> <li>• Constant orbit, eclipse, thermal, communications, and power regimes</li> </ul>	<ul style="list-style-type: none"> <li>• Less frequent intervention possible depending on relay-to-Earth link</li> <li>• Multiple phases over long duration resulting in various power and communications performance and availability and a range of thermal and perturbational environments</li> </ul>	<ul style="list-style-type: none"> <li>• Complex mission planning skills as multiple regimes are encountered in high capability but SWaP constrained missions</li> <li>• Creativity in orbit design and cadence in science data collection, communications, power usage is needed</li> </ul>
<b>Facilities</b>	<ul style="list-style-type: none"> <li>• Machine shops with CNC and 3D printing</li> <li>• Thermal vacuum chambers capable of -60°C to +120°C and 10<sup>-4</sup> Torr</li> <li>• Vibration and shock testing</li> <li>• Ground station</li> <li>• Anechoic chamber</li> <li>• Class 100,000 cleanroom</li> </ul>	<ul style="list-style-type: none"> <li>• Custom UHF antenna would need radiation pattern characterization in anechoic chamber</li> <li>• Thermal vacuum and vibration and shock testing required</li> <li>• Cleanroom assembly</li> </ul>	<ul style="list-style-type: none"> <li>• Cleanroom may need to address planetary protection concerns</li> <li>• May need larger thermal vacuum chamber</li> <li>• Vibration and shock tables may need to be rated for larger mass and volume</li> </ul>

## Chapter 14

### CONCLUSIONS AND FUTURE WORK

This exploratory study developed a mission concept to conduct science at Phobos and Deimos on a CubeSat scale, showing that a technology demonstration level mission is feasible using available technologies. The baseline design developed requires iteration but satisfies the requirements derived from the mission objectives, save for the thermal subsystem, though this is expected to be feasible within the current design. The selected subsystem components are not intended to be an endorsement for purchase and integration of those commercial products, rather use available technologies to provide guidance on the performances to target for each subsystem. The baseline offers a total of 4U volume to a science payload. If accepting 10% margin on the mass budget, 2.3 kg is available to a payload; with added margin, the CubeSat will require a waiver. Power available to a science payload ranges from ~13 W to ~38 W in the cyclical orbit phase depending on the power mode.

Through the development of this baseline, a few major conclusions for a near Mars CubeSat made by CPCL can be drawn. First, a larger bus than what CPCL currently produces is required to fit the propulsion and power subsystems when using high power electric propulsion to achieve delta-Vs on the order of km/s. In relation to this, experience in custom structural design should be developed and testing facilities will need to be rated for larger CubeSats. Second, hardware development should focus on the subsystems of propulsion, communications, power, and mechanisms. Development of electric propulsion systems in particular would enable science at interplanetary destinations in a CubeSat form factor. To facilitate electric propulsion system use, higher power generation will be required, needing deployable solar arrays and power management and distribution systems capable of higher and more varied input and output voltages.

Communications will require either a higher power radio, higher gain antenna, or combination of both to achieve useful data rates. While this design closed using a UHF link, expanding CPCL communications capability to X-band would significantly improve the data rate and reduce antenna size. This design utilizes critical deployable systems, solar arrays and an antenna, calling for development of reliable deployment mechanisms. Other takeaways for a mission at Mars include the need for student experience in advanced computational analysis and modelling for orbital trajectory design, thermal analysis, and structural analysis. Additionally, mission analysis and planning will require tools and design processes that account for the changing environment over a long duration mission affecting power modes and communications opportunities.

While one baseline was presented, other configurations and design options are possible and should be investigated in the next iteration of design. However, this research provides the subsystem performances required for a CubeSat that can host a scientific payload in a Phobos-Deimos cycler orbit around Mars which can inform that iteration. Through this research, areas for subsystem improvement within CPCL were identified both for this specific mission and interplanetary missions in general.

#### **14.1 Future Work**

Immediate future work should focus on developing the thermal protection system to close such that all components remain in their operational temperatures. This will involve investigating other mitigation methods for dissipating heat from the electric propulsion system in the low-thrust phase but balancing that dissipation with the heat retainment needed for the cycler orbit phase. Identified potential methods include phase change materials and deployable radiators. The effect on the power subsystem considering the heater power required to maintain components above their minimum temperatures should be investigated as well as part of the next iteration; effects on the power subsystem will in turn affect stowage volume and may require reconfiguration. Additionally, structural design and analysis was outside the scope of this thesis but is required to determine final



mass, volume, and configuration of the baseline. The design updates informed by structural analysis findings would in turn affect radiation and thermal modelling. The subsystem analyses performed were high level, all warranting more detailed investigation and design which would then allow interface development.

Beyond closing the design, some initial assumptions should be revisited. As low-thrust orbit optimization was outside the scope of this thesis, greater delta-V requirements were imposed. With an optimized orbit design, propulsion subsystem requirements would be reduced, and significant volume and mass could be saved such as through the removal of the chemical propulsion system, potentially reducing the overall bus size to 12U or even 6U. There are also multiple Mars SKGs that could be addressed in a lower Mars orbit and be used to develop a mission concept. For a first technology demonstration, a low-Mars orbiting CubeSat may be more feasible and offer an intermediate step between current CPCL capability and that required in this research as such a mission is more analogous to a LEO CubeSat.

Finally, for future work to remain relevant, the rapidly evolving CubeSat industry and technologies should be monitored. Enabling technologies are continually being developed and matured. These technologies, such as flexible solar arrays, have the potential to completely outdate the design decisions made in this work. Beyond software and hardware development, some processes alluded to in this research would be a novelty to CPCL, requiring investigation into how those endeavors might affect schedule and budget. As CubeSats beyond LEO are novel, near future lessons learned for flight technology and operations will be able to be gleaned from CubeSats manifested on Artemis-1. This work should be revisited as more information on those mission designs become available.

## BIBLIOGRAPHY

- [1] G. Dubos, J.-F. Castet and J. Saleh, "Statistical reliability analysis of satellites by mass category: Does spacecraft size matter?," *Acta Astronautica*, vol. 67, pp. 584-595, 9 2010.
- [2] NASA, *Jason 1 Launch Press Kit*, 2001.
- [3] NASA/CNES, *Mission to Planet Earth TOPEX/POSEIDON Press Kit*, 1992.
- [4] J.-P. Donnio, *Topex Poseidon*, 2020.
- [5] NASA, *What are SmallSats and CubeSats?*, 2015.
- [6] E. Kulu, *Nanosatellite & CubeSat Database*, 2019.
- [7] Cal Poly CubeSat Laboratory, *CubeSat Design Specification (1U - 12U), Revision 14 Draft*, 2020.
- [8] NASA CubeSat Launch Initiative, "CubeSat101: Basic Concepts and Processes for First-Time CubeSat Developers," 2017.
- [9] T. Villela, C. A. Costa, A. M. Brandão, F. T. Bueno and R. Leonardi, "Towards the Thousandth CubeSat: A Statistical Overview," *International Journal of Aerospace Engineering*, vol. 2019, pp. 1-13, 1 2019.
- [10] R. Staehle, B. Anderson, B. Betts, D. Blaney, C. Chow, L. Friedman, H. Hemmati, D. Jones, A. Klesh, P. Liewer, J. Lazio, M. W.-Y. Lo, P. Mouroulis, N. Murphy, P. Pingree, J. Puig-Suari, T. Svitek and A. W. Wilson, "Interplanetary CubeSats: Opening the Solar System to a Broad Community at Lower Cost," 2012.
- [11] NASA, *NASA Strategic Plan 2018*.
- [12] U. S. Small Business Innovation Research Program, *Deep Space Cubesat Technology*, 2014.
- [13] K. Robinson and G. Norris, "NASA's Space Launch System: Deep-Space Delivery for Smallsats," in *31st Annual AIAA/USU Conference on Small Satellites*, Logan, 2017.
- [14] NASA Jet Propulsion Laboratory, *Mars Cube One Demo*, 2019.
- [15] NASA, *Mars Reconnaissance Orbiter Launch Press Kit August 2005*, 2005.
- [16] NASA, *Cube Quest Challenge Fact Sheet*, 2019.
- [17] NASA, *CubeSat Launch Initiative*, 2020.
- [18] Cal Poly CubeSat Laboratory, *PolySat*.

- [19] Cal Poly CubeSat Laboratory, "ANNOUNCEMENT OF CUBESAT LAUNCH INITIATIVE No. NNH19ZCQ001O SLS ARTEMIS 2 DEEP-SPACE CUBESAT MISSION A Proposal Submitted by Cal Poly CubeSat Laboratory: LUNARAD A Study of Radiation Shielding Technologies in Cis-lunar Space\_".
- [20] A. Rivkin, *NEO/Phobos/Deimos Strategic Knowledge Gaps Special Action Team Final Report*, 2012.
- [21] S. Campagnola, C. H. Yam, Y. Tsuda, N. Ogawa and Y. Kawakatsu, "Mission analysis for the Martian Moons Explorer (MMX) mission," *Acta Astronautica*, vol. 146, pp. 409-417, 5 2018.
- [22] NASA, *Strategic Knowledge Gaps Associated with Potential Human Missions to the Martian System*, 2017.
- [23] D. Gilmore, *Spacecraft Thermal Control Handbook: Fundamental Technologies*, The Aerospace Corporation, 2002.
- [24] K. Mani, "Combined Chemical–Electric Propulsion Design and Hybrid Trajectories for Stand-Alone Deep-Space CubeSats," 2019.
- [25] NASA, *NASA Systems Engineering Handbook*, 2007.
- [26] EXOlaunch, *EXOpod 12U/16U CubeSat Deployment System User Guide*, 2020.
- [27] Cal Poly CubeSat Laboratory, *CubeSat Design Specification (CDS), Revision 13*, 2014.
- [28] A. Klesh, B. Clement, C. Colley, J. Essmiller, D. Forgette, J. Krajewski, A. Marinan, T. Martin-Mur, J. Steinkraus, D. Sternberg, T. Werne and B. Young, "MarCO: Early Operations of the First CubeSats to Mars," in *32nd Annual AIAA/USU Conference on Small Satellites*, Logan, 2018.
- [29] B. Sherwood, S. Spangelo, A. Frick, J. Castillo-Rogez, A. Klesh, E. J. Wyatt, K. Reh and J. Bake, "Planetary CubeSats Come of Age," in *66th International Astronautical Congress*, Jerusalem, 2015.
- [30] SolAero Technologies Corp., *COBRA-SS and COBRA-IU Composite Beam Rollout Array for SmallSats/CubeSats*, 2018.
- [31] A. Klesh and J. Krajewski, "MarCO: CubeSats to Mars in 2016," in *29th Annual AIAA/USU Conference on Small Satellites*, 2015.
- [32] F. C. Krause, J. A. Loveland, M. C. Smart, E. J. Brandon and R. V. Bugga, "Implementation of commercial Li-ion cells on the MarCO deep space CubeSats," *Journal of Power Sources*, vol. 449, p. 227544, 2 2020.
- [33] R. Hodges, N. Chahat, D. Hoppe and J. Vacchione, "A Deployable High-Gain Antenna Bound for Mars Developing a new folded-panel reflectarray for the first CubeSat mission to Mars," 2017.

- [34] E. Bering, L. Pinsky, L. Li, D. Jackson, J. Chen, H. Reed, M. Moldwin, J. Kasper, J. P. Sheehan, J. Forbes, T. Heine, A. Case, M. Stevens and D. Sibeck, "MarsCAT: Mars Array of ionospheric Research Satellites using the CubeSat Ambipolar Thruster," in *54th AIAA Aerospace Sciences Meeting*, 2016.
- [35] E. Decrossas, N. Chahat, P. Walkemeyer and B. Velasco, "Deployable Circularly Polarized UHF Printed Loop Antenna for Mars Cube One (MarCO) CubeSat," *IEEE*, 2019.
- [36] K. Lemmer, "Propulsion for CubeSats," *Acta Astronautica*, vol. 134, pp. 231-243, 5 2017.
- [37] S. Tardivel, A. Klesh and S. Campagnola, "Technology Enabling Interplanetary Trajectories for Nanospacecraft," *Journal of Spacecraft and Rockets*, vol. 55, pp. 95-105, 1 2018.
- [38] International Space Exploration Coordination Group, "The Global Exploration Roadmap," 2018.
- [39] J. Harper, "Pocket Rocket: A 1U+ Propulsion System to Enhance CubeSat Capabilities," 2020.
- [40] A. Powaser, "Colloid Thruster to Teach Advance Electric Propulsion Techniques to Post-Secondary Students," 2018.
- [41] V. L. Pisacane, *The Space Environment and Its Effects on Space Systems*, American Institute of Aeronautics and Astronautics, 2008.
- [42] J. Semkova, R. Kolevaa, V. Benghinc, T. Dacheva, Y. Matviichuka, B. Tomova, K. Krasteva, S. Maltcheva, P. Dimitrova, I. Mitrofanov, A. Malahov, D. Golovin, M. Mokrousov, A. Sanin, M. Litvak, A. K. V. Tretyakov, S. Nikiforov, A. Vostrukhin, F. Fedosov, N. Grebennikova, L. Zelenyi, V. Shurshakov and S. Drobishev, "Charged particles radiation measurements with Liulin-MO dosimeter of FRENDA instrument aboard ExoMars Trace Gas Orbiter during the transit and in high elliptic Mars orbit," *Icarus*, pp. 53-66, 2018.
- [43] D. Sinclair and J. Dyer, "Radiation Effects and COTS Parts in SmallSats," in *27th Annual AIAA/USU Conference on Small Satellites*, 2013.
- [44] B. Sabitbek, "Orbit Design for a Phobos-Deimos Cyclo Mission," 2016.
- [45] J. Sobtzak, E. Tianang, V. Joshi, B. Branham, N. Sonth, M. DeLuca, T. Moyer, K. Wislinsky and S. Palo, *A Deep Space Radio Communications Link for Cubesats: The CU-E3 Communication Subsystem*, 2017.
- [46] C. Hartzell, *On-Orbit, Collision-Free Mapping of Small Orbital Debris*, 2018.
- [47] OmniVision, *CMOS OV2640 Camera Module 1/4-Inch 2-Megapixel Module Datasheet Rev 1.0, May. 2015*, 2015.

- [48] SkyFox Labs, *Digital CubeSat Dosimeter piDOSE-DCD Product Datasheet, Rev. E/2019*, 2019.
- [49] Cal Poly CubeSat Laboratory, *ExoCube Engineering CDR*, 2012.
- [50] N. OGAWA, Y. TSUDA, Y. TAKEI, H. INOUE, S. TAKAHASHI and Y. KAWAKATSU, "Orbit Design for Martian Moons Explorer," 2017.
- [51] D. Eagle, *Optimal Impulsive Orbital Transfer*, 2020.
- [52] D. Eagle, *Low Thrust Transfer Between Non-coplanar Circular Orbits*, 2020.
- [53] D. Eagle, *A MATLAB Script for Designing Low-thrust Spiral Trajectories with Constant Periapsis Radius*, 2020.
- [54] H. Curtis, *Orbital Mechanics for Engineering Students*, Elsevier, 2014.
- [55] MIT OpenCourseWare, *Analytical Approximations for Low Thrust Maneuvers*, 2015.
- [56] NASA, "State of the Art Small Spacecraft Technology," 2018.
- [57] K. Mani, S. Boccelli, A. Cervone and F. Topputo, "Electric Propulsion Characterization for a Stand-Alone Mars CubeSat," in *36th International Electric Propulsion Conference*, 2019.
- [58] Busek Space Propulsion Systems, *BIT-3 RF Ion Thruster Datasheet*, 2019.
- [59] Aerojet Rocketdyne, *MPS-130 Innovative Propulsion Solutions for SmallSats*.
- [60] Aerojet Rocketdyne, *Modular Propulsion Systems Innovative Propulsion Solutions for CubeSats and SmallSats Datasheet*.
- [61] J. Botha, "Design of an RF Ion Thruster," 2014.
- [62] ATLAS Space Operations, *DEEP SPACE COMMUNICATIONS THE WORLDS FIRST COMMERCIAL DEEP SPACE NETWORK*, 2020.
- [63] W. Larson, *Space Mission Analysis and Design*, J. Wertz, Ed., Microcosm, 1999.
- [64] NASA, *Iris V2.1 CubeSat Deep Space Transponder*, 2016.
- [65] M. Simon, *Bandwidth-Efficient Digital Modulation with Application to Deep-Space Communications*, 2001.
- [66] N. Chahat, E. Decrossas, D. Gonzalez-Ovejero, O. Yurduseven, M. J. Radway, R. E. Hodges, P. Estabrook, J. D. Baker, D. J. Bell, T. A. Cwik and G. Chattopadhyay, "Advanced CubeSat Antennas for Deep Space and Earth Science Missions: A review," *IEEE Antennas and Propagation Magazine*, vol. 61, pp. 37-46, 2019.
- [67] EnduroSat, *X-Band Patch Antenna*, 2020.

- [68] T. Reichhardt, "Self-navigation put to asteroid fly-by test," *Nature*, vol. 400, pp. 392-392, 7 1999.
- [69] C. D. Edwards, "The Electra Proximity Link Payload for Mars Relay Telecommunications and Navigation," in *54th International Astronautical Congress of the International Astronautical Federation, the International Academy of Astronautics, and the International Institute of Space Law*, 2003.
- [70] Astronautical Development, LLC., *Lithium-1 Radio User Guide*, 2009.
- [71] A. Babuscia, D. Divsalar and K. Cheung, "CDMA communication system for mars areostationary relay satellite," in *2017 IEEE Aerospace Conference*, 2017.
- [72] S. Pirkle, "Design of a Martian Communication Constellation of CubeSats," 2020.
- [73] D. Lee and C. Lau, *Turbo-coded GMSK FER Measurements Using OQPSK Receiver*.
- [74] Arizona State University Phoenix CubeSat, *Phoenix PDR*, 2017.
- [75] J. Wertz, D. Everett and J. Puschell, Eds., *Space Mission Engineering (SME): The New SMAD, Microcosm*, 2011.
- [76] SpectroLab, *30.7% XTJ Prime Space Qualified Triple Junction Solar Cell*, 2018.
- [77] E. McNaul, *HaWK Solar Array Technology Advanced Deployable Satellite Power Solution*, 2015.
- [78] GomSpace, *Nanopower BPX Datasheet*, 2018.
- [79] GomSpace, *NanoPower BP4 Datasheet*, 2018.
- [80] GomSpace, *NanoPower P60 Dock Datasheet*, 2019.
- [81] GomSpace, *NanoPower P60 PDU-200 Datasheet*, 2018.
- [82] GomSpace, *NanoPower P60 ACU-200*, 2018.
- [83] M. H. Acuña, J. E. P. Connerney, P. Wasilewski, R. P. Lin, D. Mitchell, K. A. Anderson, C. W. Carlson, J. McFadden, H. Rème, C. Mazelle, D. Vignes, S. J. Bauer, P. Cloutier and N. F. Ness, "Magnetic field of Mars: Summary of results from the aerobraking and mapping orbits," *Journal of Geophysical Research: Planets*, vol. 106, pp. 23403-23417, 10 2001.
- [84] H. Hallock, G. Welter, D. Simpson and C. Rouff, *ACS Without an Attitude*, M. Hinchley, Ed., Springer, 2017.
- [85] New Space Systems, *Sun Sensor Datasheet*.
- [86] Sinclair Interplanetary, *Nanosatellite Reaction Wheels (RW-0.03) Datasheet*.
- [87] Adcole Maryland Aerospace, *MAI-SS Space Sextant Low Cost Miniature Star Tracker*, 2017.

- [88] Analog Devices, *Triaxial Inertial Sensor with Magnetometer ADIS16400/ADIS16405*, 2009.
- [89] NASA, *Mars Atmospheric Model*, 2015.
- [90] A. DeMasi, J. Giacomini, J. Joyce, C. Laurent and J. Stricker, "Development of a Low Cost 3-Axis Reaction Wheel System for Ultra-Fine Satellite Pointing Capabilities".
- [91] ISIS Space, *16-Unit CubeSat Structure*, 2020.
- [92] MMA Design, LLC, *eHaWK 27A-84FV Specification Sheet*.
- [93] VACCO Industries, *JPL MarCO - Micro CubeSat Propulsion System*.
- [94] K. Mani, A. Cervone and F. Topputo, "Combined Chemical–Electric Propulsion for a Stand-Alone Mars CubeSat," in *Journal of Spacecraft and Rockets*, 2019.
- [95] Honeybee Robotics, *CubeSat SADA*.
- [96] M. J. Burgdorf, T. Encrenaz, J. R. Brucato, H. Feuchtgruber, G. R. Davis, E. Lellouch, B. M. Swinyard, T. G. Müller, S. D. Sidher, P. Morris, M. J. Griffin, L. Colangeli and V. Mennella, "The Emissivity of Mars and Callisto in the Far Infrared," in *ISO Beyond the Peaks: The 2nd ISO Workshop on Analytical Spectroscopy*, 2000.
- [97] J. Henninger, "Solar Absorptance and Thermal Emittance of Some Common Spacecraft Thermal-Control Coatings," 1984.
- [98] All Flex, *Polyimide Heater 9.45" x 3.94" 6.53 Ohms*, 2020.
- [99] C. Zeitlin, D. M. Hassler, F. A. Cucinotta, B. Ehresmann, R. F. Wimmer-Schweingruber, D. E. Brinza, S. Kang, G. Weigle, S. Bottcher, E. Bohm, S. Burmeister, J. Guo, J. Kohler, C. Martin, A. Posner, S. Rafkin and G. Reitz, "Measurements of Energetic Particle Radiation in Transit to Mars on the Mars Science Laboratory," *Science*, vol. 340, pp. 1080-1084, 5 2013.
- [100] A. Good and J. Wendel, *Beyond Mars, the Mini MarCO Spacecraft Fall Silent*, 2019.
- [101] ISIS Space, *ISIS On Board Computer*.

APPENDICES

**Appendix A. Propulsion Trade and Calculations**

		Volume of req'd propellant at 100 psi (U)	Dry Mass (kg)	Power (W)	Time req'd to get to 1250 m/s (years)	TRL
<i>Ion Engine</i>	<b>BIT-3</b>	0.26	1.4	60	1.1	6
	<b>I-COUPS</b>	66.44	7.4	40	3	9
<i>Hall Effect</i>	<b>BHT-200</b>	48.64	1.1	200	0.1	8

	1	2	3	Rationale
Volume	>6U	1-6U	<1U	
Dry Mass	>6kg	6-1kg	<1kg	
Power	>70	70-20W	<20W	
Time	>5 yrs	2-5yrs	<2 yrs	Thruster lifetime
TRL	<5	5-6	7-9	Near future mission desired

<b>MPS Line Performance Analysis</b>		
	<b>12U</b>	<b>16U</b>
<b>Initial Mass (kg)</b>	24.0	32.0
<b>Propellant Expended from BIT-3 (kg)</b>	1.3	1.7
<b>Mass at Beginning of Impulsive Maneuver (kg)</b>	22.7	30.3
<b>Isp (s)</b>	235	
<b>MPS-135-4U dV (m/s)</b>	410	300
<b>MPS-135-6U dV (m/s)</b>	835	596
<b>MPS-135-8U dV (m/s)</b>	1267	878



## Appendix B. Detailed Link Budgets

### B.1 Direct to Earth Architecture

Parameter	Value	Source	
Distance (AU):	0.5		
T (K)	135	SMAD	
CubeSat Antenna Diameter Downlink X-Band	0.5		
CubeSat Antenna Diameter Downlink Ka-Band	0.28		
CubeSat RF Power (W)	3.8		
CubeSat Antenna Eff. Downlink	0.33	MarCO	
CubeSat gain uplink (dB):	12		
Earth GS X-Band Diameter (m):	70	DSN	
Earth GS Ka-Band Diameter (m):	34	DSN	
Earth GS Efficiency:	0.7	Assumed	
Earth GS RF Power (W):	20000	DSN, X-band transmit	
	<b>X-Band Up</b>	<b>X-Band Down</b>	<b>Ka-Band Down</b>
Frequency (GHz)	7.15	8.43	31.20
Distance (km)	74,800,000.00	74,800,000.00	74,800,000.00
Gtx	72.84	28.09	34.42
Ptx (dBW)	43.01	5.80	5.80
Grx	6.00	74.27	79.37
Eb/No	2.90	2.90	2.90
Rec System Temp	21.30	21.30	21.30
Free Path Loss	267.01	268.44	279.81
Other Losses	5.00	7.00	7.00
Margin	3.00	3.00	3.00
Boltzmann	228.60	228.60	228.60
R	51.24	34.12	34.18
<b>Bitrate (bps)</b>	<b>133,102.79</b>	<b>2,579.49</b>	<b>2,617.23</b>

## B.2 Relay Architecture

	<i>Far, Coded</i>		<i>Perigee, No coding</i>		<i>Perigee, Coded</i>		<i>Perigee, No coding</i>
	<i>UHF-Band Uplink</i>	<i>UHF-Band Downlink</i>	<i>UHF-Band Uplink</i>	<i>UHF-Band Downlink</i>	<i>UHF-Band Uplink</i>	<i>UHF-Band Downlink</i>	<i>X-Band Downlink</i>
<i>Uplink = Relay to Cubesat</i>							
<i>Downlink = CubeSat to Relay</i>							
Frequency (GHz)	0.45	0.39	0.45	0.39	0.45	0.39	8.40
Distance (km)	13,500.00	13,500.00	10,000.00	10,000.00	10,000.00	10,000.00	10,000.00
Gtx	0.00	3.50	0.00	3.50	0.00	3.50	12.00
Ptx (dBW)	8.45	3.98	8.45	3.98	8.45	3.98	5.80
Grx	3.50	0.00	3.50	0.00	3.50	0.00	30.00
Eb/No	2.90	2.90	9.60	9.60	2.90	2.90	9.60
Rec System Temp	23.86	23.86	23.86	23.86	23.86	23.86	23.86
Free Path Loss	168.12	166.88	165.51	164.27	165.51	164.27	190.94
Other Losses	7.00	7.00	7.00	7.00	7.00	7.00	7.00
Margin	3.00	3.00	3.00	3.00	3.00	3.00	3.00
Boltzmann	228.60	228.60	228.60	228.60	228.60	228.60	228.60
R	35.67	32.45	31.58	28.35	38.28	35.05	42.01
<b>Bitrate (bps)</b>	<b>3,693.17</b>	<b>1,756.05</b>	<b>1,439.02</b>	<b>684.23</b>	<b>6,730.80</b>	<b>3,200.40</b>	<b>15,871.53</b>

Parameter	Value
Max Distance (km):	13500
Min Distance (km):	10000
T (K)	243
CubeSat RF Power (W)	2.5
CubeSat UHF gain (dB):	3.5
Relay Antenna Gain (dB):	0
Relay Efficiency:	0.85
Relay RF Power (W):	7
Eb/No no coding	9.6
Eb/no coding	2.9
CubeSat X-band Gain (dB)	12
CubeSat X-band Power (W)	3.8
Relay X-Band Gain (dB)	30

## Appendix C. EXOlaunch Specifications [26]

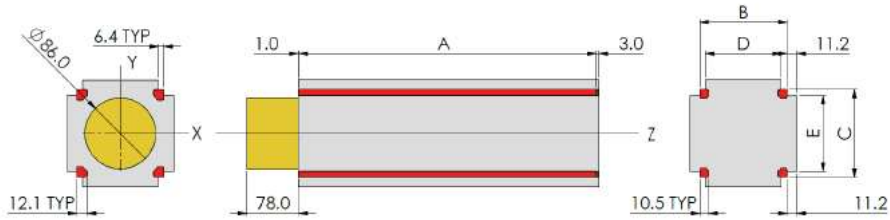


Figure 15: Maximum allowable outer dimensions for Cubesats launched in an EXOpod. Contact areas with the deployer are marked red.

Table 1: Maximum Cubesat Dimensions

Description	Letter	3U	6U	6U XL	8U	12U	16U
Cubesat Rail Length (Z) [mm]	A	340.5	340.5	365.9	454	340.5	454
Cubesat Rail Width (X) [mm]	B	100	226.3	226.3	226.3	226.3	226.3
Cubesat Rail Height (Y) [mm]	C	100	100	100	100	226.3	226.3
Maximum Space Between Rails (X) [mm]	D	87.2	213.5	213.5	213.5	213.5	213.5
Maximum Space Between Rails (Y) [mm]	E	87.2	87.2	87.2	87.2	213.5	213.5
Number of Tuna Cans	-	1	2	2	2	5*	5*
Distance Between Tuna Cans [mm]	-	-	126.3	126.3	126.3	126.3	126.3
Maximum Mass [kg]	-	5.5	11	12	15	22	24
Maximum Distance Between CoG and Geometric Center [mm]	-	20					
Rail Parallelism [mm]	-	0.05					
Surface Roughness [ $\mu\text{m}$ ]	-	1.6					

\*The fifth tuna can is located at the center of the deployment wagon. Dimensions in Figure 17 and Figure 18.

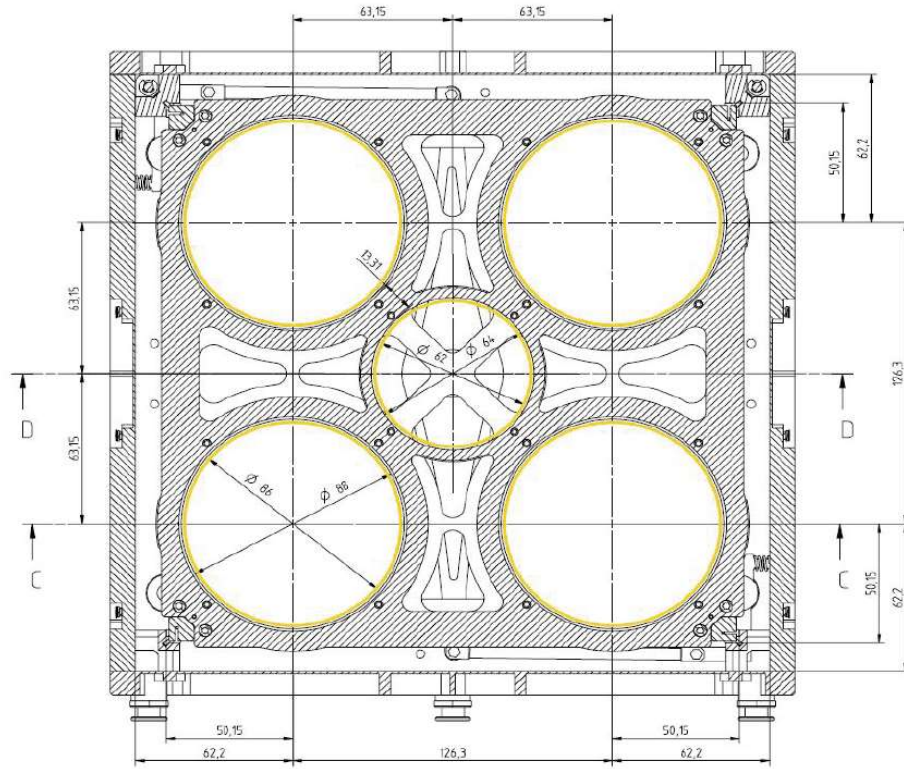
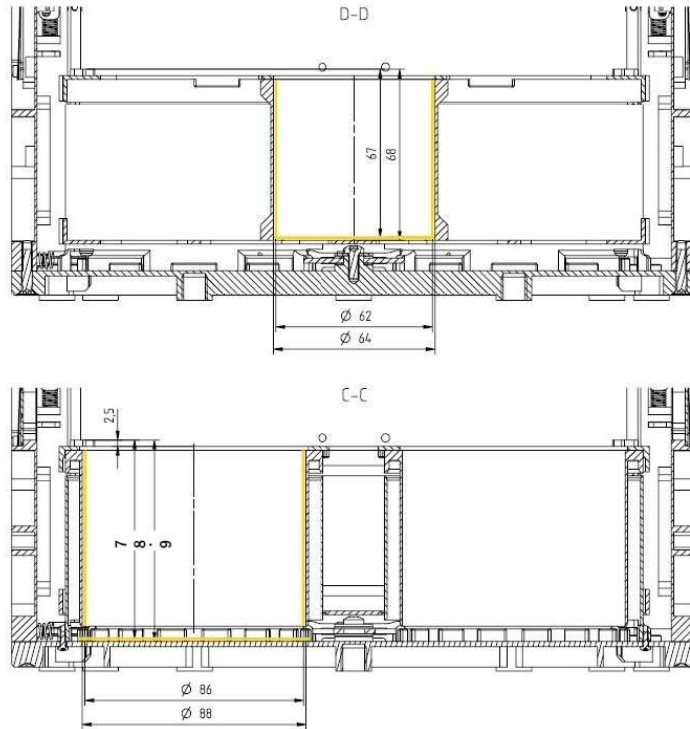


figure 17: Detailed dimensions of the tuna cans (front view). Note that the yellow area marks a required tolerance gap. E.g. the internal diameter of the cylinder is 88 mm wide, but the maximum allowed diameter for the tuna can is 86 mm.



: Detailed dimensions of the tuna cans, Sections C-C and D-D (side view). Note that the yellow area marks a required tolerance gap. E.g. the internal diameter of the cylinder is 88 mm wide, but the maximum allowed diameter for the tuna can is 86 mm.

## Appendix D. N2 Diagram for Configuration

Spacecraft Component Interfaces															
STRUCTURE	M	M		M			M	M	M		M	M	M	M	M
	BIT-3						E					E			
		MPS-135					E								
			UHF RADIO	E			E, D								
				UHF ANTENNA											
					CAMERA		E, D								
						RADIATION SENSOR	E, D								
							OBC	E	E, D	E, D	E, D	E, D			E, D
								RXN WHEELS							
									SUN SENSOR						
M	Mechanical									IMU					
E	Electrical										STAR TRACKER				
D	Data											PDU	M, E	E	
													BATTERIES		
														SOLAR PANELS	M, E
															SADA

## Appendix E. CubeSats Manifested for Artemis-1

### CubeSats manifested for SLS Artemis-1 [6, 13].

<b>CubeSat</b>	<b>Mission</b>	<b>Orbit</b>	<b>Affiliation</b>
<b>Near Earth Asteroid (NEA) Scout</b>	Rendezvous with and characterize an NEA using a solar sail as propulsion	Interplanetary	NASA
<b>Lunar Flashlight</b>	Search for ice-deposits in Moon's permanently shadowed craters using lasers and a spectrometer; will use a green-propellant system	Lunar	NASA
<b>BioSentinel</b>	Measure effects of space radiation on yeast; will enter a heliocentric orbit outside of the Van Allen belts	Lunar fly-by, heliocentric	NASA
<b>Lunar Icecube</b>	Search for water in solid, liquid, and vapor forms using an infrared spectrometer; highly inclined lunar orbit	Lunar	Morehead State University
<b>Skyfire</b>	Tech demonstration to perform spectroscopy and thermography during a lunar flyby	Lunar fly-by	Lockheed Martin
<b>CubeSat Mission to Study Solar Particles (CuSP)</b>	Study solar and interplanetary particle dynamics and provide space weather support during Solar Energetic Particle events	Interplanetary	Southwest Research Institute (SRI)
<b>LunaH-Map</b>	Understand Hydrogen deposits in lunar cold traps	Lunar	Arizona State University
<b>Outstanding MOon exploration TEchnologies demonstrated by NAno Semi-Hard Impactor (OMOTENASHI)</b>	Land smallest lunar lander to demonstrate hardware feasibility for multi-point exploration; characterize lunar radiation environment and soil	Interplanetary	Japanese Space Agency (JAXA)
<b>EQUilibriUm Lunar-Earth point 6U Spacecraft (EQUULEUS)</b>	Perform first CubeSat trajectory control techniques in a Sun-Earth-Moon libration point at Lagrange Point 2; characterize lunar meteorite impacts and geospace radiation environment	Lunar Lagrange Point 2	Japanese Space Agency (JAXA)
<b>ArgoMoon</b>	Perform proximity operations with the ICPS on its disposal trajectory, perform optical communications demonstration	Lunar	European Space Agency (ESA), Italian Space Agency (ISA)
<b>Cislunar Explorer</b>	Water-electrolysis-based propulsion system	Lunar	Cornell University
<b>Colorado University Earth Escape Explorer (CU-E<sup>3</sup>)</b>	Communications demonstration	Interplanetary	University of Colorado
<b>Miles</b>	Evolutionary plasma thrusters demonstration	Lunar	Fluid & Reason, LLC, Tampa Hackspace

### Yet to Launch Missions [6]

<b>CubeSat</b>	<b>Mission</b>	<b>Orbit</b>	<b>Affiliation</b>
<b>Garatea-L</b>	Perform biological microgravity and radiation experiments	Lunar	Airvantis
<b>INSPIRE</b>	Demonstrate deep space relay communications and navigation	Interplanetary	NASA Jet Propulsion Laboratory, California Institute of Technology
<b>Miniaturised Asteroid Remote Geophysical Observer (M-ARGO)</b>	Rendezvous with and characterize an asteroid to determine mining potential	Interplanetary	European Space Agency



## Appendix F. STK Inputs

### 1. Initial State:

Propagator: Astrogator Central Body: Mars

Elements: Spacecraft Parameters Fuel Tank User Variables

Coord.System: Mars Inertial

Coordinate Type: Keplerian

Orbit Epoch: 11 Jun 2025 00:00:00.000 UTCC

Element Type: Osculating

Semi-major Axis: 3696 km

Apoapsis Altitude: 299.81 km

Inclination: 0 deg

Right Asc. of Asc. Node: 0 deg

Argument of Periaapsis: 0 deg

True Anomaly: 301.03 deg

Initial State Tool...

Initial: 11 Jun 2025 00:00:00.000 UTCC Final: 11 Jun 2025 00:00:00.000 UTCC

### 2. Propagate one orbit:

Propagator: Astrogator Central Body: Mars

Propagator: Mars Point Mass Advanced...

Stopping Conditions

On	Name	Sequence	User Comment	Description
<input checked="" type="checkbox"/>	Duration	STOP	Stop after a specified duration	Stop after a specified duration

Trip: 6822 sec Criterion: ...

Tolerance: 1e-08 sec Repeat Count: 1

Max Trip Times: 10000

User Calc Object: ... Edit

Sequence: STOP Constraints: ...

Before: N/A  Condition Inherited by Automatic Sequences

### 3. Low-Impulse Maneuver:

Propagator: Astrogator Central Body: Mars

Maneuver Type: Finite Seed Finite From Impulsive

Attitude Engine Propagator

Attitude Control: Along Velocity Vector More Options...

Attitude Update: Update during burn

Initial: 11 Jun 2025 01:53:42.000 UTC Final: 19 Nov 2026 01:53:42.000 UTC

Results...

- Initial State
- Propagate
- Maneuver
- Propagate1
- Propagate3
- Target Sequence
  - Maneuver
- Propagate2

Propagator: Astrogator Central Body: Mars

Maneuver Type: Finite Seed Finite From Impulsive

Attitude Engine Propagator

Propulsion Type

Engine Model BIT-3 ...

Thruster Set Single Thruster ...

Pressure Mode: Blow-Down

Thrust Efficiency: 1

Thrust: Affects Accel Only

- Initial State
- Propagate
- Maneuver
- Propagate1
- Propagate3
- Target Sequence
  - Maneuver
- Propagate2

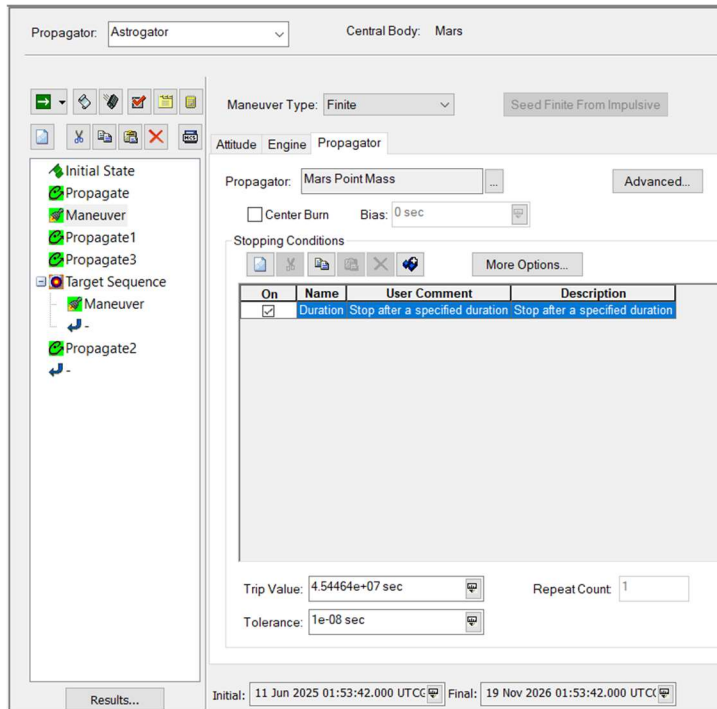
Engine Models - BIT-3

Name: BIT-3

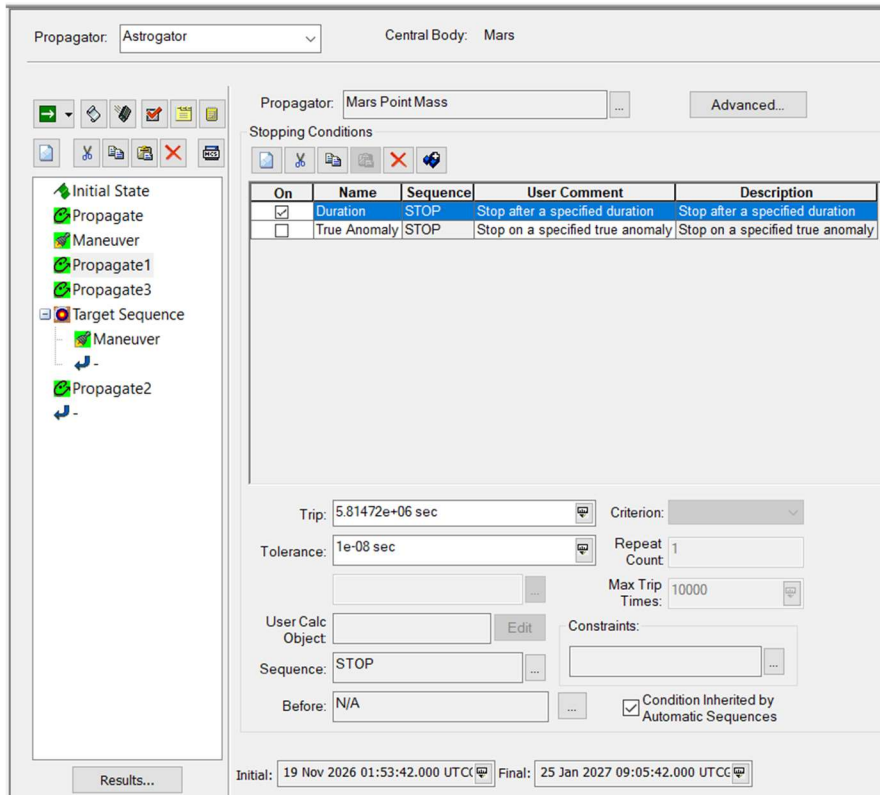
Description: Engine that has a constant Thrust and Isp

User Comment: Engine that has a constant Thrust and Isp

Name	Value	Description
ComponentName	BIT-3	Name of the component
g	0.009806650000000000 km/sec^2	Earth surface gravity accel. for Isp conver
Thrust	0.0008500000000000 N	Thrust for this engine
Isp	2300.0000000000000 s	Specific Impulse for this engine



**4. Propagate additional time to account for only thrusting in Sun:**



5. Propagate to periapsis to perform impulsive maneuver:

Propagator: Astrogator Central Body: Mars

Propagator: Mars Point Mass Advanced...

Stopping Conditions

On	Name	Sequence	User Comment	Description
<input type="checkbox"/>	Duration	STOP	Stop after a specified duration	Stop after a specified duration
<input checked="" type="checkbox"/>	True Anomaly	STOP	Stop on a specified true anomaly	Stop on a specified true anomaly
<input type="checkbox"/>	Periapsis	STOP	Stop at the point closest to the origin	Stop at the point closest to the origin

Trip: 43200 sec Criterion:   
 Tolerance: 1e-08 sec Repeat Count: 1   
 Max Trip Times: 10000

User Calc Object: Edit   
 Sequence: STOP   
 Before: N/A   
 Condition Inherited by Automatic Sequences

Initial: 25 Jan 2027 09:05:42.000 UTCC Final: 25 Jan 2027 09:57:37.484 UTCC

6. Target sequence to transfer to cycler orbit:

Propagator: Astrogator Central Body: Mars

Action: Run active profiles   
 When Profiles Converge: Run to RETURN and continue   
 Continue if profiles don't converge   
 Reset inner targeters before each run

Profiles and Corrections   
 Apply Changes   
 Reset

Profiles

Name	Reset	Apply	Mode	Status	User Comment
Differential Corrector	Reset	Apply	Iterate	Converged	Differential Corrector Description

Enable Logging

Initial: 25 Jan 2027 09:57:37.484 UTCC Final: 25 Jan 2027 09:57:37.484 UTCC

**Differential Corrector**

Variables | Convergence | Advanced | Log | Graphs | Scripting

Control Parameters

Use	Name	Final Value	Last Update	Object	Custom Display Unit	Display Unit
<input checked="" type="checkbox"/>	ImpulsiveMnr.Cartesian.XSDU	441.05 m/sec	441.05 m/sec	Maneuver	<input type="checkbox"/>	m/sec
<input checked="" type="checkbox"/>	ImpulsiveMnr.Cartesian.YSDU	0.00923759 m/sec	0.00923759 m/sec	Maneuver	<input type="checkbox"/>	m/sec
<input checked="" type="checkbox"/>	ImpulsiveMnr.Cartesian.ZSDU	31.7517 m/sec	31.7517 m/sec	Maneuver	<input type="checkbox"/>	m/sec

Initial: 441.05 m/sec | Perturbation: 0.1 m/sec | Scaling Method: By initial value | Value: 1 m/sec

Correction: 441.05 m/sec | Max. Step: 100 m/sec

---

Equality Constraints (Results)

Use	Name	Desired Value	Current Value	Object	Custom Display Unit	Display Unit
<input checked="" type="checkbox"/>	Eccentricity	0.4497	0.452222	Maneuver	<input type="checkbox"/>	

Difference: 0.00252185 | Tolerance: 0.01 | Scaling Method: By desired value | Value: 1 | Weight: 1

Propagator: Astrogator | Central Body: Mars

Maneuver Type: Impulsive | Seed Finite From Impulsive

Attitude Engine

Attitude Control: Thrust Vector | More Options...

Thrust Axes: VNC(Mars)

Cartesian  Spherical

X (Velocity): 0 m/sec | Azimuth: 0 deg

Y (Normal): 0 m/sec | Elevation: 0 deg

Z (Co-Normal): 0 m/sec | Magnitude: 0 m/sec

Allow Negative Spherical Magnitude

Initial: 25 Jan 2027 09:57:37.484 UTCC | Final: 25 Jan 2027 09:57:37.484 UTCC

Results...

Propagator:  Central Body:

Maneuver Type:

Attitude Engine

Propulsion Type

Engine Model

Thruster Set

Update Mass Based on Fuel Usage

Initial:  Final:

Engine Models - MPS-130

Name:

Description:

User Comment:

Name	Value	Description
ComponentName	MPS-130	Name of the component
g	0.009806650000000000 km/sec^2	Earth surface gravity accel. for Isp conversion
Thrust	1.2500000000000000 N	Thrust for this engine
Isp	245.00000000000000 s	Specific Impulse for this engine

*\*Note: Incorrectly named, parameters correspond to MPS-135.*

## 7. Propagate 1.88 years

Propagator: Astrogator Central Body: Mars

Propagator: Mars Point Mass Advanced...

Stopping Conditions

On	Name	Sequence	User Comment	Description
<input checked="" type="checkbox"/>	Duration	STOP	Stop after a specified duration	Stop after a specified duration
<input type="checkbox"/>	Perapsis	STOP	Stop at the point closest to the origin	Stop at the point closest to the origin
<input type="checkbox"/>	True Anomaly	STOP	Stop on a specified true anomaly	Stop on a specified true anomaly

Trip: 5.93283e+07 sec Criterion: [dropdown]

Tolerance: 1e-08 sec Repeat Count: [dropdown]

User Calc: [dropdown] Edit

Max Trip Times: 10000

Constraints: [dropdown]

Sequence: STOP

Before: N/A

Condition Inherited by Automatic Sequences

Initial: 25 Jan 2027 09:57:37.484 UTC Final: 12 Dec 2028 02:02:25.484 UTC

*Propagator used:*

Propagators - Mars Point Mass

Propagator Functions Numerical Integrator

Central Body: Mars

Name	User Comment	Description
TwoBody Force	Force from point mass of central body	Force from point mass of central body

Gravitational Parameter Source: Cb File

Gravitational Parameter: 42828.4 km<sup>3</sup>/sec<sup>2</sup>

Modify gravity model below this percentage of central body surface: 99%

## Appendix G. Thermal Desktop Inputs

*Hot Case:*

**Orbit:**

Orbit: Initial\_Circular\_300\_km

Basic Orbit | Orientation | Positions | Planetary Data | Solar | Albedo | IR Planetshine | Fast Spin | Comment

Beta Angle:  Degrees (Angle between solar vector and plane of orbit)

Altitude:  km

Calculated orbital period = 6825.33 sec

Orbit: Initial\_Circular\_300\_km

Basic Orbit | Orientation | Positions | Planetary Data | Solar | Albedo | IR Planetshine | Fast Spin | Comment

Pointing

Axis:  ▾

Nadir

Sun

Star

Right Ascension:  Degrees

Declination:  Degrees

Velocity vector

Orientation Override

Align to Celestial Coordinate System

Additional Constraint

Axis:  ▾

Nadir

Sun

Star

Right Ascension:  Degrees

Declination:  Degrees

Velocity vector

Additional Rotations

X  ▾ Degrees

Y  ▾ Degrees

Z  ▾ Degrees

Orbit: Initial\_Circular\_300\_km

Basic Orbit | Orientation | Positions | Planetary Data | Solar | Albedo | IR Planetshine | Fast Spin | Comment

Radius of Planet:  km

Gravitational Mass (GM):  km<sup>3</sup>/s<sup>2</sup>

Inclination of Equator:  Degrees

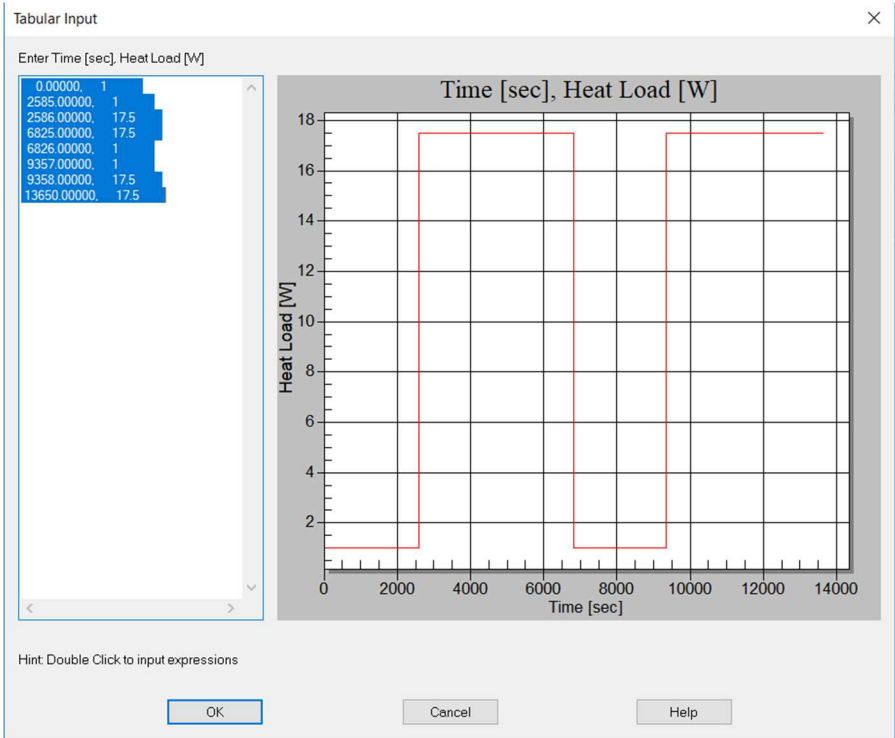
Sidereal Period:  sec

Mean Solar Day:  sec

Reset to:  ▾



**BIT-3 Heating Profile:**



**Cold Case:**

**Orbit:**

Heating Rate Case: Cyclor

Keplerian Orbit Orientation Positions Planetary Data Solar Albedo IR Planetshine Fast Spin Comment

Orbit Definition

Orbit Inclination:  Degrees

R.A. of Ascending Node:  Degrees

Argument of Periaapsis:  Degrees

Date Dependent Right Ascension Definitions

User Specified

Sun:  Degrees

Prime Meridian:  Degrees

Use Date/Time

Orbit Shape Definition - Select 2

Minimum Altitude:  km

Maximum Altitude:  km

Eccentricity:

Period:  sec

Calculated Beta Angle: 0.000000e+00

Heating Rate Case: Cyclor

Keplerian Orbit Orientation Positions Planetary Data Solar Albedo IR Planetshine Fast Spin Comment

Pointing

Axis:

Nadir

Sun

Star

Right Ascension:  Degrees

Declination:  Degrees

Velocity vector

Orientation Override

Align to Celestial Coordinate System

Additional Constraint

Axis:

Nadir

Sun

Star

Right Ascension:  Degrees

Declination:  Degrees

Velocity vector

Additional Rotations

X:  Degrees

Y:  Degrees

Z:  Degrees

Heating Rate Case: Cyclor

Keplerian Orbit Orientation Positions Planetary Data Solar Albedo IR Planetshine Fast Spin Comment

Radius of Planet:  km

Gravitational Mass (GM):  km<sup>3</sup>/s<sup>2</sup>

Inclination of Equator:  Degrees

Sidereal Period:  sec

Mean Solar Day:  sec

Reset to:

**Thermal and optical properties:**

**Edit Optical Properties**

Current Optical Property Database:  
 ..\rcoptics.rco

New property to add:

Name	Solar Absorp...	IR Emissivity	a/e
Aluminum	0.090	0.030	3.000
Barium Sulphate with Polyvinyl Alcohol	0.060	0.880	0.068
Black paint	0.960	0.890	1.079
EH	0.900	0.100	9.000
Martin Black Velvet Paint	0.910	0.940	0.968
Mirror	0.110	0.080	1.375
MLI	0.001	0.007	0.143
polished gold BOL	0.300	0.050	6.000
Solar Cells	0.860	0.850	1.012
Teflon	0.080	0.680	0.118
Titanium	0.400	0.550	0.727
tube black effective	0.800	0.800	1.000
vacuum deposited gold	0.030	0.030	1.000
z93	0.170	0.920	0.185

**Edit Thermophysical Properties**

Current Thermophysical Property Database:  
 ..\tdthermo.tdp

New property to add:

Name	Cond [W/m/C]	Dens [kg/m^3]	Cp [J/kg/C]	Eff Emiss
aluminum	167	2700	921.096	
Aluminum Honeycomb	167	909.1	0.896	
Carbon Fiber Skin	75	1780	710	
Copper C10200	391.2	8860	385.2	
DEFAULT	1	1	1	
Delrin	0.4	1300	1465.2	
GalnAs	4	5500	300	
Helium	0.02	125	5000	
Honeycomb	20	0	0	0.05
lithium ion	167	2747.25	960	
MLI	4e-05	0	0	0.001
MMH	0.32	874	2950	
NTO-MON-3	0.29	1442.46	1550	
pcm	0.148	790	FUSION	
Titanium	7.8	4430	522	